CAPITAL UNIVERSITY OF SCIENCE AND TECHNOLOGY, ISLAMABAD

SC-FDMA Radar: Waveform Design and Signal Processing

by

Rahat Saadia

A thesis submitted in partial fulfillment for the degree of Doctor of Philosophy

in the

Faculty of Engineering
Department of Electrical Engineering

2021

SC-FDMA Radar: Waveform Design and Signal Processing

By

Rahat Saadia

(PE131009)

Dr. Muhammad Imran, Professor

University of Glasgow, UK

(Foreign Evaluator 1)

Dr. Raja Syamsul Azmir Abdullah, Professor

Universiti Putra Malaysia, Malaysia

(Foreign Evaluator 2)

Dr. Noor Muhammad Khan

(Thesis Supervisor)

Dr. Noor Muhammad Khan

(Head, Department of Electrical Engineering)

Dr. Imtiaz Ahmad Taj

(Dean, Faculty of Engineering)

DEPARTMENT OF ELECTRICAL ENGINEERING

CAPITAL UNIVERSITY OF SCIENCE AND TECHNOLOGY

ISLAMABAD

2021

I would like to dedicate this thesis to my loving parents

CAPITAL UNIVERSITY OF SCIENCE & TECHNOLOGY
ISLAMABAD
Expressway, Kahuta Road, Zone-V, Islamabad
Phone:+92-51-111-555-666 Fax: +92-51-4486705
Email: info@cust.edu.pk Website: https://www.cust.edu.pk

CERTIFICATE OF APPROVAL

This is to certify that the research work presented in the thesis, entitled "**SC-FDMA Radar: Waveform Design and Signal Processing**" was conducted under the supervision of **Dr. Noor Muhammad Khan**. No part of this thesis has been submitted anywhere else for any other degree. This thesis is submitted to the **Department of Electrical Engineering, Capital University of Science and Technology** in partial fulfillment of the requirements for the degree of Doctor in Philosophy in the field of **Electrical Engineering.** The open defence of the thesis was conducted on **November 11, 2021.**

Student Name : Rahat Saadia (PE-131009)

The Examination Committee unanimously agrees to award PhD degree in the mentioned field.

Examination Committee :

(a) External Examiner 1: Dr. Shahid Khattak
Professor
UET, Mardan

(b) External Examiner 2: Dr. Tauseef Jamal
Professor
PIEAS, Islamabad

(c) Internal Examiner : Dr. Imtiaz Ahmad Taj
Professor
CUST, Islamabad

Supervisor Name : Dr. Noor Muhammad khan
Professor
CUST, Islamabad

Name of HoD : Dr. Noor Muhammad Khan
Professor
CUST, Islamabad

Name of Dean : Dr. Imtiaz Ahmad Taj
Professor
CUST, Islamabad

AUTHOR'S DECLARATION

I, **Rahat Saadia (Registration No. PE-131009)**, hereby state that my PhD thesis titled, "**SC-FDMA Radar: Waveform Design and Signal Processing**" is my own work and has not been submitted previously by me for taking any degree from Capital University of Science and Technology, Islamabad or anywhere else in the country/ world.

At any time, if my statement is found to be incorrect even after my graduation, the University has the right to withdraw my PhD Degree.

(Rahat Saadia)

Registration No : PE-131009

Dated: November, 2021

PLAGIARISM UNDERTAKING

I solemnly declare that research work presented in the thesis titled "**SC-FDMA Radar: Waveform Design and Signal Processing**" is solely my research work with no significant contribution from any other person. Small contribution/ help wherever taken has been duly acknowledged and that complete thesis has been written by me.

I understand the zero tolerance policy of the HEC and Capital University of Science and Technology towards plagiarism. Therefore, I as an author of the above titled thesis declare that no portion of my thesis has been plagiarized and any material used as reference is properly referred/ cited.

I undertake that if I am found guilty of any formal plagiarism in the above titled thesis even after award of PhD Degree, the University reserves the right to withdraw/ revoke my PhD degree and that HEC and the University have the right to publish my name on the HEC/ University Website on which names of students are placed who submitted plagiarized thesis.

(**Rahat Saadia**)

Dated: November, 2021

Registration No : PE-131009

List of Publications

It is certified that following publication(s) have been made out of the research work that has been carried out for this thesis:-

1. **R. Saadia**, and N. M. Khan, "Single Carrier-Frequency Division Multiple Access Radar: Waveform Design and Analysis," *IEEE Access, IEEE*, vol. 8, pp. 35742-35751, 2020.

(Rahat Saadia)

Registration No: PE131009

Acknowledgement

This dissertation would not have been possible without the inspiration and support of a number of wonderful individuals. I owe my gratitude and appreciation to all of them for being part of this experience and making this thesis possible.

I owe my deepest gratitude to my research supervisor, Dr. Noor Muhammad Khan, for his valuable guidance throughout my doctoral research. With extraordinary prescience, he led me to explore the novel and innovative research ideas. His technological foresight aims at looking into the long-term future of science, technology and innovation. He has this amazing knack of thinking out-of-the-box that led us to the idea of pushing the boundaries of wireless-communication and radar technologies for the development of futuristic radars. This thesis would not have been completed if not for his support and guidance. It has been a great honor for me to work under his supervision and a part of his excellent research team.

I would like to thank Dr. Raza Samar, Dr. Amir Qayyum, and Dr. Aamer Iqbal Bhatti for their inspiration, guidance and support during this time.

I extend my heartfelt thanks and warm regards to Dr. Mansoor Ahmed (Vice Chancellor, CUST) , Dr. Imtiaz Ahmad Taj (Dean Faculty of Engineering) and Dr. Noor Muhammad Khan (HoD Electrical Engineering) for providing administrative support to carry on this research work. I am also very grateful to all the teaching and research staff of Capital University of Science and Technology, Islamabad, who made this prestigious institution not only a great place for research but also a place for fun that I will always cherish.

I owe special thanks to Engr. Khalid Mahmood (Director, Graduate Studies) for his timely support and guidance.

I also extend my thanks to Dr. Muhammad Iqbal, who helped me as my mentor throughout the journey of my research work. Without his enthusiasm, encouragement, support and continuous optimism this thesis would hardly have been completed.

Finally, my profound and heartfelt appreciation to my family for their affection and constant support. I am always indebted to my loving parents who inspired me selflessly to pursue new paths in life and to discover my own destiny. They provided me the opportunities and experiences that have made me who I am. I would like to convey my deepest gratitude to my beloved children, Maryam and Abdullah, and my caring husband whose unceasing encouragement and commitment to me never once diminished, even in the toughest hours of this journey.

(Rahat Saadia)

Registration No: PE131009

Abstract

In a pulsed radar, the range resolution and the target detectability are usually coupled in an inverse relationship. Pulse compression is considered as a viable solution for this perplexity. However, the existing single-carrier and multicarrier pulse compression waveforms suffer from several setbacks that lead to undesirable trade-offs.

Pushing the boundaries of wireless communication and radar technologies, this thesis proposes Single-carrier Frequency Division Multiple Access (SC-FDMA) waveform for radar applications, which has it origin in Cellular Communications such as LTE. The proposed SC-FDMA radar system is not only a solution to the perplexity of range resolution and target detectability but also exploits all the benefits of single and multicarrier waveforms and offers null PAPR and improved Ambiguity Function and autocorrelation properties.

The thesis begins with the proposed interleaved SC-FDMA radar signal design while presenting a complete radar architecture and signal processing mechanism. The proposed radar system is analyzed for its ambiguity function and autocorrelation properties. The autocorrelation properties include autocorrelation function (ACF), and autocorrelation peak-to-sidelobe ratio (PLSR) of the radar waveform. The performance of the proposed radar waveform is compared with those of the notable existing radar waveforms including a standard OFDM radar, Cyclic Algorithms - New (CAN), Hadamard, and Periodic correlation Weighted Cyclic Iteration Algorithm (PWCIA). It is observed from the comparative analysis that the proposed scheme exhibits a higher PLSR and better autocorrelation properties as compared to OFDM and other notable radar waveforms.

Since the proposed interleaved SC-FDMA waveform aims at reducing the time-domain fluctuations of the signal, which is a major issue in multicarrier radar systems such as OFDM, therefore, a comparative analysis of the PAPR values of the proposed and OFDM radar waveforms is carried out using the same number of subcarriers for different fixed and random phase-coded initiating sequences. In

each case, the proposed interleaved SC-FDMA signal exhibits a constant envelope resulting in a PAPR value of almost 0 dB as compared to the chaotic fluctuating envelope exhibited by OFDM signal resulting in a high PAPR value. It is, therefore, concluded from the PAPR analysis results, that the proposed Interleaved SC-FDMA waveform is the most suitable waveform for multicarrier radar systems in term of achieving minimum possible PAPR. This enables the power amplifier of the radar transmitter to utilize its maximum capability without compromising its power efficiency and hence consequently extends the detection range of the radar many folds.

In order the evaluate the performance of the proposed interleaved SC-FDMA radar in terms of target detection and parameter estimation, a complete end-to-end radar is simulated with monostatic configuration for single and multiple moving target scenarios. The target parameters include pulse delay and Doppler shift, referring to range and radial speed of the target respectively. The comparative analysis of the simulation results for each scenario show that the proposed radar outperforms the Linear Frequency Modulated (LFM) and OFDM radars while offering extremely high range and velocity resolutions. This shows that the proposed radar exhibits the ability to pinpoint and discriminate a target, even with a very small radar cross-section (RCS), in single as well as multiple target scenarios, at any unambiguous range and speed.

The proposed radar design opens portals to multiple research realms for the development of futuristic high performance radars. The wideband characteristics of the proposed SC-FDMA waveform makes it resistant against active and passive interference. As a future work, the performance of the proposed SC-FDMA radar can be analyzed in terms of this feature against jammers and electronic deception devices. Moreover, the proposed work can be extended to develop multiple tasking radars, as the different source signals can correspond to independent tasks to be performed simultaneously. The proposed extension can not only find its applications in Radar-Communications (Rad-Comm) hybrid systems but also in multiple target tracking radars. In addition to this, as a future work, the SC-FDMA waveform can be implemented in MIMO radars. Exploiting the spatial diversity provided by MIMO systems, the SC-FDMA-MIMO duo would be able to achieve not only a higher angle estimation accuracy and better sensitivity for moving target detection but also higher range and Doppler resolutions as compared to the conventional single as well as multicarrier radars.

Contents

List of Figures

List of Tables

Abbreviations

2-D	2-Dimension
3-D	3- Dimension
8PSK	8-Phase Shift Keying
ACF	Autocorrelation Function
AF	Ambiguity Function
ATC	Air Traffic Control
BPSK	Binary Phase Shift Keying
CAN	Cyclic Algorithms - New
CCDF	Complementary Cumulative Distribution Function
CDMA	Code Division Multiple Access
CP	Cyclic Prefix
CW	Continuous Wave
dB	Decibel
DFT	Discrete Fourier Transform
DFT-S-OFDM	Discrete Fourier Transform Spread OFDM
DOA	Direction of Arrival
DS-CDMA	Direct-Sequence Code Division Multiple Access
EM	Electromagnetic
FFT	Fast Fourier Transform
FMCW	Frequency-Modulated Continuous Wave
GHz	Gigahertz
HPA	High Power Amplifier
IDFT	Inverse Discrete Fourier Transform
IFFT	Inverse Fast Fourier Transform

ISC-FDMA	Interleaved SC-FDMA
LFM	Linear Frequency Modulation
LOS	Line-of-Sight
LSC-FDMA	Localized SC-FDMA
LTE	Long-Term Evolution
MCPC	Multicarrier Phase-Coded
MHz	Megahertz
MIMO	Multi-Input and Multi-Output
Msps	Mega samples per second
OFDM	Orthogonal Frequency Division Multiplexing
PAM	Pulse Amplitude Modulation
PAPR	Peak-to-Average Power Ratio
PMEPR	Peak-to-Mean Envelope Power Ratio
PN	Pseudo-Noise
PNLFM	Piecewise Nonlinear Frequency Modulated
PRF	Pulse Repetition Frequency
PRI	Pulse Repetition Interval
PRN	Pseudo Random Number
Prob	Probability
PSLR	Peak-to-Sidelobe Ratio
PWCIA	Periodic correlation Weighted Cyclic Iteration Algorithm
QPSK	Quadrature Phase Shift Keying
Rad-Comm	Radar-Communications
Radar	Radio Detection and Ranging
RCS	Radar Cross-Section
SAR	Synthetic Aperture Radar
SC-CFDMA	Single Carrier Code-Frequency Division Multiple Access
SC-FDMA	Single-Carrier Frequency Division Multiple Access
SISO	Single-Input and Single-Output
SNR	Signal-to-Noise Ratio
STAP	Space-Time Adaptive Processing

WeCAN	Weighted-CAN

Symbols

$*$	Complex conjugate
α	Gain constant
σ	Radar Cross Section
τ	Delay shift
B	Bandwidth
c	Speed of light in free space
f_c	Carrier frequency
f_d	Doppler frequency
f_{PRF}	Pulse repetition frequency
Δf_d	Doppler frequency resolution
$h(t)$	Impulse response of the matched filter
K	Bandwidth spreading factor
n	Source symbol index
N	Number of input data symbols
m	Subcarrier index
M	Number of subcarriers
r	Initial sequence number of the source symbol
R	Range of a target
R_{ch}	Channel transmission rate
R_{sr}	Source symbol rate
$\triangle R$	Target range resolution
t_o	Time delay of the received pulse
T	Pulse width

T_s	Chip rate
v	Radial speed of a target
$x(t)$	Transmitted source signal
$\tilde{x}(t)$	Received source signal
x_n	Transmitted source data symbols
$\tilde{x}_n$	Received source data symbol
X_q	Frequency domainsource symbols
$\widetilde{X}_q$	Frequency domain demapped source symbols
$y(t)$	Baseband transmitted signal
$y_c(t)$	Complex passband transmitted signal
Y_l	Frequency domain mapped symbols
$\widetilde{Y}_l$	Received frequency domain symbols
y_m	Transmitted SC-FDMA symbols
$\tilde{y}_m$	Received SC-FDMA symbols

Chapter 1

Introduction

Radar is a remote sensing system that uses electromagnetic waves to detect and locate different reflecting objects such as aircrafts, spacecrafts, missiles, vehicles, ships, and even the natural environment. In this chapter, a brief history and applications of radar are given along with the basic radar functions and salient target parameters, the concept of pulse compression, and types of radar waveforms. The chapter also includes radar waveform performance metrics, research objectives, and the organization of the thesis.

1.1 A Brief History of Radar and its Applications

The term radar was devised by the US Navy in 1940 as an acronym of Radio Detection and Ranging. Radar was first developed in 1930s for the defense applications and since then it has been used to aid in the detection of targets of interest [1]. It has its use in multiple disciplines, ranging from micro-scale radar applications in biomedical engineering to macro-level uses in radio astronomy [2–5]. The major application of radar is the detection of moving targets and parameter estimation [2]. In the military, it is additionally used for weapon guidance and fire control. The basic use of today's Radar is to perform parameter estimation of any desired target. The significant target parameters include range, velocity, acceleration, angle, and radar cross section (RCS).

Radars are classified into many categories on the basis of specific characteristics regarding waveform type, frequency band, number of antennas, antenna configuration, and signal processing specifications. These include monostatic, bistatic, pulsed, pulse-Doppler, continuous wave, and FMCW radars. Radars are also classified based on their mission type and applications such as search radar, tracking radar, early warning radar, weather radar, air traffic control (ATC) radars, synthetic aperture radar (SAR), fire control radar, track-while-scan radar and over-the-horizon radar.

Radars are divided into two main categories depending on the type of their waveform; continuous wave (CW) and pulsed or pulse-Doppler radars. A continuous-wave radar transmits energy continuously in the form of a constant frequency signal. After reflecting from a remote moving object, there is a shift in the frequency of the signal, known as Doppler shift. The radar detects the speed of the moving object on the basis of this Doppler shift. In contrast to CW radar, a pulsed radar transmits energy for short periods of time known as pulses. The radars generate pulses with or without some form of modulation such as frequency, amplitude, and phase modulation. Fig.1.1 shows a pulsed-radar that consists of time control, transmitter, receiver, duplexer and signal processing blocks. During the time between two subsequent pulses, the transmitter is in Off state while the receiver is active so that any signal reflected by a target can be detected. Fig.1.2 shows a pulsed-radar transmitted and a received signal scattered by a target.

Based on their antenna configuration, radars are divided into two categories, namely single antenna and multiple antenna radars. Multiple antennas are usually in the form of arrays. Array antenna radars are further categorized into phased array and multi input and multi output (MIMO) radars. Array antennas are used in radars, based upon the idea that signals can be coherently processed. The array antenna is used at the transmitter to steer the beam in a particular direction. At

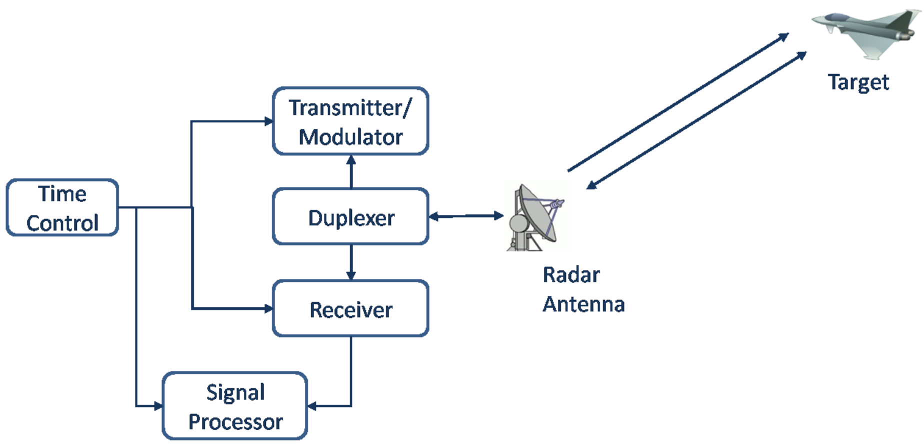

FIGURE 1.1: A pulsed-radar block diagram with monostatic configuration

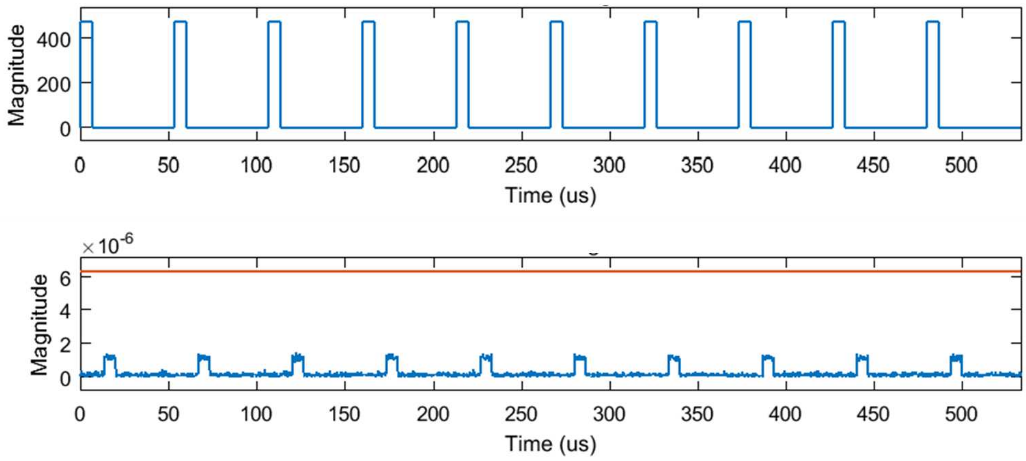

FIGURE 1.2: Pulsed radar signal (a) Transmitted signal (b) Received signal reflected by a target

the receiver, the receiving array forms a beam in space providing array gain. The corresponding radar is known as a phased-array radar [6–11]. Phased array radars have got much attention due to their multi-function applicability and use as shipboard, airborne, and land-based [12]. The other category of radars, based upon antenna configuration, is MIMO radars. MIMO radar is a promising technology that has received increased attention from researchers and radar engineering professionals in recent years. In contrast with a standard phased array radar that transmits scaled versions of a single waveform, a MIMO radar can transmit multiple signals independent from each other [5, 13, 14]. The MIMO radars can be classified into two categories based on the antenna distribution; widely separated antennas also known as multi-static MIMO [6] and collocated antennas also known as monostatic MIMO [7][15]. Each distribution has its own merits and demerits [8]. MIMO radars provide higher resolution, higher sensitivity for detection of moving objects [9], a better capability to identify the maximum number of targets distinctively, as compared to traditional radars. This waveform diversity enables the superiority of MIMO radar over the performance of a standard phased array radar.

Present-day radars are more sophisticated and can provide more information about its target such as its size, shape, motion type, and trajectory. Radar signals are designed to improve the target detectability, range resolution, velocity resolution, and discrimination between different objects (especially in the presence of heavy clutter).

Designing a radar waveform that complies with all these requisites, is a challenging task as it involves multiple analytical and practical trade-offs. For example the range resolution and target detectability in pulsed radars are usually coupled in an inverse relationship. Pulse compression has been proposed as a possible solution to this conundrum. Existing single-carrier and multicarrier pulse compression waveforms, on the other hand, suffer from a number of setbacks that result in undesirable trade-offs. One such waveform that belongs to the family of multicarrier waveforms is OFDM (Orthogonal Frequency Division Multiplexing) waveform. OFDM is a spread spectrum technique in which the digital data symbols are multiplexed over multiple carrier frequencies which are orthogonal to each other. OFDM waveform is widely used in MIMO radars to achieve high resolution in the measurement of the target range, speed, and direction. However, OFDM is also used independently as a pulse compression technique [16]. OFDM being a multicarrier radar system, not only provides improved range resolution and spectral efficiency but also offers frequency diversity to the radar system. OFDM Radar provides a range of performance improvements in the radar system as compared to the conventional radars including better discrimination between clutter and moving targets. However, OFDM exhibits few weaknesses like high peak-to-average power ratio (PAPR), and frequency offsets for non-synchronized channels.

1.2 Basic Radar Functions and Salient Target Parameters

The basic radar functions are target detection, parameter estimation, and target tracking or imaging. For these function the salient target parameters are: radar cross-section (RCS), range, range resolution, speed, and speed resolution.

1.2.1 Target RCS

A target can be characterized by its radar cross-section (RCS). In general, there is no simple way to compute RCS. It can be defined, as given in [17], as

$$\sigma = \frac{\text{power reradiated towards the source per unit solid angle}}{\text{incident power density}/4\pi} \tag{1.1}$$

The unit for RCS is m^2. In general, the RCS of an object depends upon its orientation relative to the line-of-sight (LOS). Most of the targets are not just simple mathematical shapes. Targets like airplanes are comprised of multiple different shapes in different orientations. Further, when a moving target shifts its position relative to the radar, the orientations of various shapes change considerably. Consequently, a general plot of target RCS versus its orientation relative to LOS is very complicated. If the airplane is moving towards the radar, its orientation with respect to the radar will change continuously.

The fluctuations in the RCS are characterized by different Swerling models developed by Peter Swerling [18]. These models are the statistical representation of the changes in the orientation of the targets relative to its motion. Table

1.1 provides the description of different Swerling models regarding target RCS fluctuations.

Target model	Description
Swerling Case 0	Non-fluctuating target; usually a spherical structure that have constant RCS for all dimensions
Swerling Case I	RCS fluctuates slowly over time and changes on a scan-to-scan basis; Complex targets (targets have a large amount of surfaces, many independent scatterers of roughly equal areas, RCS with two degrees of freedom)
Swerling Case II	RCS fluctuates rapidly over time and changes on a pulse-to-pulse basis; Complex targets; (targets have a large amount of surfaces, many independent scatterers of roughly equal areas, RCS with two degrees of freedom)
Swerling Case III	RCS fluctuates slowly over time, RCS changes on a scan-to-scan basis; Simple targets (A dominant isotropic reflector, comprised of many small reflectors, RCS with four degrees of freedom)
Swerling Case IV	RCS fluctuates rapidly over time; RCS changes on a pulse-to-pulse basis; Simple targets (A dominant isotropic reflector, comprised of many small reflectors, RCS with four degrees of freedom))

TABLE 1.1: RCS Swerling Models for diverse range of targets

1.2.2 Target Detection

Target detection is one of the most important functions that has been widely used in radars. Detection is performed on the received signal to determine whether target information is present in it or not. For a received signal under test, a genuine target echo is detected as a peak in the signal. The radar signal processor discriminates the target echo from noise and clutter. For a received signal, a threshold is set to detect the presence of a target. If the signal strength is less than the threshold, then the radar will miss the target that is called a *target miss*. If a threshold is set too low to avoid a target miss then it is possible that a random noise signal crosses the threshold, which results in an erroneous target detection decision. This is known as a *false alarm* [19]. Therefore an optimal threshold is selected very carefully so that it avoids a false alarm and a target miss, simultaneously [20].

1.2.3 Target Range

The range of a target is computed by estimating the time delay t_o, i.e. the time that a pulse takes to travel the two-way path between the radar and the target [21]. When a radar receives an echo of a target, the delay of the received pulse is characterized as the range of the target. The relation between the time delay and the radial distance between the radar and the target is given as:

$$R = \frac{ct_o}{2} \tag{1.2}$$

where c is the speed of light in the free space, R is the radial distance or the range of the target, t_o is the time delay of the received pulse, and 2 in the denominator compensates for the two-way travel of the radar pulse.

1.2.4 Target Range Resolution

Range resolution of a target is another important parameter, linked to radar performance. It is the capability of a radar to resolve a target along the range axis. Range resolution depends upon the pulse width of a pulsed radar and is given by.

$$\triangle R = c\frac{T}{2} \tag{1.3}$$

where T is the pulse width of the radar.

1.2.5 Target Speed

For a moving object, the relative motion between the radar and the object results in the change in the carrier frequency of the transmitted signal referred to as the

Doppler shift. Estimation of the Doppler frequency gives the relative radial speed of a moving object by using the following relation.

$$f_d = \pm\frac{2v}{\lambda} = \frac{2f_c v}{c} \tag{1.4}$$

where f_d is the Doppler frequency, v is the radial speed, f_c is the carrier frequency, and λ is the wavelength of the carrier frequency. Since the Doppler shift affects the incident wave on the moving object as well as the reflected wave therefore the change in the frequency is twice as compared to that of a moving object emitting a wave. The positive or negative Doppler shift corresponds to the target, moving towards or moving away from the radar respectively.

The Doppler shift in the carrier frequency of the transmitted signal is estimated by performing pulse-Doppler processing [21] that is explained in detail in chapter 3.

1.2.6 Target Speed Resolution

Speed resolution of a target is linked inversely with the ambiguity in the measurement of Doppler shift. The ambiguity in Doppler measurement depends upon the number of pulses that a radar integrates to estimate the Doppler shift in the frequency. The ambiguity decreases with the increased number of integrated pulses and hence the speed resolution increases.

1.3 Radar Waveform and Pulse Compression

A pulsed-radar transmits energy in a repetitive train of short duration pulses by using a single antenna for transmitting and receiving signals with the help of a duplexer. The range resolution of a pulsed-radar depends upon the duration of the pulse in a pulse modulated fixed frequency signal. To improve the range resolution the width of the transmitted pulse is shortened. This reduction in pulse width costs the radar with increased bandwidth.

$$\triangle R \approx \frac{c}{2B} \tag{1.5}$$

where $\triangle R$ is the range resolution and B is the bandwidth of the signal.

The detection probability increases with the increase in pulse transmit energy. That can be achieved by transmitting pulses with long duration or with very high peak power but a radar usually transmits pulses close to its peak power limitation. For a rectangular pulse, the duration of the radar transmitted waveform and the processed echo is effectively the same. Thus range resolution and target detectability (energy in the pulse) is coupled in an inverse relationship. The solution to this perplexity of pulse duration is provided in the form of pulse compression.

The idea of pulse compression evolved in the late 50s and early 60s [22]. The idea behind pulse compression was to use long duration pulses with increased bandwidth so that high range resolution of short duration pulses and high detection energy of long duration pulses are achieved simultaneously with the same pulse. The use of pulse compression techniques enables decoupling of pulse duration from its pulse energy by creating different time durations of the transmitted pulse and processed echo [23, 24].

We categorize pulsed-radar waveforms into single-carrier and multicarrier. The single-carrier waveforms uses a single carrier frequency to transmit pulses with or without any form of modulation such as frequency, amplitude and phase. Whereas multicarrier wavefroms use multiple carrier frequencies to transmit the pulsed signals. A brief description of these wavefroms is given in section 1.5.

1.4 Radar Waveform Performance Metrics

In general, the metrics that are used for the performance analysis of the radar waveforms, are ambiguity function, waveform correlation properties, and the peak-to-average power ratio (PAPR). The detailed description of these metrics are given in their respective chapters, however, a brief introduction is given in this section.

1.4.1 Ambiguity Function

Ambiguity function (AF) is a two-dimensional correlation between a transmitted signal and its time-delayed and frequency-shifted version [25–27]. The time delay refers to as range resolution and frequency shift refers to as the speed resolution of the moving target. In another interpretation [28, 29], the AF is a two-dimension point spread function. Ambiguity function (AF) is an analytical tool that is useful for designing a waveform and analyzing its behavior coupled with its matched filter [30, 31] . It has been used as a performance tool for studying the effects and performance of different radar waveforms [32]. Ambiguity function is important when choosing a waveform in any radar as it helps to analyze the characteristics of the waveform [33, 34]. Radar designers usually use the ambiguity function to evaluate the performance of a waveform in terms of range and Doppler resolutions. AF does not depend upon any specific target scenario despite it is determined by pulse waveform specifications and the matched filter [21]. Fig.1.3 shows a normalized ambiguity function diagram for a Barker code of length 11.

1.4.2 Waveform Correlation Properties

1.4.2.1 Autocorrelation

For many radar applications, good auto-correlation properties of a waveform are required. Good auto-correlation means a waveform being transmitted is uncorrelated to the time-shifted versions of itself. If a transmitted waveform

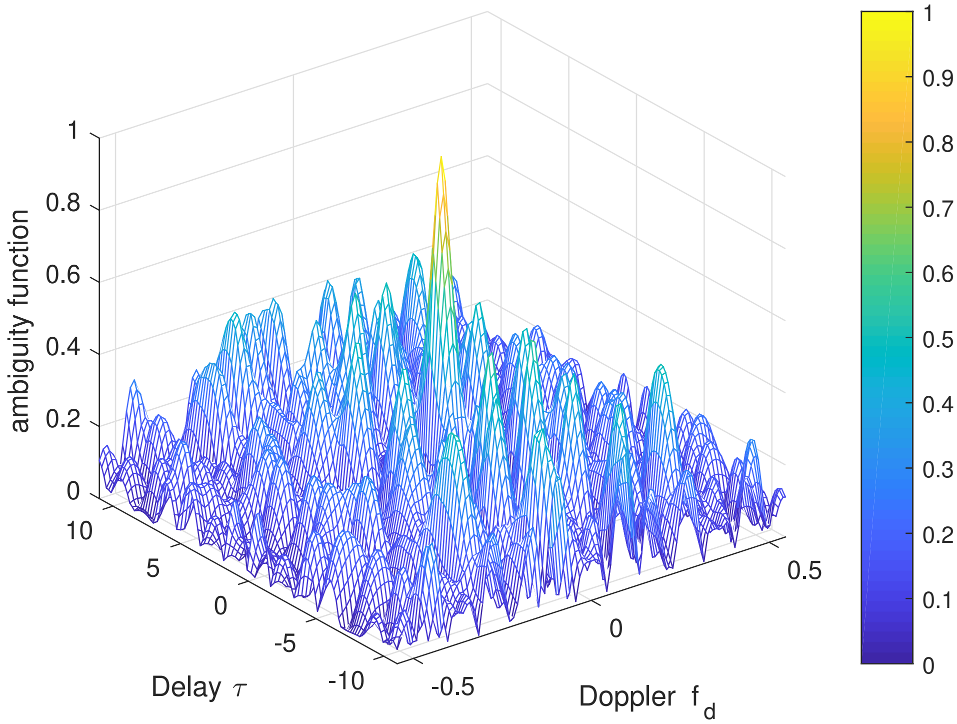

(a)

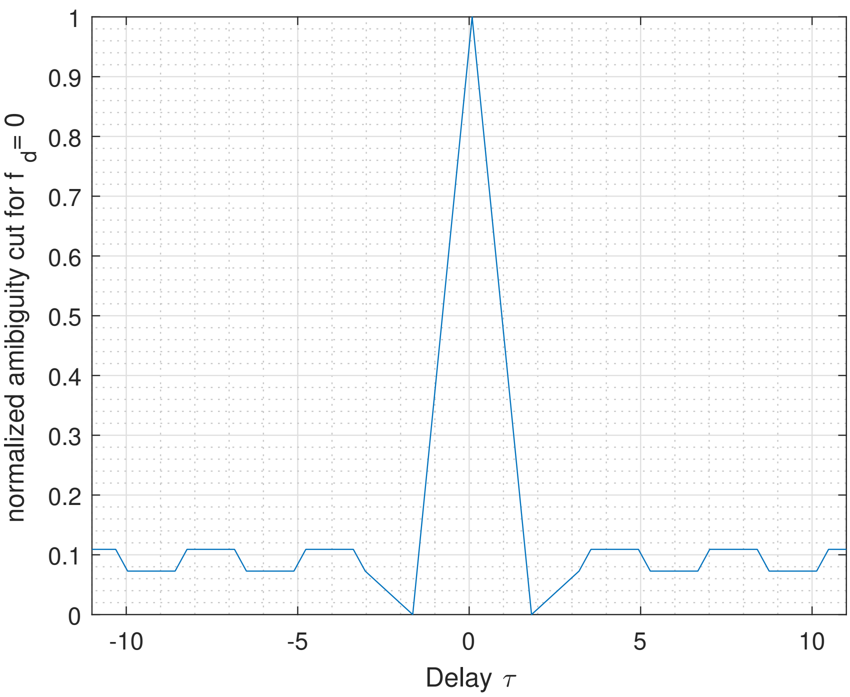

(b)

FIGURE 1.3: (a) Normalized Ambiguity Function and (b) Zero Doppler cut of Ambiguity Function for Barker Code for $N = 11$.

possesses strong auto-correlation properties then the matched filter at the receiving end collects the backscattered signal for a specified range bin and attenuates the backscattered signals from other range bins [21].

1.4.2.2 Peak-to-Sidelobe Ratio

Peak-to-sidelobe ratio (PSLR) is a significant parameter in an auto or cross-correlated signal while analyzing a radar waveform. It is defined as the ratio of the most prominent sidelobe peak intensity to the mainlobe peak intensity in a correlated signal.

1.4.3 Peak-to-Average Power Ratio

The measure of the envelope variations in a given transmitting signal is known as Peak-to-Average Power Ratio (PAPR). It is the ratio of the instantaneous peak power to the average signal power. The high PAPR in the transmitting signal causes serious issues by producing signal excursions into the nonlinear operation region of the transmitter amplifier that results in nonlinear distortions leading to inter-carrier interference and spectral spreading [35]. High PAPR in the transmitting signal degrades the performance of the overall system. Therefore it is necessary to reduce PAPR in such Radar waveforms or selecting such a waveform that provides negligible PAPR.

1.5 Notable Radar Waveforms

As mentioned earlier in section 1.3, we divided the radar waveforms into two categories i.e. single-carrier waveforms and multicarrier waveforms. A brief description of these waveforms is given below.

1.5.1 Single-Carrier Radar Waveforms

Various single-carrier waveforms are used for different radar applications. The following are some notable single-carrier radar waveforms.

1.5.1.1 Rectangular Pulse

A rectangular wave is used in pulsed radars to generate a pulsed signal, also known as pulse amplitude modulation (PAM) signal. It is used to pulse-modulate the constant frequency carrier to produce the radar signal generator output. It is defined as

$$x(t) = a(t)\sin(\omega t) \qquad a(t) = \begin{cases} 1 & 0 \leq t \leq T \\ 0 & \text{otherwise} \end{cases} \tag{1.6}$$

where T is the duration of the pulse also known as pulse width and ω is the carrier frequency of the passband signal.

The complex envelope of a constant-frequency pulsed radar signal is given by

$$x(t) = \frac{1}{\sqrt{T}}\text{Rect}\left(\frac{t}{T}\right) \tag{1.7}$$

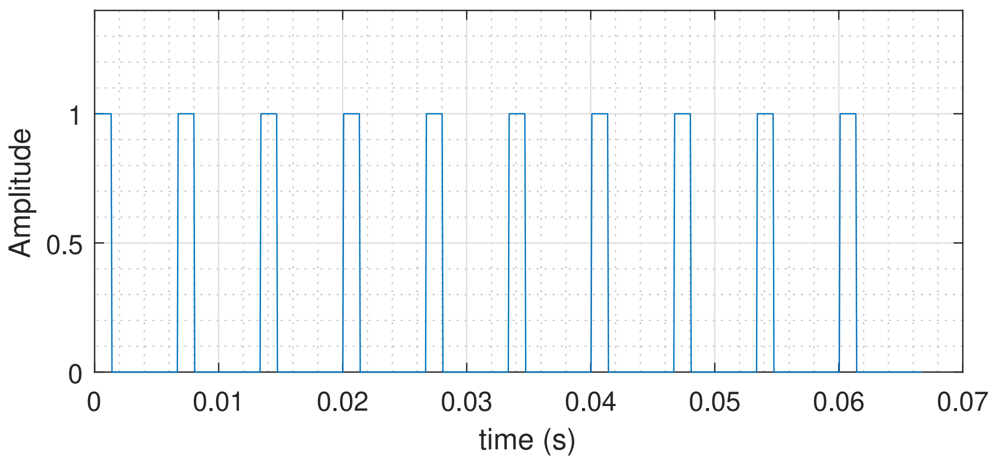

FIGURE 1.4: Rectangular wave pulse train

Fig.1.4 shows a pulse train of rectangular pulses. The repetition time interval of each pulse is constant and is known as the pulse repetition interval.

1.5.1.2 Linear Frequency Modulation (LFM)

LFM is a type of modulation that employs a linear sweep in instantaneous carrier frequency over a desired bandwidth during the pulse duration [36]. LFM is also referred to as the chirp signal. It employs a continuous quadratic phase shift on the transmitted pulse during the pulse interval. The transmitted signal of an LFM pulse compression radar consists of a rectangular pulse with a fixed amplitude. The frequency varies linearly throughout the pulse duration. On reception of the echo of an LFM signal the received signal is passed through a pulse compression filter. The output is the autocorrelation of the modulated pulse. The peak power of the autocorrelation output signal is dependent upon the pulse compression ratio. It increases with the increase in the compression ratio. If the frequency of the signal increases along the pulse duration, the chirp signal is up chirp and otherwise is known as down chirp [37].

A linear frequency modulated signal $x(t)$ is described as

$$x(t) = \frac{1}{\sqrt{T}}\mathrm{Rect}\left(\frac{t}{T}\right)\exp(j2\pi\mu t^2) \tag{1.8}$$

where T is the pulse width and μ is the LFM coefficient with bandwidth B, given as

$$\mu = \pm\frac{B}{T} \tag{1.9}$$

The positive or negative sign in the selection of α stands for the up or the down chirp of the LFM signal. Fig.1.5 shows an LFM pulse along with its frequency domain signal which is approximately rectangular in shape.

LFM pulse provides a very high range and Doppler resolution. Ambiguity function is used as a tool for the realization of range and Doppler resolution. The ambiguity function of the LFM pulse will be discussed in detail in chapter 4.

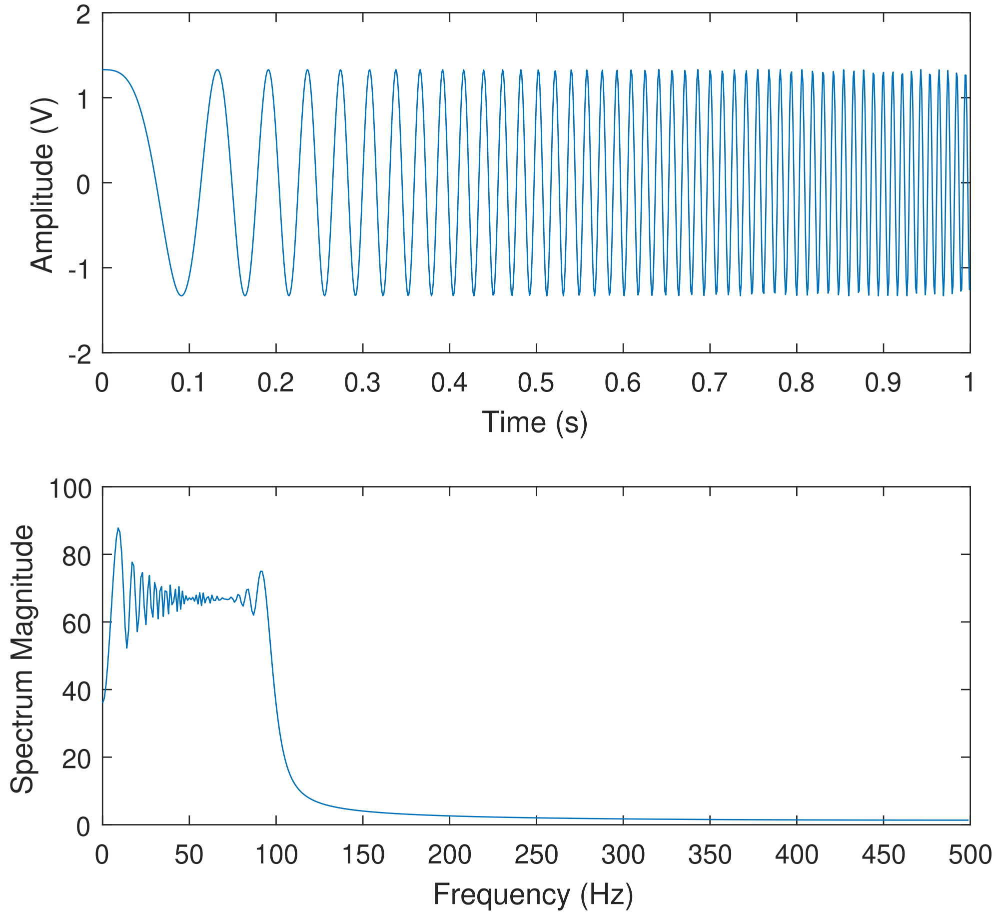

FIGURE 1.5: Linear frequency modulated pulse waveform with initial frequency $f_1 = 1$ Hz and final frequency $f_2 = 100$ Hz (a) Time domain signal (b) Spectrum (an approximately rectangular shape within the bandwidth).

1.5.1.3 Phase-Coded Pulse

In phase coding, each pulse is divided into sub-segments equally and each segment is encoded separately with a different phase. It is well known that the time rate of change of phase is referred to as frequency. Therefore phase coding involves bandwidth increase and hence increases the range resolution of the target. One of its example is Barker code which is a binary phase coding technique and is the simplest one [38]. More than two phases are also used in phase coding refer to as polyphase codes and their examples are Frank code [39, 40], Zadoff-Chu code, and Px codes [41, 42]. Fig.1.6 shows Zadoff-Chu (Poly Phase) pulse compression waveform with 20 number of chips and each chip has 5 μs chip width.

On the other hand Barker codes are the simplest binary phase codes designed to yield a peak to peak sidelobe ratio equal to N for a pulse with N sub-segments. There are only seven known Barker codes with $N = \{2, 3, 4, 5, 7, 11, 13\}$ given in Table 1.2.

Code Length	Code Values	Sidelobe Reduction (dB)
2	10 or 11	6.0
3	110	9.5
4	1110 or 1101	12.0
5	11101	14.0
7	1110010	16.9
11	11100010010	20.8
13	1111100110101	22.3

TABLE 1.2: List of binary Barker codes

1.5.1.4 CDMA Radar Waveform

Code Division Multiple Access (CDMA) is a spread spectrum technique that has been used to generate radar signals for target detection and ranging [43] and vehicle to vehicle communication [44]. A CDMA based Radar for collision avoidance in automobiles was proposed in [45]. However, CDMA Radar does not offer the level of control on the spectral properties as does the OFDM based radar.

1.5.2 Multicarrier and OFDM Radar Signals

The concept of Multicarrier signals was introduced by Levanon for radar applications [16]. The previously used phase-coded waveforms which are basically single-carrier waveforms have some drawbacks. The main drawback is the Sinc i.e. $\sin x/x$ shape of the frequency spectrum, imposing higher out-of-band interference and losses. Multicarrier radar signals ware generated by using phase-coded sequences. These signals known as multicarrier phase-coded (MCPC) exhibited

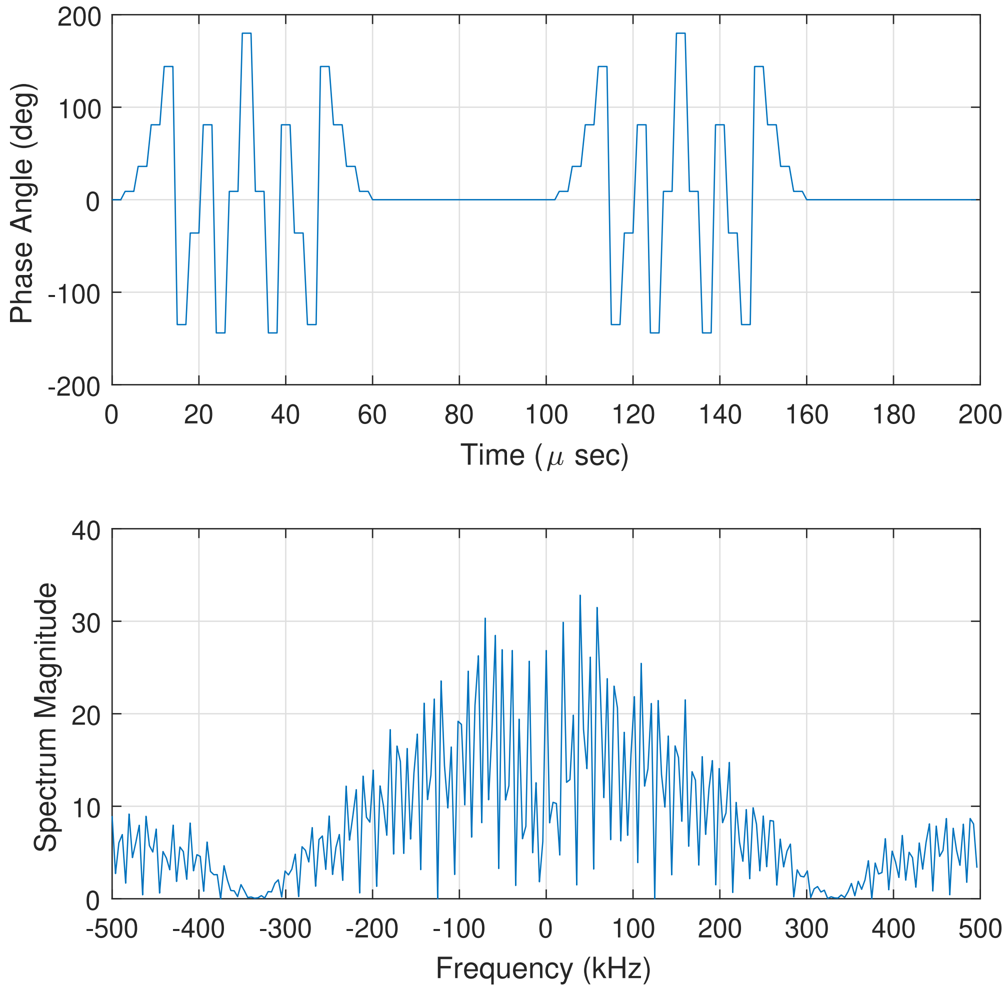

FIGURE 1.6: Zadoff-Chu Code (Poly Phase) pulse compression waveform with number of chips = 20 and chip width = 5 μs . (a) phase angle variations along the time axis (b) Frequency domain signal (spectrum is not regular)

the advantage of relatively lower PAPR, lower autocorrelation function (ACF) sidelobes, and simultaneously have a higher frequency spectrum efficiency than that of the single carrier waveform signals.

Orthogonal Frequency Division Multiplexing (OFDM) is a form of the multicarrier signal in which the use of phase coded sequence was proposed by Levanon *et al.* in [16, 46]. OFDM is a spread spectrum technique in which the digital data symbols are multiplexed over multiple carrier frequencies which are orthogonal to each other. Fig.1.7 shows the consecutive OFDM subcarriers which are orthogonal to each other. In radars, OFDM was proposed as a pulse compression technique

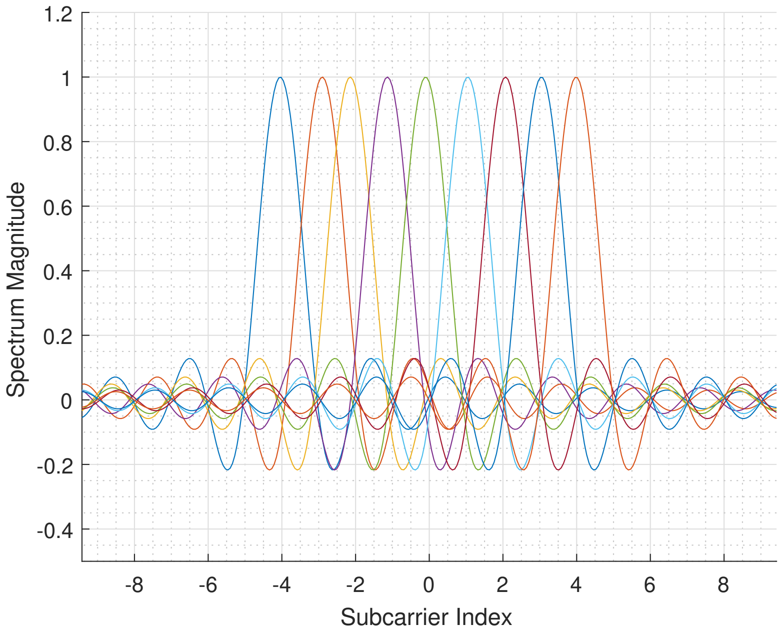

FIGURE 1.7: Consecutive OFDM Subcarriers

for waveform generation. OFDM being a multicarrier radar system, not only offers improved range resolution and spectral efficiency but also provides frequency diversity to the radar system [47]. OFDM Radar provides a range of performance improvement over the conventional radar systems including better discrimination between clutter and moving targets.

The OFDM signal is created by multiplexing the data on a set of subcarriers that are orthogonal to each other. OFDM places data on these narrowband subcarriers with effectively using Inverse Fast Fourier Transform (IFFT). Data on these subcarriers are transmitted in parallel. Each subcarrier contains an integer number of cycles over the symbol duration. A block of redundant data referred to as cyclic prefix is added between symbols in the time domain as guard interval to battle the adverse channel conditions. Fig.1.8 shows the OFDM radar block diagram displaying each block of the radar transmitter and receiver. The phase and amplitudes of OFDM subcarriers carry the information [48]. Each of the subcarriers may carry information (phase and amplitude) independent from other subcarriers. Therefore, the spectrum can be controlled as per our requirement.

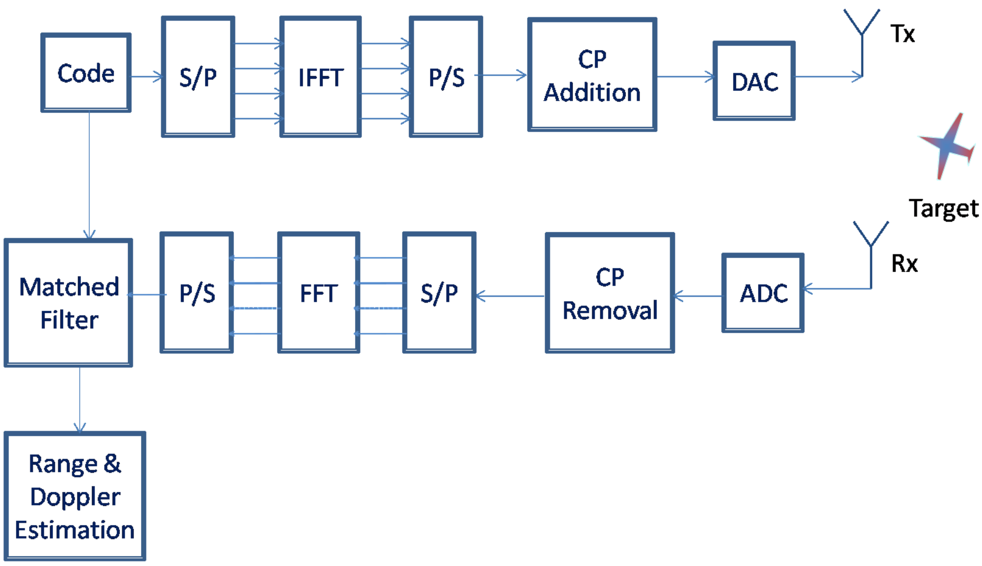

FIGURE 1.8: OFDM radar block diagram

For an OFDM symbol, the frequency spacing between each subcarrier is given as

$$\Delta f = \frac{B}{M} \tag{1.10}$$

where Δf is frequency spacing between two consecutive subcarriers, B is the available bandwidth, and M is the total number of OFDM subcarriers.

The time duration T of the signal will be as

$$T = \frac{1}{\Delta f} \tag{1.11}$$

In OFDM, the modulation and demodulation are performed by employing IFFT and FFT operations respectively, so these algorithms help to achieve the overall system efficiency.

1.5.2.1 Benefits of OFDM Radar

The wideband characteristics of OFDM are desirable to achieve high resolution for radar applications as narrowband subcarriers collectively make a large bandwidth signal. The remarkable structure of OFDM symbols consisting of a linear combination of narrowband subcarriers provides the opportunity to achieve frequency agility [49]. The instantaneous selection of desired subbands are digitally controllable at the transmitter end. The subcarriers can be turned ON and OFF independent from each other. That provides flexibility in the selection of subcarriers and control over the spectrum and bandwidth of the overall signal [48].

In case of external interference or jamming the frequency agility forces the jammer to spread its power over a wide bandwidth. The jammer power density is reduced when it has to transmit in a wideband with the same power for jamming a narrowband radar [49].

Another benefit of OFDM radar is its sensitivity to Doppler frequency that is caused by moving targets. Conventional pulse compression radars use Doppler matched filter banks for Doppler processing that is considered disadvantageous in search radars. OFDM radar with a multi-carrier structure compensates for the Doppler effect in the digital domain by a computationally efficient way as the frequency components (subcarriers) can be controlled in OFDM independent to each other [50].

1.5.2.2 Applications of OFDM Radar

OFDM waveform has been investigated for multiple radar applications. Few of these are given below:

1. A coexistent design of transmit and receive waveform for a joint system of radar and communications, also known as RadCom [51–80].
2. Range and Doppler processing for single and multiple moving targets [81–85].
3. Simultaneous surveillance and tracking operations including task scheduling, allocation of optimized power for different tasks, and robustness against unfavorable channel conditions [86, 87].
4. Target detection by implementing space-time adaptive processing (STAP) [88–92].

5. OFDM-MIMO radar integration [93–98] for achieving high probability of target detection and high direction of arrival (DOA) estimation accuracy [99–104].

6. Synthetic Aperture Radar (SAR) for 2-D and 3-D imaging [105–119].

1.5.2.3 Issues of OFDM Radar

In communication, the main issue of OFDM is the synchronization, which is based on the fact that the time and frequency synchronization is essential in preserving subcarrier orthogonality. However, for radars, the OFDM sensitivity to frequency and time synchronization is advantageous as the radar receiver uses pre-stored copies of the transmitted signal in the match filtering process of the received signals. We know that the OFDM signal spectrum is obtained by the summation of Sinc functions associated with each subcarrier. In the case of moving targets, the return signal is affected by the Doppler shift, resulting in a shift in the OFDM spectrum keeping a constant space between each subcarrier that is the inverse of the signal duration. However the structure of OFDM is still vulnerable to frequency offsets especially in bistatic radar configurations and airborne applications.

In radars, the major weakness of the OFDM signal is the high peak-to-average power ratio (PAPR). The OFDM signal is the sum of all modulated orthogonal subcarriers. However, for some input sequences, many subcarriers are in phase resulting in some high amplitude peaks [35]. These peaks impose a heavy load on the transmitter power amplifier. The issue of high PAPR in OFDM systems reduces the efficiency of the transmitter power amplifier and forces the amplifier to operate in the non-linear region. However, nonlinearity in the power amplifier is the imperfection that degrades the performance of frequency-division techniques. Therefore, the peak to average power ratio control is an essential task in OFDM radars.

The other weakness of OFDM is its vulnerability to spectral nulls [120]. In OFDM receivers, the detection is performed in the frequency domain and detection action is performed on each subcarrier separately which is vulnerable to spectral nulls [121].

1.6 Research Objectives

The research objectives of this research are:

- To design a radar waveform that provides all of the benefits of multicarrier waveforms such as OFDM radar and non of their weaknesses such as spectral nulls and frequency offsets.
- To achieve 0 dB PAPR and very good autocorrelation properties.
- To achieve extremely narrow mainlobe peak and lower or negligible sidelobe peaks in an ambiguity function plot for both range and Doppler as compared to the existing radar waveforms.
- To achieve high accuracy in target detection and very high range and Doppler resolutions.

1.7 Organization of the Dissertation

The rest of the dissertation is organized as below:

Chapter 2 provides the literature review and research directives in radar waveforms. The literature review leads to the gap analysis and motivation for the proposed Single Carrier-FDMA radar waveform. In the next sections the chapter includes problem statement, the research methodology, and finally the contributions of this dissertation.

Chapter 3 presents signal modeling and the complete architecture of the proposed SC-FDMA radar. The signal modeling includes the analytical expressions for the SC-FDMA transmit and receive signals. This chapter also presents the signal processing mechanism of the proposed radar in terms of target range and Doppler estimation.

Chapter 4 provides a detailed description of the Ambiguity Function (AF), the correlation properties and PAPR analysis of the proposed waveform. Initially, a generalized ambiguity function and its properties are discussed. Then a complete derivation of the analytical expression of AF and Autocorrelation function of the proposed waveform is performed in this chapter along with their plots by using the different number of initial sequences and subcarriers. For performance evaluation, the results are then compared with that of OFDM and some existing notable waveforms. In the end of this chapter, the analytical expression for the PAPR of the proposed waveform is given, the PAPR values of SC-FDMA waveforms for different initial sequences and the number of subcarriers are computed and compared with those of prominent existing waveforms.

In chapter 5, an end-to-end radar using the SC-FDMA waveform is simulated and analyzed for its performance for target detection and range and Doppler estimation and compared it with those of OFDM and LFM in the context of range and Doppler resolutions.

Finally, Chapter 6 summarizes the major achievements of the research work presented in this thesis, presents conclusion, and sets out some suggestions for potential future work.

Chapter 2

Literature Review, Gap Analysis and Problem Formulation

In this chapter, section 2.1 discusses the literature review and research directives in radar waveforms. The research work mentioned in this review includes books, journal articles, conference papers, and PhD. theses. The literature review helped to find out the gray areas in the previous research work leading us to the gap analysis given in section 2.2. In the next sections the chapter includes motivation for Single Carrier-FDMA, problem statement, the research methodology, and finally the contributions of this dissertation.

2.1 Existing Research Directives in Radar Waveforms

The fundamental task of a radar is to detect the presence of a target and to determine the target's features such as range, range resolution, Doppler, Doppler resolution, and azimuth, and elevation angles. Out of these features, the ability to resolve a target in range and speed plays a pivotal role in the detection of a target in the presence of background noise and clutter.

It is well established that the high range resolution is achieved at the cost of large bandwidth [2]. It is also evident that the detection probability increases with the increase in transmit pulse energy which can be achieved by transmitting pulses either with large duration or with high peak power. Since a radar usually transmits pulses with the available peak power within its power amplifier limitations; therefore, the only possibility to increase the transmit energy is to widen the pulse in time which results in the shortening of the bandwidth and consequently degrades range resolution. Thus the range resolution and target detectability are coupled in an inverse relationship. The solution to this perplexity of pulse energy and range resolution is the pulse compression [22–24]. As already discussed in chapter 1, the use of pulse compression enables decoupling of pulse duration from its pulse energy. LFM waveform is an example of pulse compression. LFM provides very high range resolution and solves the issue of pulse duration and pulse energy perplexity altogether [36, 37].

LFM provides good spectrum efficiency but lacks diversity at sub-pulse level. The other pulse compression technique, the phase-coding, divides each pulse into segments and these segments are then encoded independently with different phase values [38, 40, 41]. The resulting phase-coded waveforms though provide diversity at sub-pulse level but fail to achieve spectrum efficiency. Moreover, most of the pulse compressed waveforms (i.e. LFM [37] and Barker [38] etc.) also exhibit poor peak to sidelobe ratios.

Nevertheless, the issue of these tradeoffs was later addressed by N. Levanon *et al.* by proposing OFDM waveform for radar applications [16] in 2000. The authors were inspired from the work of Jankiraman *et al.* [122] in which they simultaneously used multiple subcarriers for PANDORA FMCW radar. They used 8 LFM channels each with a sweep bandwidth of 48 MHz achieving a total bandwidth of 384 MHz. The multi-carrier signal was characterized by varying amplitude. For transmission, such signals need linear amplifiers which are less efficient. Jankiraman *et al.* mostly addressed power combining and amplification issues of multicarrier signals.

OFDM had been investigated for almost two decades and was considered as a promising candidate for future radar systems. The work related to the use of OFDM as a multicarrier waveform in radars and its relevant multi-frequency applications is performed in [114, 123–130]. Advancing the work on OFDM waveform, N. Levanon *et al.* introduced a multicarrier phase-coded signal to generate a pulse train [131] using the P3 codes and managed to reduce autocorrelation sidelobes by assigning suitable weights to the carriers. Fuhr *et al.* used Software Defined Radio based experimental testbed to test OFDM Radar performance for range measurement of moving and stationary objects [132, 133].

The performance of OFDM radar was compared with that of LFM pulse radars in [134, 135] that showed promising results about the use of OFDM waveform in radars. Though LFM and OFDM waveforms were earlier treated separately for radars; however, in [136, 137], hybrid designs of OFDM and LFM waveforms were proposed. In addition, a similar approach was adopted in [138] to generate a hybrid design of multicarrier and phase-coded signals. These hybrid designs showed significant improvements in parameter estimation and high range resolution profiling. Despite the performance improvements, there were still shortcomings in the performance of these OFDM waveforms such as low peak to sidelobe ratio of its autocorrelation function. This issue was addressed by Ruggiano *et al.* who performed sidelobe suppression in multi-target environment by implementing the reiterated LMMSE-based adaptive pulse compression in OFDM Radar [139]. Although, this solution provided with the suppressed autocorrelation sidelobes; however, the cyclic iterative algorithm introduced a high computational load. Lately, the same issue was addressed by Zuo *et al.* in [140] by introducing a waveform design, which only transmits data in the sub-carriers with preferable channel quality. However, their design was flawed with a decrease in bandwidth leading to achieve a poor range resolution.

Large time-bandwidth product is considered to be useful in resolving closely-spaced targets. Wang *et al.* proposed a large time-bandwidth product for OFDM Radar in [141]. Although, they achieved good range resolution but were not able to attain uniform spectrum which results in low spectrum efficiency.

Cheng *et al.* used Direct Sequence Spread Spectrum coding and OFDM chirp waveform to design a MIMO radar and achieved large time-bandwidth product in [142]. Though their proposed waveform offered high range resolution by achieving large time-bandwidth product but their design suffered from high computational load while selecting optimum code and optimized subcarrier spacing to maintain orthogonality.

Ambiguity function is generally used when studying the performance of different radar waveforms. Optimization of ambiguity function was considered for the design of OFDM radar in [143, 144]. A solution to Doppler ambiguity for speed measurement in OFDM radars was proposed in [145].

High PAPR is usually thought to be the major factor involved in the performance degradation of OFDM radar [146]. As discussed earlier in chapter 1, the high PAPR produces signal excursions into the nonlinear region of the operation of transmitter amplifier that results in nonlinear distortions leading to inter-carrier interference and spectral spreading. It is, therefore, necessary to use linear amplifiers in the transmitters [147] which are difficult to be employed in many radars applications such as airborne and vehicular applications where power is a constraint. Therefore, the peak to average power ratio must be controlled in these systems.

In the literature, many techniques have been evolved to reduce the PAPR. We categorize these PAPR reduction techniques into two major groups for radar applications. The first group contains *Explicit PAPR reduction techniques* while the second encompasses *Implicit PAPR reduction techniques*. The explicit reduction techniques include the classical methods that have been traditionally used to reduce PAPR. These techniques are further classified into three major families i.e. signal distortion techniques, distortionless techniques, and coding techniques. Signal distortion techniques reduce PAPR at the expense of distorting the transmitted OFDM signal. These techniques include clipping [148–150], companding [151], peak cancellation [152] and peak windowing [153, 154]. However, the simplest among these techniques is the clipping method, which has usually been used for OFDM systems [155]. In this method, the peaks in the OFDM signal are deliberately clipped before amplification. Although clipping action eliminates high peaks in OFDM signals; however, this is a nonlinear process that results in inband and out-of-band interference among the subcarriers destroying the orthogonality among them. The out-of-band interference can be removed by employing iterative filtering after clipping action. This imparts additional complexity to the radar system.

Distortionless approaches maintain orthogonality between subcarriers and make it possible for the radar to process each subcarrier independently. One of such approaches is the tone reservation method [156]; however, it only reduces the peaks while ignoring the structure of the rest of the wave that is also littered with envelope fluctuations. The other distortionless techniques include selective mapping [157], partial transmit sequence [158], interleaved OFDM [159, 160], Interleaved Spread Spectrum OFDM [161], tone injection [156], active constellation extension [162], constrained constellation shaping [163] and Partial Transmit Sequence (PTS) approach based upon adaptive particle swarm optimization [164]. All of these techniques add up redundancy in the transmitted signal increasing overhead to the transmitted signal and hence extending the complexity of the overall system.

The third family of Explicit PAPR reduction techniques, i.e. the coding technique, works on the principle of selecting appropriate codewords to reduce PAPR in the OFDM radar signals [165]. Examples include Linear Block Coding [166], Golay sequences [167], and Turbo coding [168]. However, these coding techniques show better performance only at the cost of coding rate and high computational load.

Implicit PAPR reduction techniques are based on waveform designs that achieve high performance in target detection and parameter estimation while providing very low PAPR. One such waveform design, proposed by Zhao *et al.* [169], referred to as piecewise nonlinear frequency modulated (PNLFM) waveform, exhibited good auto-correlation properties. This waveform design provided a high degree of freedom, achieving high range resolution and low PAPR up to 3dB. Although this PAPR value was small though still was not 0 dB. In [170], the authors used phase and amplitude weighted carriers to reduce the Peak-to-Mean Envelope Power Ratio (PMEPR) and peak sidelobe levels in the region around the mainlobe peak. Their proposed approach was flawed with the lower bandwidth efficiency and high correlation sidelobes. Balal *et al.,* in their work in [171], addressed the Peak-to-Mean Envelope Power Ratio issue and proposed a solution for it by generating constant envelope OFDM. Nevertheless, meanwhile, some other implicit PAPR reduction techniques with constant envelope were also reported in the literature, that provided 0dB PAPR, such as Cyclic Algorithms - New (CAN), Weighted-CAN (WeCAN) [172, 173], and Periodic correlation Weighted Cyclic Iteration Algorithm (PWCIA) [174]. However, the operation of these cyclic waveform design algorithms is iterative in nature that not only enhances the complexity of the radar system but also increases its computational load. In addition, the selection of suitable weights for the improvement of Peak-to-Sidelobe Ratio (PSLR) [172, 174] aggravates this issue further. In a similar work, proposed by Mietzner [29], they used DFT-Spreaded OFDM waveform for radar application to reduce PAPR or crest factor. Their proposed waveform, however, suffered from energy leakage into range sidelobes. This leakage entails a certain power penalty regarding the mainlobe of the ambiguity function and turns out to cause blurred target images. In nutshell, none of the above-mentioned PAPR reduction techniques is exempted from setbacks. Moreover, the OFDM systems even after using these PAPR reduction techniques are still vulnerable to frequency offsets due to their multicarrier structure.

2.2 Gap Analysis

The grey areas in the existing research work are listed in Table 2.1. As discussed earlier, the rectangular pulse or PAM signal suffers from the pulse energy and the range resolution perplexity. In order to address this issue, the bandwidth of the radar signal needs to be increased in such a way that its energy is not compromised. This increase in bandwidth, thus, results in improved detection probability, high range estimation accuracy, increased range resolution, increased radar's covertness, reduced effects of active and passive interference, and improved radar immunity to external narrowband electromagnetic (EM) radiation effects.

The most common method to increase the bandwidth of a radar signal, as already discussed, is pulse compression that includes LFM, phase-coding, and CDMA in the case of single carrier and OFDM in the case of multicarrier radar systems. LFM waveform has good spectral efficiency but lacks the sub-pulse level diversity whereas the phase-coded compression offers diversity at sub-pulse level but fails to achieve spectral efficiency as its resulting spread spectrum is not effectively rectangular due to abrupt changes in the phase. Likewise, CDMA does not provide control over spectral properties of the signal and OFDM possesses inherited weaknesses, such as the high peak-to-average power ratio (PAPR) and its vulnerability to spectral nulls.

As reported earlier, in the literature, many techniques categorized into *Explicit* and *Implicit* techniques, have been used to reduce the PAPR. Explicit techniques are sub-categorized into three major families i.e. signal distortion techniques, distortionless techniques, and coding techniques. Though these techniques reduce PAPR but at the expense of some performance degradation of the waveforms. The signal distortion techniques reduce PAPR at the expense of distorting the transmitted OFDM signal resulting in inband and out-of-band interference among the subcarriers destroying their orthogonality. The distortionless approaches maintain orthogonality between subcarriers but these techniques add redundancy in the transmitted signal and increase the complexity of the system. The coding techniques impose high computation load on the system to search the suitable codewords. The Implicit techniques include designing and/or selection of a waveform that has an inherent capability to reduce PAPR. The waveforms that fall in this category reduce PAPR effectively but do not exhibit good autocorreleation properties.

Due to the shortcomings of previously utilized radar waveforms, we have come to the conclusion that a robust waveform is required, with all of the benefits of the existing waveforms and none of the flaws. Therefore, research needs to be carried out in order to explore more favourable waveform designs that not only provide the benefits of the previously mentioned waveforms but also do not suffer from the above mentioned issues.

2.3 Motivation for SC-FDMA Radar

The gap analysis presented in the previous section leads the authors to a conclusion that the existing waveforms cannot be modified further for significant improvements in terms of waveform resilience, radar covertness, target detection, parameter estimation and PAPR reduction. This motivates the authors to explore some other waveform design such as SC-FDMA for its use as a radar waveform (also known as DFT-Spreaded OFDM or Linearly Pre-coded OFDM) instead of previously used single and multicarrier waveforms. Therefore, before moving towards the problem formulation, we come up with the idea of suggesting Single-carrier Frequency Division Multiple Access (SC-FDMA), as a strong candidate for multicarrier radar signaling.

SC-FDMA exploits not only the benefits of single carrier modulation schemes but also embraces the blessings of the multicarrier modulation techniques. It has been in use in the uplink of LTE cellular communication systems due to its intrinsic properties of no inter-channel interference, in addition to all those possessed by OFDM. Since its advent, it has not only been regarded as a more robust technique in terms of PAPR characteristics as compared to its other multicarrier competitors but has also been considered more resilient to frequency offsets [120, 175]. Due to its wideband characteristics, it is less sensitive to frequency selective fading as compared to OFDM, which transmits symbols in relatively narrow sub-bands if the same number of subcarriers are considered [121].

SN	Research topics			References	Issues
1	Pulse Amplitude Modulation			[1, 2]	• Low detection probability • Range resolution and pulse-energy perplexity
2	LFM			[36, 37]	• Lack of sub-pulse level diversity • Low PSLR
3	Phase-coded			[38, 40, 41]	• Less spectrum efficiency
4	CDMA			[43–45]	• Lack of control on the spectral properties
5	OFDM			[16, 46, 131] [114, 123–127, 146, 170, 176]	• High PAPR • Low PSLR
6	PAPR Reduction	Explicit techniques	Signal distortion techniques	[48, 148, 151–153, 155, 177]	• In and out-of-band interference
			Distortionless techniques	[156–163]	• Added up redundancy • Enhanced complexity
			Coding Techniques	[48, 178]	• High computational load
		Implicit techniques	Waveform selection/ Design	[169–174, 179, 180]	• Low PSLR

Table 2.1: Research gap analysis

In SC-FDMA, DFT and IDFT operations are performed a prior and a posterior to subcarrier mapping respectively. These prevent the subcarriers to overlap and eventually result in either very low or no PAPR. Moreover, SC-FDMA offers robustness to the spectral nulls and provides good spectral efficiency due to its interleaved multicarrier mapping structure. The resulting wideband signal, if used for radar applications, would certainly offer the opportunity to achieve high range resolution of the target.

2.4 Problem Statement

The research gap analysis, presented in section 2.2, shows that there is a need to design a waveform that possesses the expediencies of all radar waveforms discussed in the literature review on one hand and none of their drawbacks on the other hand. This means, we require a waveform that:

- Possesses large bandwidth and high detection probability.
- Resolves the high PAPR issue.
- Provides high range resolution.
- Acquires favourable ambiguity function.
- Achieves good autocorrelation properties.

None of the radar waveforms other than SC-FDMA seems to deliver all these perks as a single suit. We, therefore, build our research problem on the idea of using SC-FDMA as a radar waveform and aim to design and analyze a complete architecture of an SC-FDMA radar.

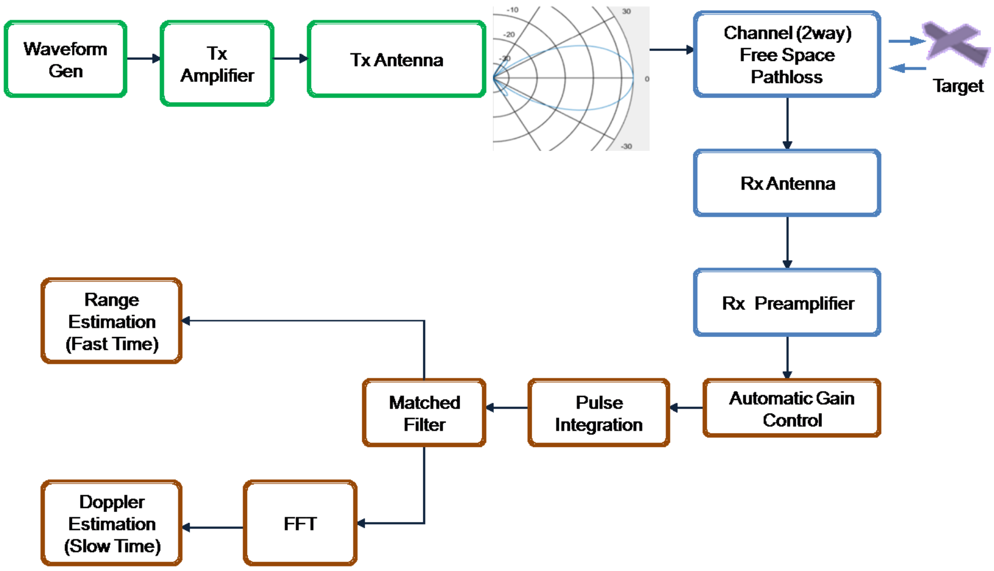

FIGURE 2.1: Block diagram of a Radar System Architecture

2.5 The Proposed Research Methodology and Scope of the Thesis

Our methodology to provide a solution to the research problem set out in the previous section is twofold.

In the first part of the research, we aim to design an SC-FDMA radar waveform and analyze it properties on the basis of the performance metrics described in chapter1. This part is subdivided into four stages. In the first stage, we aim to develop the analytical expression for the proposed waveform i.e. SC-FDMA with interleaved sub-carrier mapping, and design the transmitter, receiver, and signal processing unit of the proposed radar. In the second stage, an expression for the ambiguity function of the proposed waveform is derived and analyzed. The third stage focuses on the statistical properties of the proposed waveform including its correlation function and peak-to-sidelobe ratio (PSLR). In the fourth stage, we focus on determining the PAPR of the proposed waveform for different codes as initial sequences by using the standard PAPR measuring formulas. For random initial sequences, we aim to use CCDF plots for the analysis of PAPR of the proposed SC-FDMA waveform after running Monte Carlo simulation.

The second part of the research methodology is based on implementing the proposed SC-FDMA waveform into a monostatic radar for target detection and parameter estimation. Initially, we aim to model all the necessary blocks of an end-to-end radar, described in Fig. 2.1. These blocks include waveform generation and transmitter amplifier at the radar transmitter side, and preamplifier, automatic gain control, pulse integration, matched filter, and range and Doppler estimation on the receiver side. This stage also includes target modeling, signal propagation modeling, and motion modeling of the target and the sensor platforms.

In the next stage of part II, we aim to characterize a general interleaved SC-FDMA radar and simulate it for an end-to-end monostatic configuration to detect moving and static targets in single and multiple target environment. The final goal of this stage is to estimate the target parameters; i.e. range, speed and the resolutions of target in range and speed. Here, we intend to construct a standard data matrix after receiving echoes of a burst of pulses from the target, and determine the speed and the range by processing along the slow time and fast time of the data matrix respectively.

2.6 Contributions

The contributions of the research conducted for this dissertation are given below.

1. We propose the complete architecture of a wideband SC-FDMA radar.
2. We analyze the SC-FDMA waveform for its correlation properties and ambiguity function. The analytical expression for the ambiguity function of the proposed SC-FDMA are derived. The 3-D AF diagrams are simulated by using the numerical method for the proposed waveform. Also, 3-D AF diagrams of some notable existing waveforms are plotted including OFDM, Phase-coding, and LFM waveforms for comparison. Signal correlation properties for the proposed waveform such as autocorrelation and peak to sidelobe ratio are analyzed and compared with those of existing OFDM and phase coded waveforms.

3. We compute the peak to average power ratio of the proposed SC-FDMA waveform (with interleaved sub-carrier mapping) for different numbers of subcarrier frequencies by using different radar phase-coded waveforms as the initial sequences.

4. We evaluate the performance of the proposed waveform in the context of achieving high range resolution and discriminating between very close targets in range and speed. We simulate the proposed SC-FDMA end-to-end radar that includes SC-FDMA waveform generator, transmitter, receiver, and signal processing modules. The purpose of these simulations is to evaluate the performance of the proposed radar and compare it with that of other existing radars. We present four different scenarios that include clutter and moving targets with different ranges and radial velocities.

Chapter 3

Proposed SC-FDMA Radar Architecture

In this chapter, the proposed SC-FDMA radar architecture is discussed in detail. In section 3.1. the building blocks of the architecture are elaborated. SC-FDMA radar signal modeling is given in section 3.2, that includes subcarrier mapping, transmitted signal model and the received signal model. Section 3.3 discusses SC-FDMA radar signal processing in terms of target detection and range and Doppler estimation.

3.1 Single Carrier FDMA Radar Architecture

SC-FDMA is a multiple access technique that uses single carrier modulation, orthogonal frequency division multiplexing, and frequency domain equalization. Single carrier FDMA is a linear precoded interpretation of OFDMA. SC-FDMA is also known as DFT-Spreaded OFDMA, as it has an additional DFT process prior to the conventional OFDMA processing.

The proposed architecture of a generic SC-FDMA radar is shown in Fig. 3.1, which includes SC-FDMA modulator and demodulator as its two major blocks. In SC-FDMA, the symbols are transmitted sequentially, as compared to the

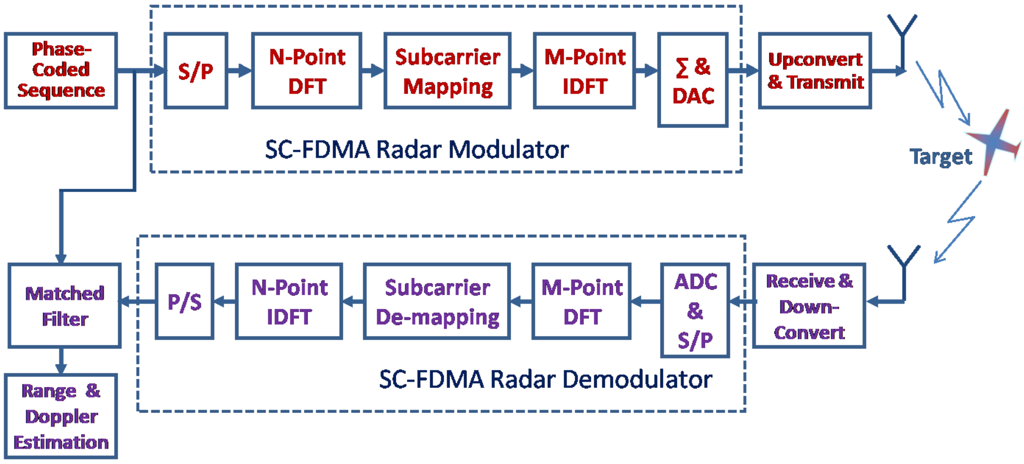

FIGURE 3.1: Architecture of Proposed Single Carrier FDMA Radar

parallel transmission of OFDM symbols in OFDM radar, over multiple subcarriers. Multiple source signals are multiplexed and demultiplexed in the frequency domain by subcarrier mapping that provides SC-FDMA, an aspect of OFDM.

In the proposed model, we combined the SC-FDMA waveform (previously used in LTE) with a radar system using phase-coded waveforms. Phase-coded waveform preferably Frank or P-codes are used as initial sequence for generating SC-FDMA waveform. The whole signal modeling is for single source (or user, as the term used in communications). However for multiple sources this waveform has the provision to accommodate other phase-coded sequences or LFM signal simultaneously in the same SC-FDMA signal. That is the beauty of SC-FDMA as it is a multiple access scheme. However, for the sake of simplicity in this chapter and in the subsequent chapters single source is used for analysis purposes.

The input to the SC-FDMA radar modulator and the output at the demodulator is a phase-coded pulse sequence. The only difference between these two is that the signal at the output of the demodulator contains information of the target parameters including range and speed.

As shown in Fig. 3.1, the SC-FDMA modulator consists of a serial to parallel conversion block followed by an N-point DFT block, where N is the number of the transmitted symbols. This N-point DFT converts the time domain data to frequency domain symbols. SC-FDMA is also known as Discrete Fourier

Transform Spread OFDM (DFT-S-OFDM) because of this process, though this term is less common. The frequency domain symbols are then mapped to N out of M subcarriers according to some suitable mapping scheme, where M is the total number of subcarriers. The mapping techniques are discussed in detail in the next section of this chapter. After symbols to subcarriers mapping, an M-point IDFT is implemented that converts the mapped frequency domain symbols to time domain signals. All the parallel streams are added in the time domain and then a digital to analog conversion is applied. After using a mixer to upconvert this baseband signal, a passband signal is transmitted from the radar.

A target is illuminated by this signal and an echo of the same signal is received by the radar. At the receiver end, the signal is downconverted to baseband and then is transformed from analog to the digital domain. In the SC-FDMA demodulator block, in Fig. 3.1, the DFT operation is performed. It transforms the received baseband signal to the frequency domain to retrieve N subcarriers. The de-mapping procedure separates N frequency domain symbols that belong to each source, in the case when multiple sources are used for SC-FDMA signal generation. Then the N point IDFT operation transforms these frequency domain symbols to N time domain samples. Then after applying the matched filter, a detector recovers the original phase-coded sequences associated to each source. This signal carries the target range and velocity information in the form of delay and Doppler shift.

3.2 SC-FDMA Radar Signal Model

At the transmitter, the input is most desirably a code taken from the family of phase-coded waveforms. The code consists of N complex symbols generated at a rate of R_{sr} symbols/sec. N-point DFT is performed to create N frequency domain symbols that modulate N out of M subcarriers, given that $M \geq N$, occupying the entire bandwidth

$$B = M\,\Delta f \tag{3.1}$$

Where $\triangle f$ is the spacing between the subcarriers and B is the total bandwidth. The channel transmission rate in symbols per second is given as

$$R_{\text{ch}} = \frac{M}{N} R_{\text{sr}} \tag{3.2}$$

where R_{sr} is the rate at which radar source symbols are generated and M is the total number of subcarriers. If we denote K as the bandwidth spreading factor and M being an integral multiple of N, then

$$K = \frac{R_{\text{ch}}}{R_{\text{sr}}} = \frac{M}{N} \tag{3.3}$$

3.2.1 Subcarrier Mapping

There are two ways of subcarrier mapping in SC-FDMA; interleaved and localized. In interleaved SC-FDMA (named as ISC-FDMA), the data symbols of a single source are equally distributed over complete frequency band whereas in localized SC-FDMA (LSC-FDMA) the data symbols of a single user are mapped on a consecutive set of frequencies.

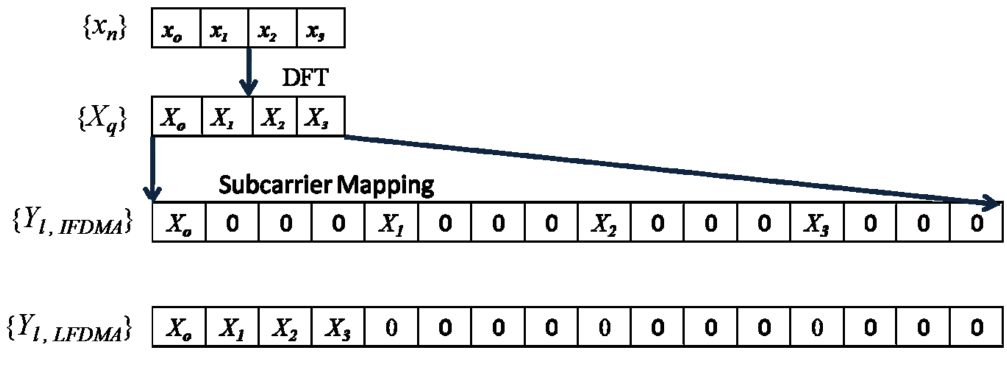

Figure 3.2: Subcarrier Mapping in SC-FDMA with N=4 and K=4 and M=16

The SC-FDMA radar can handle up to K independent signal sources each carrying N symbols. K is referred to as the number of users in communication systems; however, in case of radar, this concept can be used differently as the multiple tasks performed by a single radar. However, in this research work, we take a single source scenario in which data from a single source is spreaded over the entire frequency range with equal frequency spacing. The mapping scheme used is interleaved subcarrier mapping which is more robust against fading and external interference by achieving maximum frequency diversity.

3.2.2 Transmitted Signal

We assume $\{x_n : n = 0, 1, \ldots, N-1\}$ as the modulation symbols, we take from the family of phase-coded waveforms. The waveform uses fixed carrier frequency but different phases that are switched between a total of N different fixed values after regular intervals within a pulse duration. This waveform can be modeled as N contiguous subpulses of duration T_s also known as chips or elements. In this work, we are using 4-phase Frank code with 16 elements, 8-phase Frank code with 64 elements, and P3 code with 40 elements. The phase coded symbols $\{x_n : n = 0, 1, \ldots, N-1\}$ are generated by using following relation

$$x(t) = \sum_{n=0}^{N-1} x_n g(t - nT_s) \tag{3.4}$$

In the same way, nth symbol of kth source would be denoted by $x_{n,k}$ with $(k = 0, 1, \ldots, K-1)$ and $(n = 0, 1, \ldots, N-1)$. We assume data symbols from a single source and hence for simplicity, use the notation x_n instead of $x_{n,k}$. These symbols are then converted to frequency domain symbols X_q by performing DFT

$$X_q = \sum_{n=0}^{N-1} x_n \exp(-j\frac{2\pi}{N}nq) \tag{3.5}$$

where q is the index representing the frequency domain symbol and N is the length of DFT. After performing DFT, the frequency domain symbols X_q are mapped to subcarriers according to one of the previously-mentioned subcarrier mapping schemes. We take the case of interleaved SC-FDMA and hence denote the resulting frequency domain symbols as Y_l with $(l = 0, 1, ..., KN-1)$. The frequency domain symbols Y_l, mapped to corresponding subcarriers, are then subjected to IDFT operation and the resulting time domain symbol can be written as

$$y_m = \frac{1}{M}\sum_{l=0}^{M-1} Y_l \exp(j\frac{2\pi}{M}ml) \tag{3.6}$$

where M being the length of IDFT is equal to the number of subcarriers such that $M \geq N$. The index m is given as $m = n + kN$ where $(0 \leq n \leq N-1)$ and $(0 \leq k \leq K-1)$.

The resulting time domain interleaved SC-FDMA signal represented by symbols$\{y_m : m = 0, 1, ..., M-1\}$ are basically a K times repetition of the original time domain signal represented by symbols $\{x_n : n = 0, 1, ..., N-1\}$ with a scaling factor $1/K$. In general for multiple source symbols, the subcarrier allocation starts with rth subcarrier and y_m can be written as

$$y_m = \frac{1}{K} x_n(m)_{mod\,N} \ \exp(j2\pi\frac{rm}{M}) \tag{3.7}$$

where $e^{(j2\pi rm/M)}$ represents a phase rotation of in the time domain SC-FDMA signal and r is the initial sequence number of the source symbol and $(0 \leq r \leq K-1)$.

The transmitted interleaved SC-FDMA signal for passband is a complex signal represented as

$$y_c(t) = e^{j2\pi f_c t}\sum_{m=0}^{M-1} y_m g(t - mT_s) \tag{3.8}$$

where f_c is the carrier frequency of the system and $g(t)$ is the pulse shaping function. $y_c(t)$ can be represented in baseband form as

$$y(t) = \sum_{m=0}^{M-1} y_m g(t - mT_s) \tag{3.9}$$

Since $y(t)$ is a periodic signal in which the source signal is repeated K times after T interval. We consider the transmitted signal as a continuous wave for length KT with a periodic complex envelope $y(t)$ with period T.

In (3.7), for a single source with $r = 0$, there is no phase rotation and we can write $y(t)$ as

$$y(t) = \sum_{k=0}^{K-1} \sum_{n=0}^{N-1} \frac{1}{K} x_n g[t - (n + kN)T_s] \tag{3.10}$$

$y(t)$ is a periodic function repeating after K intervals and can be written as

$$y(t) = \frac{1}{K} x(t \pm kT) \qquad k = 0, 1, , ..., K - 1 \tag{3.11}$$

In general, to avoid intersymbol interference, the transmitted signal is added by a cyclic prefix (CP) of some appropriate length. CP could merely be zeros that is added at the beginning of the SC-FDMA data block or a copy of the last part of the data block. In the case of radar, the CP being a sequence of zeros is characterized by the maximum unambiguous range of the radar. From 3.11, it is obvious that the proposed waveform not only retains all the benefits of the original phase-coded waveform but also improves range resolution by a factor K through repetitions as the bandwidth of the proposed signal increases K times.

3.2.3 Received Signal

The returning echo from a target is a passband RF signal $\tilde{y}_c(t)$ that a radar receiver down-converts to the baseband signal $\tilde{y}(t)$ which is a continuous time representation of a periodic sequence $\tilde{y}_m$; the received version of the transmitted symbols y_m. The symbols $\{\tilde{y}_m : m = 0, 1, \dots, M - 1\}$ are then demultiplexed by performing DFT and IDFT operations subsequently to achieve the associated symbols of each transmitting source.

Initially, M point DFT is performed and the received frequency domain symbols $\widetilde{Y}_l$ are acquired with $(l = 0, 1, ..., KN - 1)$, which are given below

$$\widetilde{Y}_l = \sum_{m=0}^{M-1} \tilde{y}_m \exp(-j\frac{2\pi}{M} ml) \tag{3.12}$$

The DFT operation transforms the received time domain symbols to frequency domain symbols, to retrieve the data of all sources, mapped on $M = KN$ subcarriers.

In the next step, subcarrier demapping is performed that separates N frequency domain symbols $\widetilde{X}_q$, with $(q = 0, 1, ..., N-1)$, for each source k. Then the N point IDFT operation transforms these frequency domain symbols to N time domain symbols represented by $\tilde{x}_n$, as given below.

$$\tilde{x}_n = \frac{1}{N}\sum_{q=0}^{N-1} \widetilde{X}_q \exp(j\frac{2\pi}{N}nq) \tag{3.13}$$

The associated waveform can also be written as

$$\tilde{x}(t) = \sum_{n=0}^{N-1} \tilde{x}_n g(t - nT_s) \tag{3.14}$$

3.3 Radar Signal Processing

3.3.1 Match Filtering and Range Estimation

After obtaining the individual signal for each source k given in 3.14, a matched filter is applied to the received signal. The matched filter provides a processing gain that improves the performance metric at the detection threshold. At its output, it provides a maximum signal-to-noise ratio (SNR) at the sampling instant with some delay t_o corresponding to the true target range R [21], such that

$$t_o = \frac{2R}{c} \tag{3.15}$$

where c is the speed of light in free space.

The input to the matched filter is $\tilde{x}(t)$ that contains the target information and a noise component. The output of the matched filter is given by

$$z(t) = \int_{-\infty}^{\infty} \tilde{x}(\tau)\, h(t-\tau)\, d\tau \tag{3.16}$$

where $h(t)$ is the impulse response of the matched filter and is given by

$$h(t) = \alpha x^*(T_M - t) \tag{3.17}$$

Here, we consider T_M as an arbitrary time at which SNR of the matched filter output signal is maximum i.e. T_M is equal to sampling interval. For $h(t)$ to be causal, T_M is required to be $T_M \geq t$ i.e. the current time instant. In Eq. 3.17, α is the gain constant and usually set equal to unity. Eq. 3.16 shows that the impulse response of the optimum filter is matched to the demultiplexed received signal. The matched filter performs convolution of the received signal with a conjugated time-reversed local copy of the transmitted signal.

Thus Eq. 3.16 becomes

$$z(t) = \alpha \int_{-\infty}^{\infty} \tilde{x}(\tau)\, x^*(\tau + T_M - t)\, d\tau \tag{3.18}$$

Eq. 3.18 is also known as the cross-correlation of the target and noise containing signal $\tilde{x}(t)$ with the transmitted signal $x(t)$ at a lag $T_M - t$. The matched filter is designed to maximize the output signal to noise ratio at the sampling instant T_M.

We choose $T_M = T_s$, the minimum value that makes the matched filter a causal filter. Let us consider the input to the matched filter is signal $\tilde{x}(t)$ that contains the information of the range R of the target as given in Eq. 3.15 along with a noise component

$$\tilde{x}(t) = x(t - t_o) + n(t) \tag{3.19}$$

Ignoring the noise component, the output of the matched filter can be written as

$$z(t) = \alpha \int_{-\infty}^{\infty} x(\tau - t_o)\, x^*(\tau + T_s - t)\, d\tau \tag{3.20}$$

which is simply the correlation of the time delayed echo signal with the impulse response of the matched filter. The output of the matched filter will have its peak at zero correlation lag, i.e. at the sampling instant creating the condition

$$\tau - t_o = \tau + T_s - t \tag{3.21}$$

We denote this time at which the peak occurs as t_{peak}. Hence

$$t_o = t_{peak} - T_s \tag{3.22}$$

Now the range R of a target can be determined by substituting t_o from Eq. 3.22 into Eq. 3.15, we get

$$R = \frac{c(t_{peak} - T_s)}{2} \tag{3.23}$$

3.3.2 Pulse Integration

Pulse integration is performed when the outputs of the matched filter are combined at the receiver. Radar returns from a target associated with each pulse repetition interval (PRI) at each sensor (in case of multi-antenna radar) are stored in a memory to form a data cube or a block data matrix. This data cube consists of three dimensions; fast-time, slow time, and the third one representing the received sensor array as shown in Fig. 3.3. However, when a single sensor is used, as the case considered in this research work, the datacube is converted to a data matrix with only two dimensions; fast-time and slow-time as shown in Fig. 3.4. In a data matrix, the fast time refers to as the time slots within each PRI along each column and the slow time is along each row refers to as the time between pulses that is updated after each PRI. Number of fast time blocks depends upon the sampling rate and the values of these blocks correspond to the output of the matched filter at corresponding time slots.

The samples along the fast-time, referred to as range bins or range gates, are converted to distance using the signal propagation speed. These sample intervals are referred to as range bins or range gates.

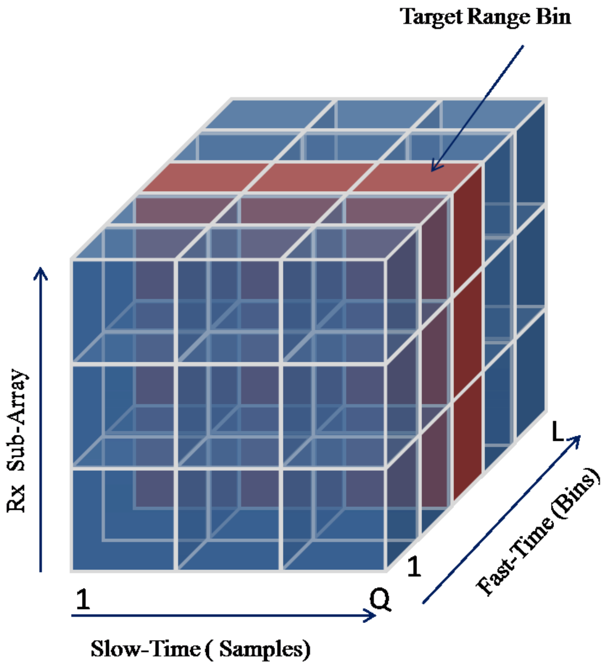

FIGURE 3.3: Radar processing data cube

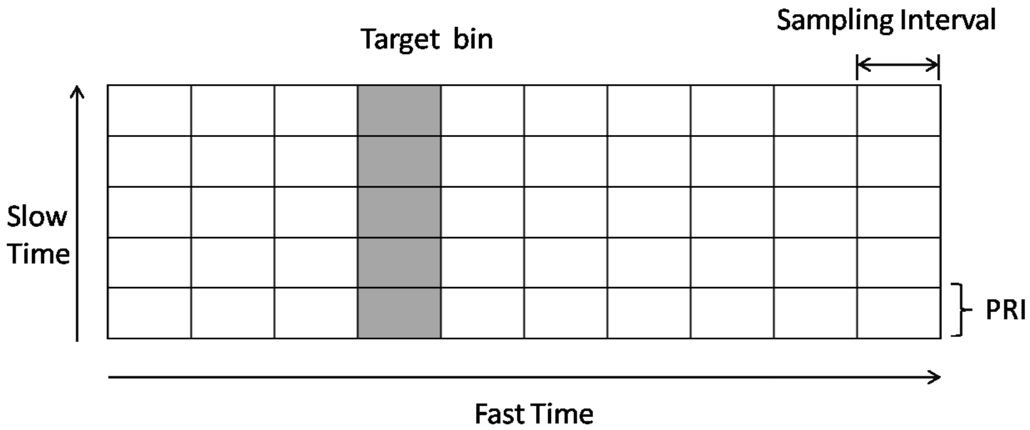

FIGURE 3.4: Data Matrix representing Fast time and Slow time

Pulse integration is performed to improve the detection probability and signal to noise ratio. In pulse integration, a gain is achieved by adding the radar returns from a sequence of pulses. There are two kinds of pulse integration, one is coherent and the other is non-coherent [21]. The coherent pulse integration is performed when there is no information lost in the form of phase and amplitude in the return signal. If we denote the data matrix by D, then D_{lq} will be the (l, q)th entry of the matrix of order $L \times Q$. Then we can define coherent pulse integration as

$$Z_q = \sum_{l=1}^{L} D_{l,q} \tag{3.24}$$

The non-coherent pulse integration is performed when the information of the phase is lost i.e. the phase of the signal is corrupted. It is also known as video integration and is mathematically defined as

$$Z_q = \sqrt{\sum_{l=1}^{L} |D_{l,q}|^2} \tag{3.25}$$

In many cases, coherent integration is more efficient as compared to non-coherent. For coherent integration, if a perfect integrator is used i.e. with 100% efficiency, then integrating pulses would improve the SNR by the same factor. In this research work, we use coherent integration for pulse detection as we are not considering any active or passive interference to distort the phase of the received signal. In case of multicarrier radar processing, another dimension of radar returns received at different subcarriers, is added which may further improve the SNR many folds.

After the pulse integration, a detector is used to compare the signal power to a given threshold. For that, the threshold is chosen such that the probability of false alarm is below a certain level. The corresponding range bin gives the value of time delay t_o from which we retrieve the range of the target as given in Eq. 3.15. There is always an ambiguity in the measurement of range that is equivalent to the range resolution. In chapter 4, we will discuss this in detail.

3.3.3 Doppler Estimation

After the range estimation, we determine the Doppler information of the target. Relative motion between the radar and the target results in the change in the carrier frequency of the signal referred to as the Doppler shift. Estimation of this Doppler frequency gives the relative radial speed of a moving object.

The radial velocity of a moving target can be estimated by performing pulse-Doppler processing. In pulse-Doppler processing, the Doppler shift is estimated through spectrum estimation by performing DFT along the slow time, in the data matrix [181]. The maximum Doppler shift that could be estimated depends upon the pulse repetition frequency (PRF) of the transmitting pulse. The maximum unambiguous Doppler frequency that can be measured by any radar is half the value of its PRF.

$$f_{d_{\max}} = \frac{f_{\text{PRF}}}{2} \tag{3.26}$$

In Doppler processing, the first step is to generate the Doppler spectrum from the received signal. For that purpose, a DFT operation is applied on the slow time data of the data matrix in order to estimate the spectral density of the received signal. In the data matrix, the slow time data is sampled at the rate of the pulse repetition frequency, and therefore the DFT along the slow time data for a particular range bin gives the estimate of the Doppler spectrum ranging from $-\frac{f_{\text{PRF}}}{2}$ Hz to $+\frac{f_{\text{PRF}}}{2}$ Hz. For illustration, we take an example of a signal that contains echoes from two targets moving at different speeds. The Doppler frequency of target 1 and target 2 is $f_1 = 100$ Hz and $f_2 = 250$ Hz respectively. Figure 3.5 shows the power spectral density of this signal both in linear and dB scale.

The resolution in Doppler measurement Δf_d can be given as

$$\Delta f_d = \frac{f_{\text{PRF}}}{Q} \tag{3.27}$$

where Q is the number of slow-time samples.

For a small number of samples along the slow-time grid, a common approach is to interpolate the DFT grid by padding it with zeros. Though, this approach does not improve the Doppler resolution; however, it can improve the estimation of the locations of the peaks in the spectrum.

The Doppler shift estimated from the DFT process is then converted to velocity. A narrowband signal propagating at the speed of light has the Doppler shift in hertz as follows:

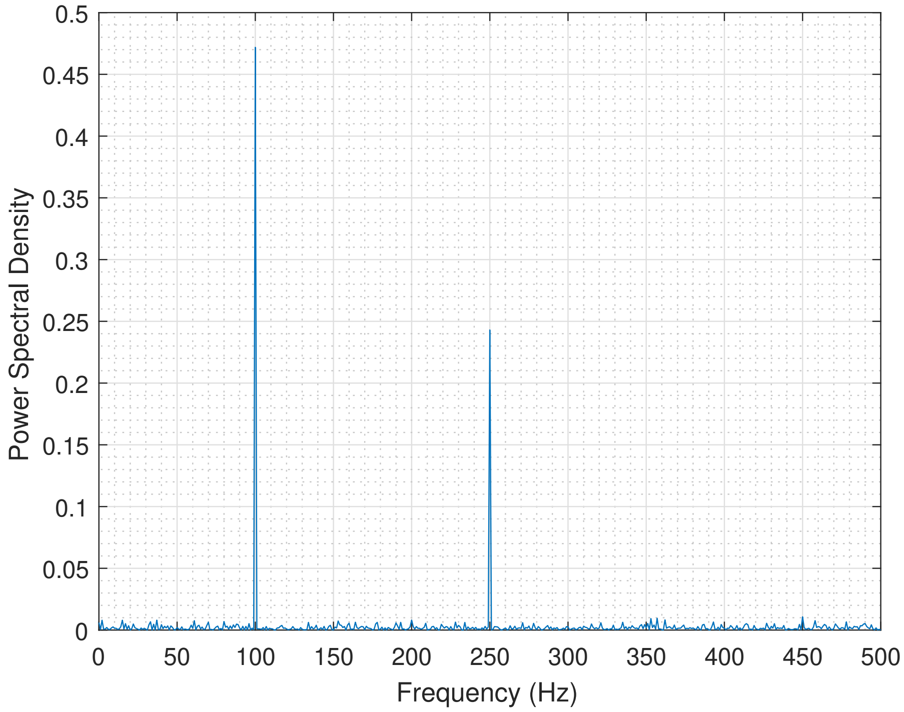

(a)

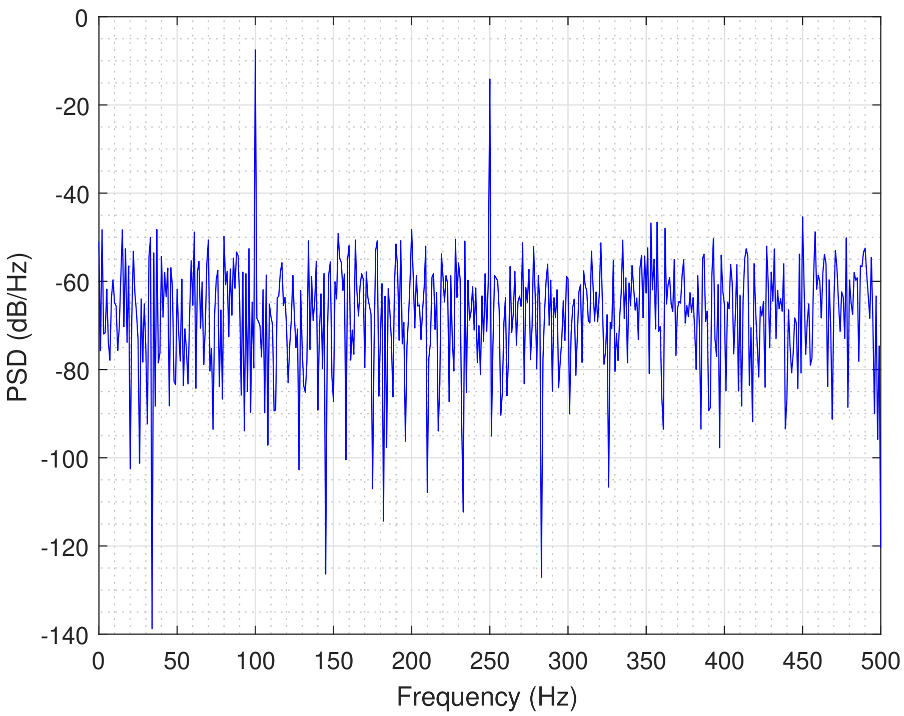

(b)

FIGURE 3.5: Power spectral density of a combined signal with frequency $f_1 =$ 100 Hz and $f_2 = 250$ Hz (a) Linear scale (b) dB scale

$$f_d = \pm \frac{2v}{c} f \tag{3.28}$$

$$f_d = \pm \frac{2v}{\lambda} \tag{3.29}$$

where v is the radial speed of the target, c is speed of light, and λ is the wavelength of the carrier. The positive Doppler shift indicates that the target is approaching towards the radar and negative Doppler shift declares that the target is moving away from the radar.

Chapter 4

Ambiguity Function, Correlation Properties, and PAPR Analysis of SC-FDMA Radar Waveform

In this chapter, a generic Ambiguity function (AF) is defined along with its properties in section 4.1 and 4.2 respectively. In sections 4.3, an ideal ambiguity function is described as a reference, while in section 4.4 some examples of commonly used AFs are given. The commonly used AFs include the AFs of linear frequency modulation (LFM) and phase-coded waveforms. In section 4.5, the analytical expression for the AF of the proposed interleaved SC-FDMA waveform is formulated. In section 4.6, the AF correlation properties of the proposed waveform are discussed and analyzed in detail and further compared with those of OFDM and other notable radar waveforms. In the subsequent sections, the peak-to-average power ratios (PAPR) analysis of the proposed interleaved SC-FDMA waveform has been performed. In section 4.7, an expression for the PAPR of a multicarrier radar is given. Section 4.8, presents the proposed interleaved SC-FDMA waveform as a constant envelope signal that aims at reducing the PAPR. In section 4.9, the PAPR of the proposed interleaved SC-FDMA waveform using different phase-coded sequences are computed and compared with those of OFDM and other notable radar waveforms. These phase-coded sequences include PRN, Barker, Frank, Zadoff-Chu, P1, P3, and Px codes.

4.1 Ambiguity Function

As discussed in chapter 1, ambiguity function (AF) is a two-dimensional correlation between a transmitted signal and its time-delayed and frequency-shifted version. The time delay refers to as range resolution and frequency shift refers to as the speed resolution of the moving target. Ambiguity function is a tool used as a means to analyze the characteristics of a radar waveform [30]. It provides insight when dealing with range and Doppler resolution of any object of interest [31]. AF does not depend upon any specific target scenario despite it is determined by pulse waveform specifications and the matched filter [21].

For a complex baseband pulse signal $x(t)$, the ambiguity function [21] is defined as

$$A(\tau,\, f_d) = \left|\tilde{A}(\tau,\, f_d)\right| = \left|\int_{-\infty}^{\infty} x(t)\, \exp(j2\pi f_d t) x^*(t-\tau)dt\right| \tag{4.1}$$

where $\tilde{A}(\tau,\, f_d)$ represents the output of the two dimensional matched-filter, $*$ denotes the complex conjugate, τ represents time delay and f_d represents Doppler frequency linked to the motion of the target.

AF are also presented in one-dimension by employing zero-delay cut $A(0, f_d)$ and zero-Doppler cut $A(\tau, 0)$ on the AF plot of the radar waveform. For a target moving at constant speed, the time domain output of a matched filter is a Doppler cut $A(\tau, f_d)$ at a fixed frequency f_d referred to as Doppler shift generated by the relative motion of the target and the radar. If the target is not moving with respect to the radar then $f_d = 0$ and the ambiguity function becomes

$$A(\tau,\, 0) = \left|\int_{-\infty}^{\infty} x(t)\, x^*(t-\tau)dt\right| \tag{4.2}$$

which is the autocorrelation function of $x(t)$ with a delay τ.

4.2 Properties of Ambiguity Function

Radar ambiguity function features the following properties [46].

1. Ambiguity function is symmetric with respect to the origin i.e.

$$A(\tau, f_d) = \left|\tilde{A}(\tau, f_d)\right| = \left|\tilde{A}(-\tau, -f_d)\right| \tag{4.3}$$

2. If the waveform energy is denoted by E, then

$$\left|\tilde{A}(\tau, f_d)\right| \leq \left|\tilde{A}(0, 0)\right| = E \tag{4.4}$$

i.e. the response of the filter is maximum when it is matched in both range and Doppler. When the filter is not matched in either range or Doppler or both, then the response is less than the maximum.

3. The total volume under the ambiguity surface is constant, independent of the waveform i.e.

$$\int_{-\infty}^{\infty}\int_{-\infty}^{\infty} \left|\tilde{A}(\tau, f_d)\right|^2 d\tau df = \left|\tilde{A}(0, 0)\right|^2 = E^2 \tag{4.5}$$

The property given by Eq. 4.5, is also known as the conservation of energy property. It states that while designing a waveform, energy cannot be removed from any portion of the AF without placing it somewhere else at the AF surface.

4. For a complex envelope $x(t)$, the AF is given as $\left|\tilde{A}(\tau, f_d)\right|$. In the same manner, for a linear frequency modulated (LFM) signal, the AF is given as

$$x(t)e^{j\pi\alpha t^2} \iff \left|\tilde{A}(\tau, f_d - \alpha\tau)\right| \tag{4.6}$$

where α is the LFM coefficient. This property states that adding LFM modulation to a waveform results in a sheared AF. This property is also known as the linear FM effect.

4.3 Ideal Ambiguity Function

The ideal ambiguity function of a radar waveform is represented by a spike of infinite height and infinitesimal width which is a 2-dimensional Dirac Delta function that lies at origin (0,0) and zero at everywhere else.

$$A(\tau, f_d) = \delta(\tau)\delta(f_d) \tag{4.7}$$

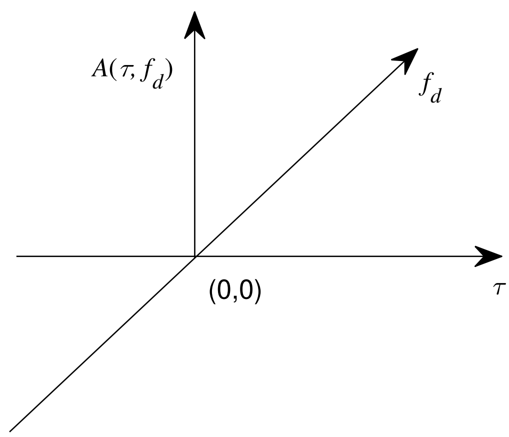

FIGURE 4.1: An ideal Ambiguity Function

In an ideal Ambiguity function, each of the zero delay and zero-Doppler cuts is an impulse function. It means that an ideal ambiguity function offers high resolution for multiple targets no matter how close they are to each other [21]. This sort of ambiguity function has no ambiguity at all. An ideal ambiguity function is physically not realizable. As it requires infinite energy to exist that is not possible in reality.

4.4 Commonly Used Ambiguity Functions

The 3-dimensional plot of range and Doppler versus ambiguity function is called "Radar Ambiguity Diagram". Different waveforms have different ambiguity functions and hence exhibit different ambiguity diagrams. Ambiguity function is important when choosing as a waveform for any radar. Few of the waveforms with their ambiguity functions are described in this section. These include pulse amplitude modulation (PAM), linear frequency modulation, and phase-coded modulation waveforms.

4.4.1 Rectangular Pulse

Let us consider a rectangular pulse $x(t)$ of pulse width T, given as

$$x(t) = \frac{1}{\sqrt{T}} \mathrm{Rect}\left(\frac{t}{T}\right) \tag{4.8}$$

Then the ambiguity function for this pulse [46] is as following.

$$\left|\tilde{A}(\tau, f_d)\right| = \left|(1 - \frac{|\tau|}{T})\frac{\sin(\pi f_d(T - |\tau|))}{\pi f_d(T - |\tau|}\right| \quad |\tau| \leq T \tag{4.9}$$

The AF along delay axis is given by substituting $f_d = 0$ in Eq.4.9

$$\left|\tilde{A}(\tau, 0)\right| = \left|(1 - \frac{|\tau|}{T})\right| \quad |\tau| \leq T \tag{4.10}$$

The ambiguity function along the Doppler axis is a sinc function that is obtained by substituting $\tau = 0$ in Eq.4.9, given as

$$\left|\tilde{A}(0, f_d)\right| = \left|\frac{\sin(\pi f_d T)}{\pi f_d T}\right| \tag{4.11}$$

Fig. 4.2 (a) gives the ambiguity diagram of a rectangular pulse along with its zero delay cuts in Fig. 4.2(b). Fig. 4.3(b) shows the zero-Doppler cut of the same AF of rectangular pulse in (a) and its contour plot in (b) part. We see the poor performance of rectangular pulse in the form of poor bandwidth efficiency and poor range and Doppler resolutions.

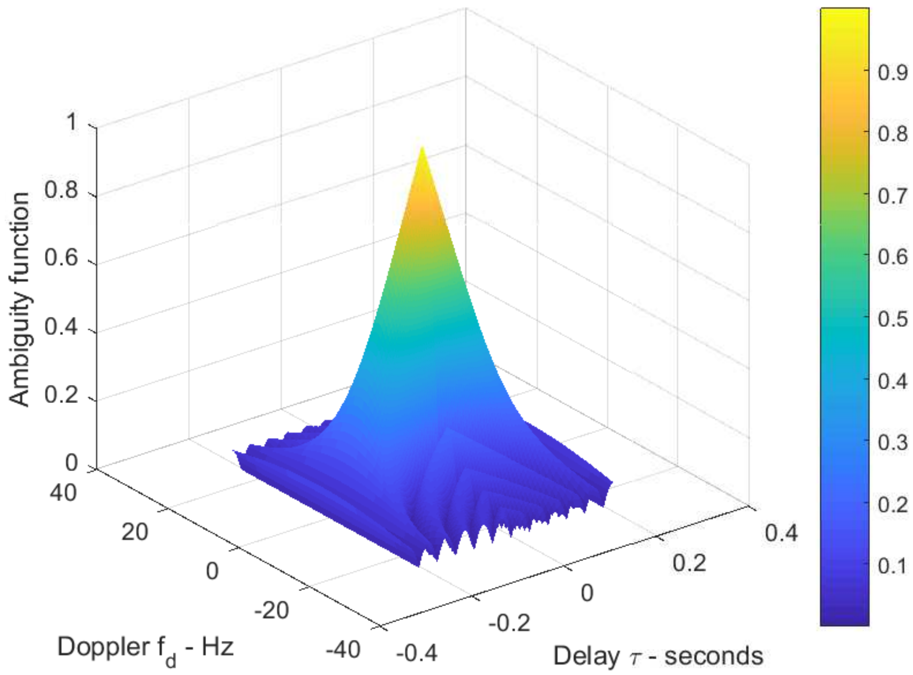

(a)

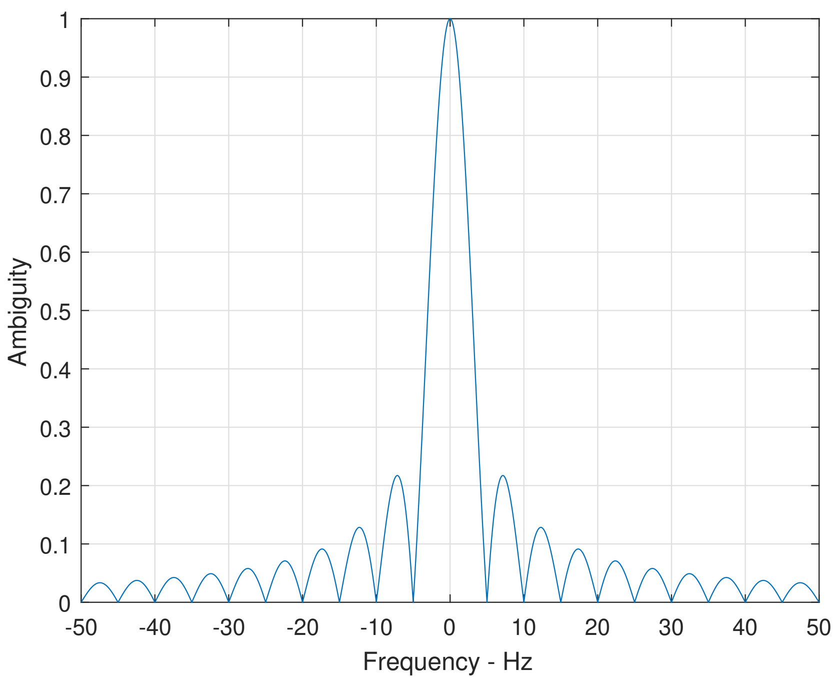

(b)

FIGURE 4.2: A rectangular pulse with pulse width = 0.2 sec (a) Ambiguity function (b) Zero-delay cut along Doppler axis.

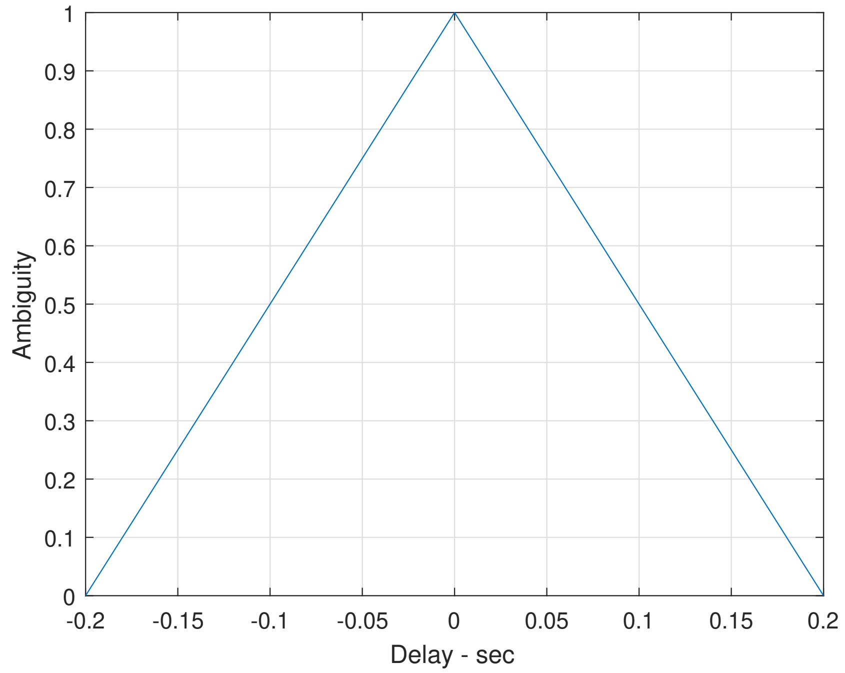

(a)

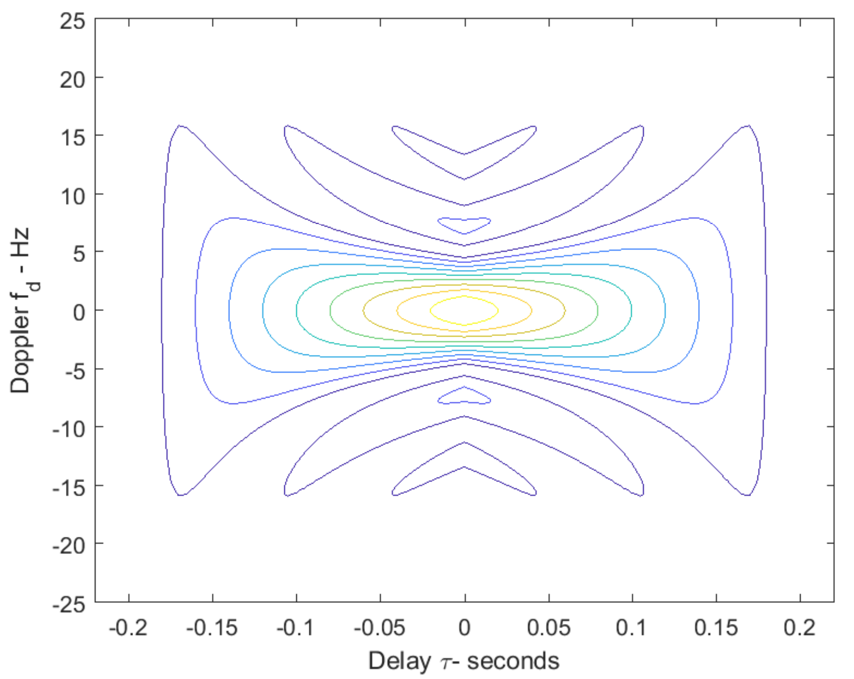

(b)

FIGURE 4.3: Ambiguity function for rectangular pulse with pulse width = 0.2 sec (a) zero-Doppler cut off along delay axis (b) Contour plot

4.4.2 LFM Pulse

A linear frequency modulated or a chirp signal $x(t)$ described in Eq. (1.8) is

$$x(t) = \frac{1}{\sqrt{T}}\text{Rect}\left(\frac{t}{T}\right)\exp(j2\pi\mu t^2)$$

where T is the pulse width and μ is LFM coefficient with bandwidth B, given as

$$\mu = \pm\frac{B}{T}$$

B is also known as the frequency deviation. The ambiguity function for a chirp pulse is given as

$$A(\tau,\ f_d) = \left|\tilde{A}(\tau, f_d)\right| = \left|(1-\frac{|\tau|}{T})\frac{\sin(\pi T(\mu\tau + f_d)(1-\frac{|\tau|}{T}))}{\pi T(\mu\tau + f_d)(1-\frac{|\tau|}{T})}\right| \quad |\tau| \leq T \tag{4.12}$$

The ambiguity function along delay axis for a chirp signal is given by substituting $f_d = 0$ in Eq.(4.12) and we get

$$\left|\tilde{A}(\tau, 0)\right| = \left|(1-\frac{|\tau|}{T})\frac{\sin(\pi T(\mu\tau)(1-\frac{|\tau|}{T}))}{\pi T(\mu\tau)(1-\frac{|\tau|}{T})}\right| \quad |\tau| \leq T \tag{4.13}$$

The ambiguity function along Doppler axis for the chirp signal is given by substituting $\tau = 0$ in Eq.(4.12) and we get

$$\left|\tilde{A}(0, f_d)\right| = \left|\frac{\sin(\pi T f_d)}{\pi T f_d}\right| \quad 0 \leq T \tag{4.14}$$

LFM has good range resolution due to its large bandwidth structure as shown in Fig.4.4 (a) and Fig.4.5. However, as can be observed in Fig.4.4 (b) its autocorrelation plot has significant high sidelobe peaks.

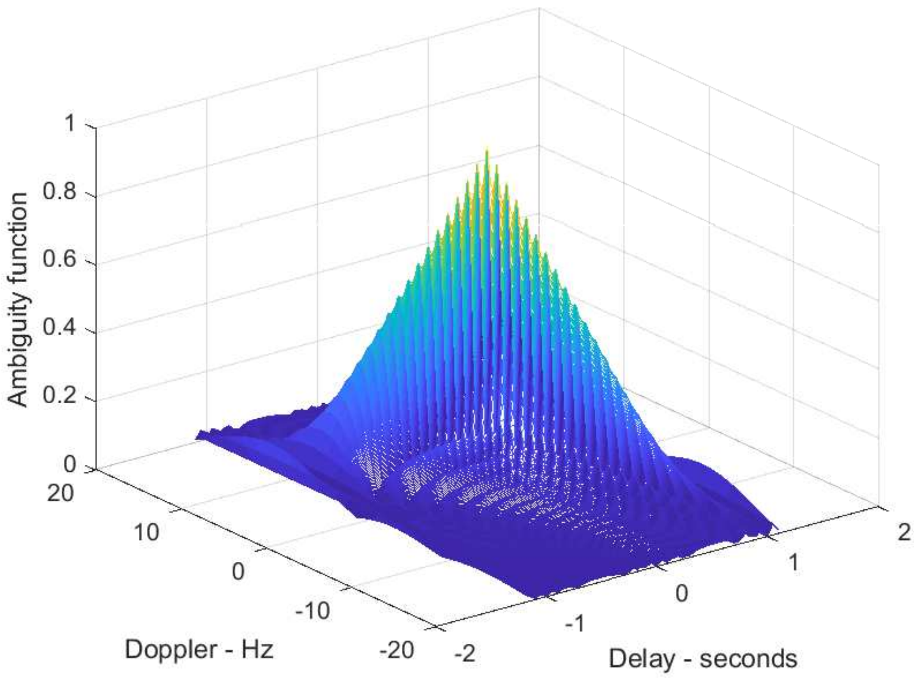

(a)

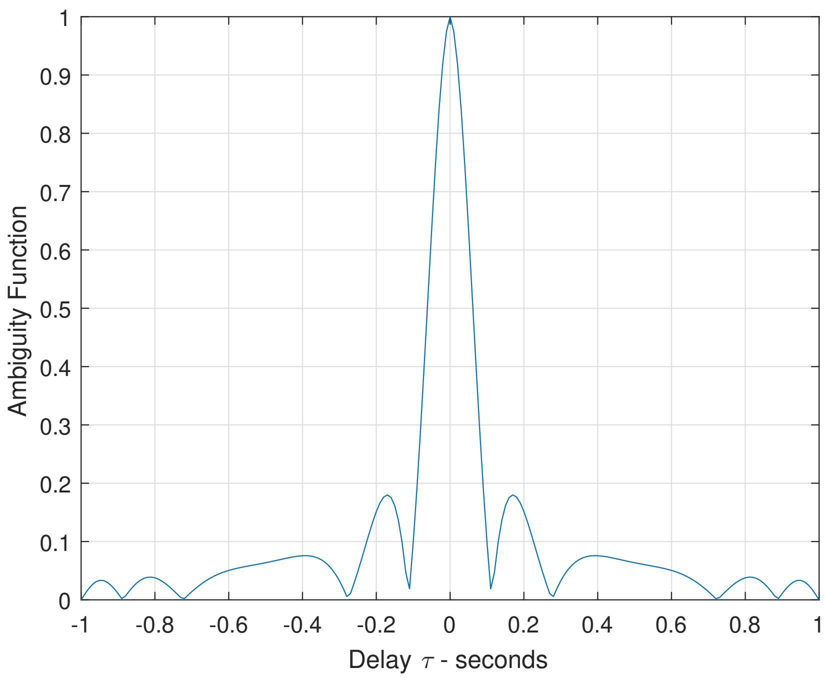

(b)

Figure 4.4: LFM Waveform (a) Ambiguity Function (b) Zero-Doppler cut of ambiguity function along delay axis

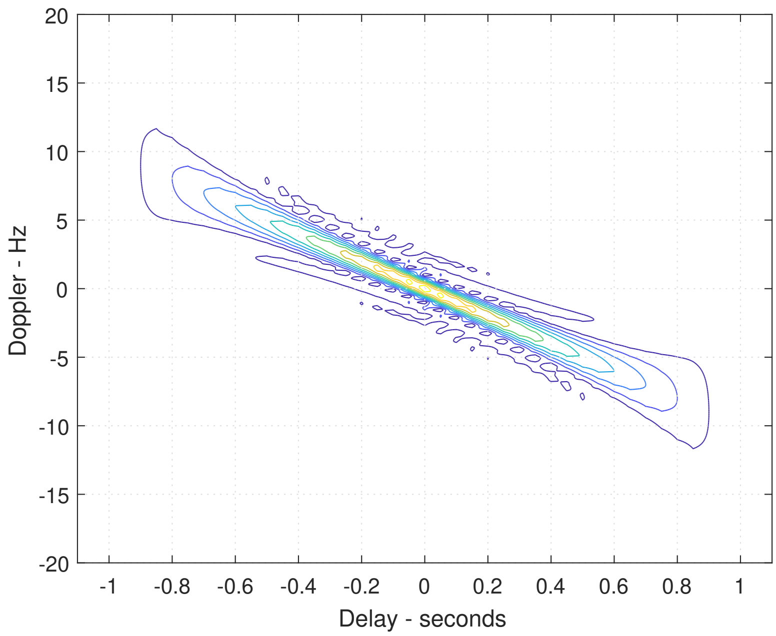

FIGURE 4.5: Contour Plot for Ambiguity Function of LFM Waveform

4.4.3 Phase Coded Waveform

In the case of phase-coded radar signals, a relatively long waveform of pulse duration T is divided into N smaller subpulses each of identical duration $T_s = \frac{T}{N}$. Each of these subpulses is coded with a different pulse code. The complex envelope of the phase-coded waveform [46] is represented by

$$x(t) = \frac{1}{\sqrt{T}} \sum_{n=1}^{N} x_n \mathrm{Rect}\left(\frac{t-(n-1)T_s}{T_s}\right) \tag{4.15}$$

where $x_n = \exp(j\phi_n)$ and a set of N number of phases $\{\phi_1, \phi_2, \ldots, \phi_N\}$ is the phase code for $x(t)$.

The autocorrelation function (which is an approximation of matched filter output or alternatively known as ambiguity function) of phase coded waveform is a continuous function with τ delay. The autocorrelation function properties are investigated with the condition $\tau < |T|$ for all values of τ. According to [46], it is sufficient to calculate ambiguity function at integral multiples of subpulse duration T_s.

Most popular among phase codes are Barker Codes, Zadoff-Chu codes, Frank codes, and P1, P2, P3, P4, and Px codes. The autocorrelation properties of binary-phase codes such as Barker codes are not good, as can be seen in Fig. 1.3 in chapter 1. Therefore, we use poly-phase codes like 4 and 8-phased Frank code and 4 and 8-phased P3 codes, for initiating the radar waveform in the proposed work.

4.4.3.1 Frank Codes

Frank codes possess phases with quadratic functions [40]. Frank codes are applicable only to the square lengths of the number of elements. We define the elements of a Frank code $s_n (1 \leq n \leq N)$ of a sequence length $N = L^2$ as

$$s_{(m-1)L+k} = \exp(j\Phi_{m,k}) \tag{4.16}$$

for $(1 \leq m \leq L)$ and $(1 \leq k \leq L)$, where

$$\Phi_{m,k} = 2\pi(m-1)(k-1)/L \tag{4.17}$$

The 16-element Frank code containing total number of elements, $N = 16$ and number of phases, $L = 4$ is given by

$$[\ 0 \quad 0 \quad 0 \quad 0 \quad 0 \quad \tfrac{\pi}{2} \quad \pi \quad \tfrac{3\pi}{2} \quad 0 \quad \pi \quad 0 \quad \pi \quad 0 \quad \tfrac{3\pi}{2} \quad \pi \quad \tfrac{\pi}{2}\ ] \tag{4.18}$$

Frank codes are used as initial sequences to generate the proposed SC-FDMA waveform as these provides low sidelobe peaks and good autocorrelation properties.

4.4.3.2 P3 Codes

In the proposed work we also use P3 codes as initial sequence as it exhibits good autocorrelation properties and offers good range and Doppler resolution [41]. Unlike Frank codes, P3 codes are applicable to any length N of the elements.

For any length N of P3 codes, the phase of P3 codes can be defined as

$$\Phi_n = \frac{2\pi}{N}\frac{(n-1)^2}{2} \tag{4.19}$$

The benefits of using P3 codes is that it does not apply any limitation on the length of code sequence and it offers high range and Doppler resolution. Fig.4.9 shows a 64-element P3 code signal with phase-time plot in (a) and frequency spectrum in (b). Fig.4.10 and Fig.4.11 show AF plots of 16-element P3 code.

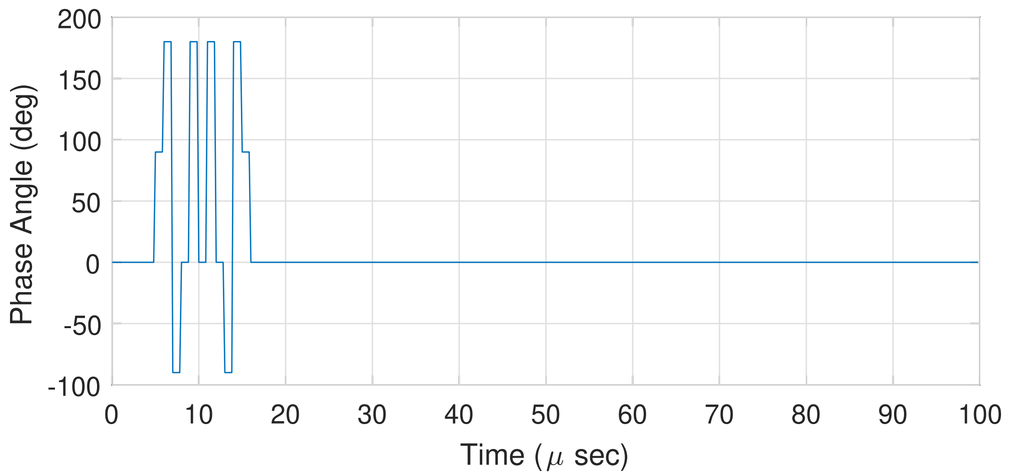

(a)

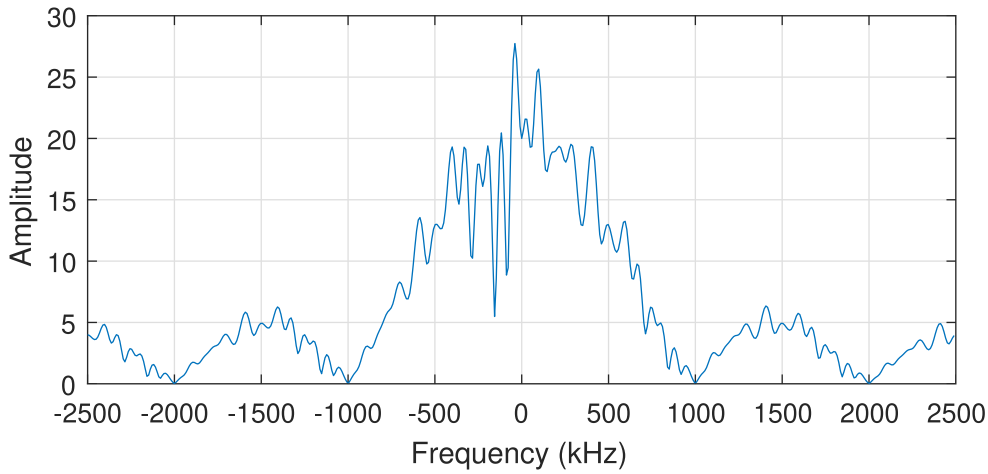

(b)

FIGURE 4.6: 4-Phased, 16-element Frank Code for phase coded pulse compression, single pulse (a) Phase Angle (b) Frequency domain signal (spectrum)

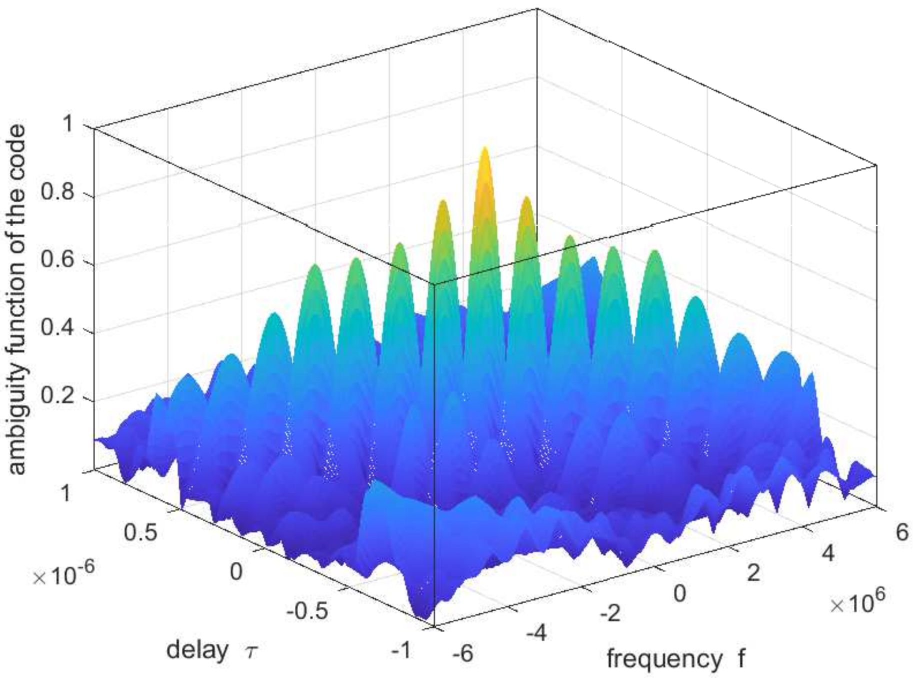

(a)

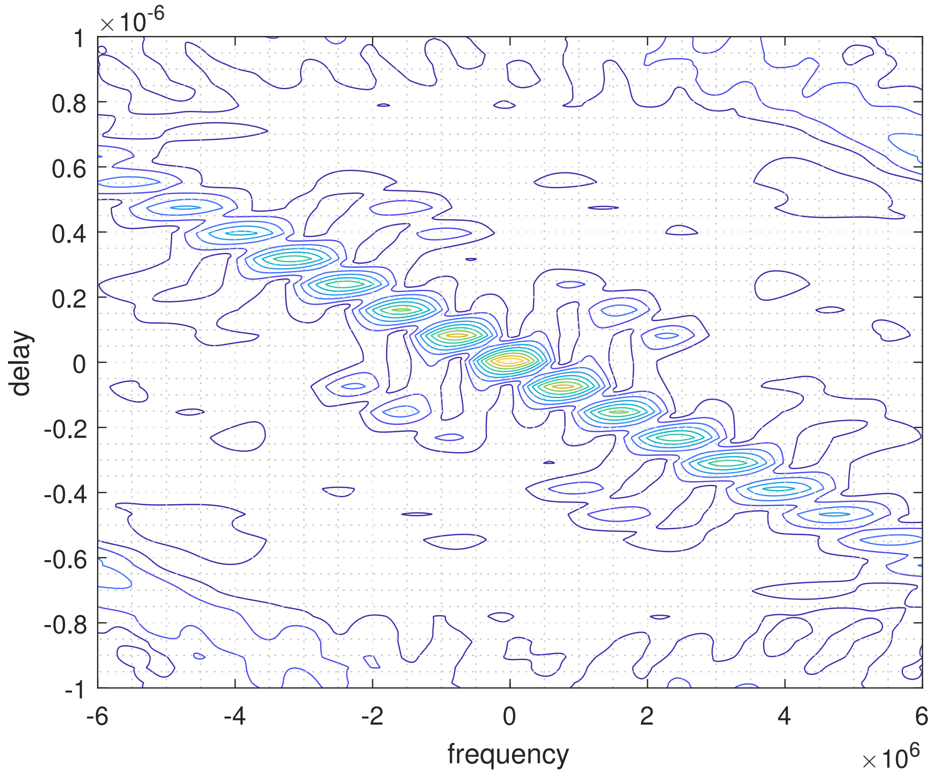

(b)

FIGURE 4.7: Ambiguity function plots for 4-phased Frank code of 16 elements a) 3-D Ambiguity diagram b) Contour plot of AF

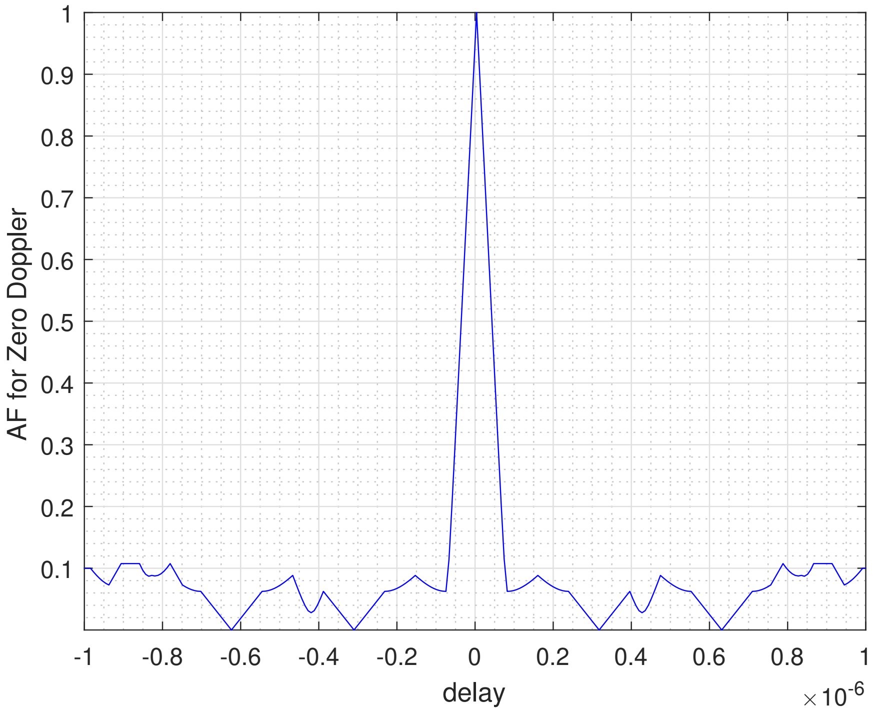

(a)

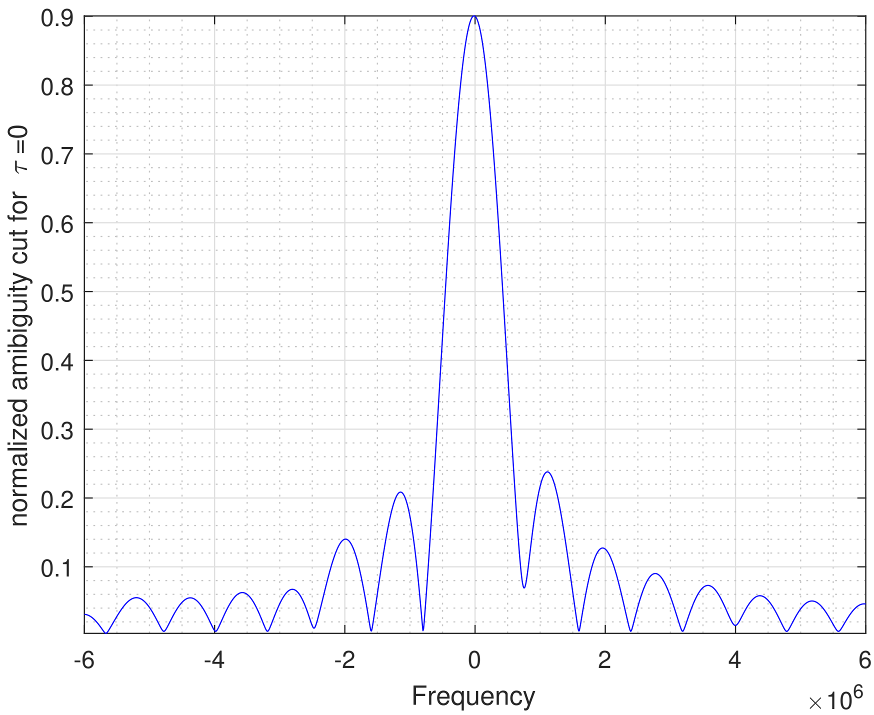

(b)

FIGURE 4.8: 4-phased Frank code with 16 elements a) Zero-Doppler cut of AF b) Zero-delay cut of AF

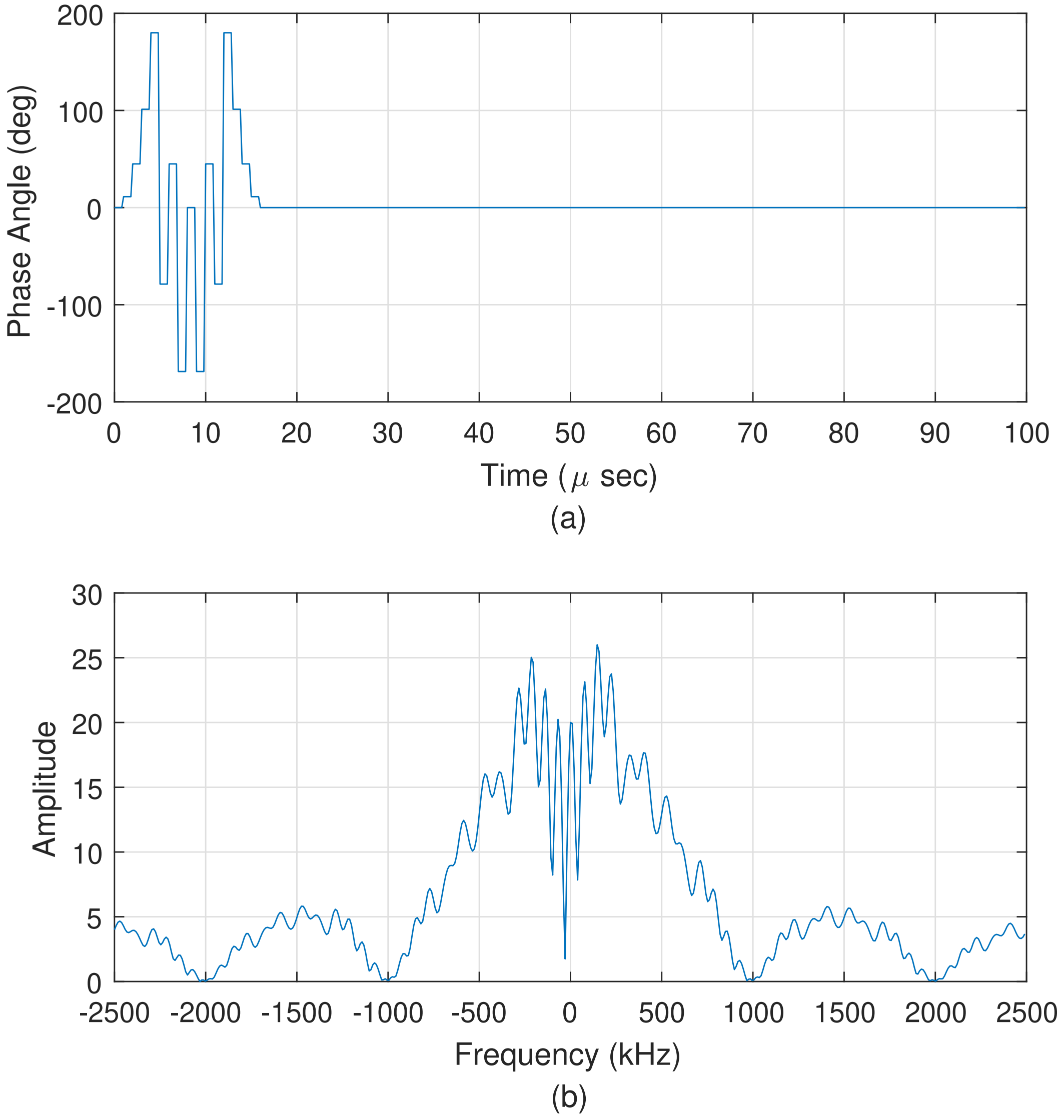

FIGURE 4.9: 64-Element P3 Code for phase-coded pulse compression a) Phase Angle in degrees vs time in *mu* seconds (b) Spectrum

4.5 Ambiguity Function of the Proposed SC-FDMA Waveform

For a complex baseband pulse signal $y(t)$, the ambiguity function [21] is defined by

$$\left|\tilde{A}(\tau,\, f_d)\right| = \left|\int_{-\infty}^{\infty} y(t)\, y^*(t-\tau)\exp(j2\pi f_d t)\, dt\right| \tag{4.20}$$

where $*$ denotes complex conjugate, τ represents time delay and f_d represents Doppler shift. The function for a zero-Doppler cut becomes the autocorrelation function of the waveform sequence as given below.

$$\left|\tilde{A}(\tau,\, 0)\right| = \left|\int_{-\infty}^{\infty} y(t)\, y^*(t-\tau)\, dt\right| \tag{4.21}$$

The single period ambiguity function of finite energy interleaved SC-FDMA signal of length T with periodic complex envelope is given as

$$\tilde{A}_T(\tau,\, f_d) = \frac{1}{T}\int_{0}^{T} y(t+\frac{\tau}{2})\, y^*(t-\frac{\tau}{2})\exp(j2\pi f_d t)\, dt \tag{4.22}$$

As we know that the reference signal $y(t)$ is of duration KT, the response of the correlation receiver is the ambiguity function for K periods which after normalization will be

$$\tilde{A}_{KT}(\tau,\, f_d) = \frac{1}{KT}\int_{0}^{KT} y(t+\frac{\tau}{2})\, y^*(t-\frac{\tau}{2})\exp(j2\pi f_d t)\, dt \tag{4.23}$$

The interleaved SC-FDMA signal is a periodic sequence of original signal $x(t)$ divided by K, therefore

$$\tilde{A}_T(\tau,\, f_d) = \frac{1}{K^2}\frac{1}{T}\int_{0}^{T} x(t+\frac{\tau}{2})\, x^*(t-\frac{\tau}{2})\exp(j2\pi f_d t)\, dt \tag{4.24}$$

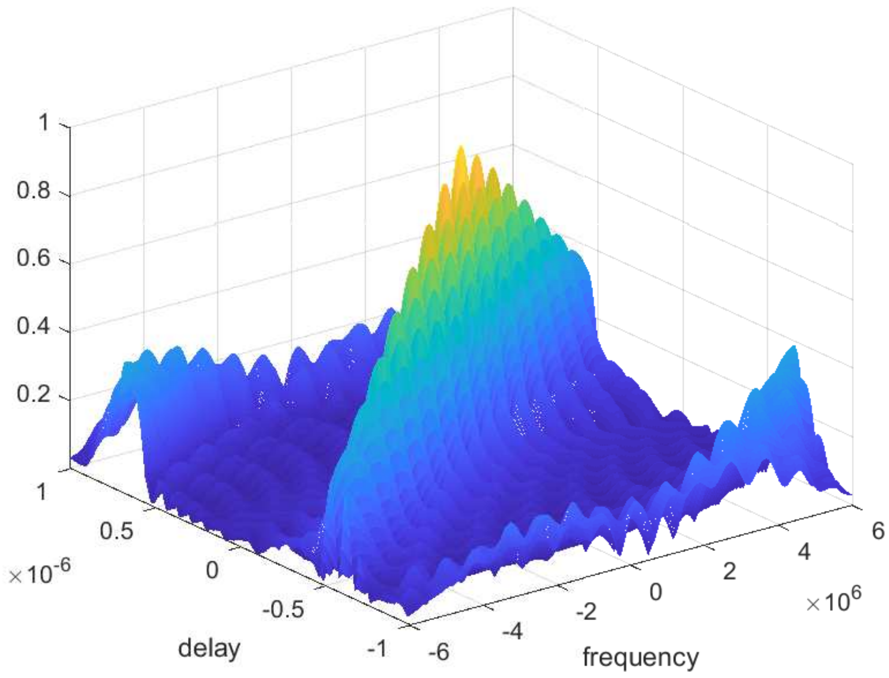

(a)

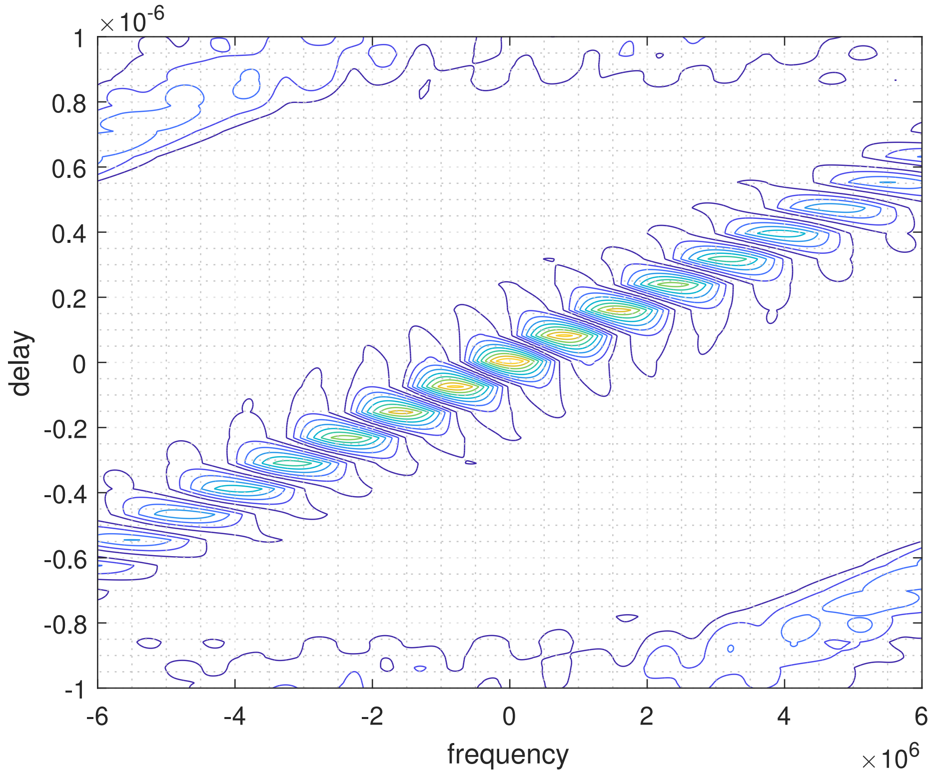

(b)

FIGURE 4.10: Ambiguity function plots for 16-Element P3 code, a) 3-D ambiguity diagram b) Contour plot of AF

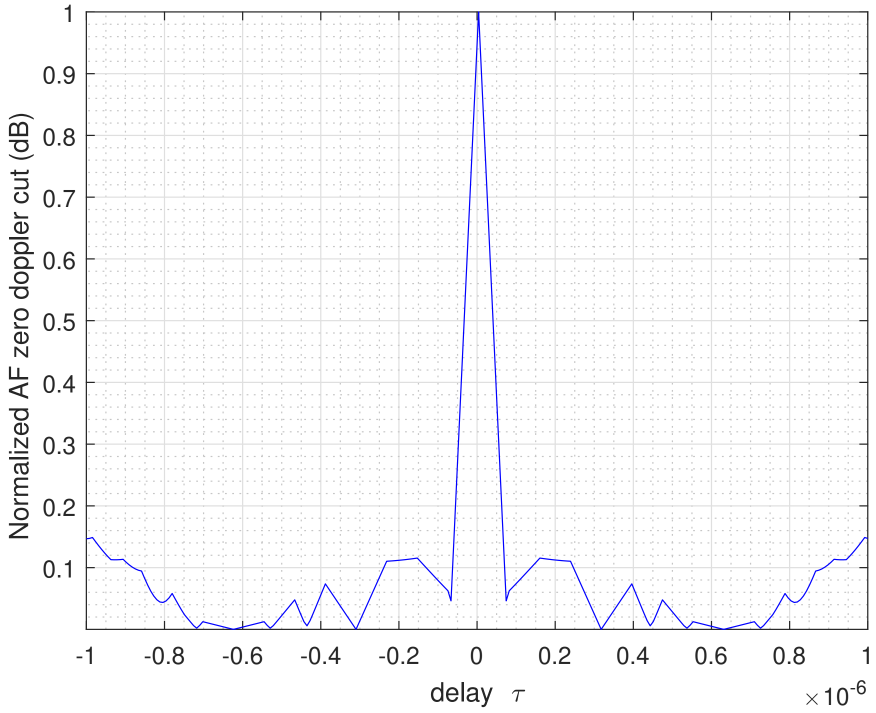

(a)

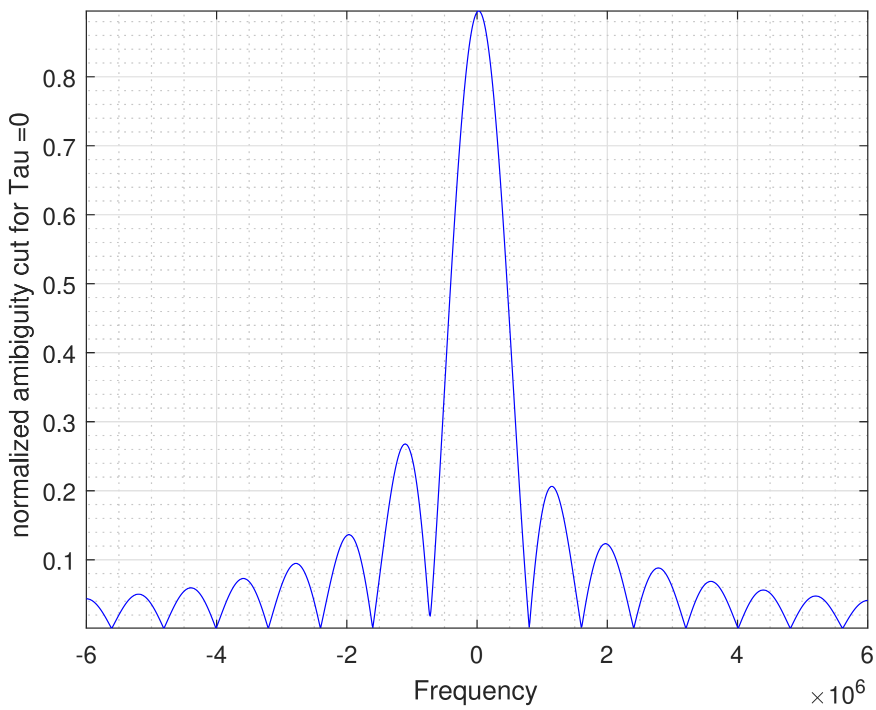

(b)

FIGURE 4.11: 16-Element P3 code, a) Zero-Doppler cut of AF b) Zero delay cut of AF

Dividing the integral in equation (4.23) into K sections and substituting for $y(t)$

$$\tilde{A}_{KT}(\tau,\, f_d) = \frac{1}{K^3T} \sum_{k=1}^{K} \int_{(k-1)T}^{kT} x(t+\frac{\tau}{2}) \times x^*(t-\frac{\tau}{2}) \exp(j2\pi f_d t)\, dt \tag{4.25}$$

by substituting $t = t' + (k-1)T$ in equation (4.25) we get

$$\tilde{A}_{KT}(\tau, f_d) = \frac{1}{K^3T} \sum_{k=1}^{K} \int_{0}^{T} x(t'+(k-1)T+\frac{\tau}{2}) x^*(t'+(k-1)T-\frac{\tau}{2}) \exp[j2\pi f_d(t'+(k-1)T)]\, dt' \tag{4.26}$$

Since the transmitted signal is periodic i.e. $x(t' \pm \frac{\tau}{2}) = x(t' + (k-1)T \pm \frac{\tau}{2})$, then we have

$$\tilde{A}_{KT}(\tau, f_d) = \frac{1}{K} \sum_{k=1}^{K} \exp[j2\pi f_d(k-1)T] \times \frac{1}{K^2T} \int_{0}^{T} x(t'+\frac{\tau}{2})\, x^*(t'-\frac{\tau}{2}) \exp(j2\pi f_d t')\, dt' \tag{4.27}$$

$$\tilde{A}_{KT}(\tau,\, f_d) = \frac{1}{K}\, \tilde{A}_T(\tau,\, f_d) \sum_{k=1}^{K} \exp[j2\pi f_d(k-1)T] \tag{4.28}$$

$$\tilde{A}_{KT}(\tau,\, f_d) = \frac{1}{K} \tilde{A}_T(\tau,\, f_d) \frac{1-\exp[j2\pi f_d KT]}{1-\exp[j2\pi f_d T]} \tag{4.29}$$

$$\tilde{A}_{KT}(\tau,\, f_d) = \tilde{A}_T(\tau,\, f_d) \frac{\sin(\pi f_d KT)}{K\sin(\pi f_d T)} \exp[j\pi f_d(K-1)T] \tag{4.30}$$

Now we have the AF, given as

$$\left|\tilde{A}_{KT}(\tau,\, f_d)\right| = \left|\tilde{A}_T(\tau,\, f_d)\right| \left|\frac{\sin(\pi f_d KT)}{K\sin(\pi f_d T)}\right| \tag{4.31}$$

Simulations are performed to obtain ambiguity functions of OFDM and SC-FDMA waveforms to analyze and compare their performance in radar applications.

The ambiguity function has been determined by numerical method which is given by;

1. Calculating Fourier transforms of $y(t)$ and $y^*(t)\exp(j2\pi f_d t)$ for different values of f_d.

2. After taking Fourier transform we get the frequency domain of these signals. These frequency domains are multiplied with each other and we get the Fourier transform of the ambiguity function.

3. In next step, ambiguity function is obtained by taking inverse Fourier transform.

In an ambiguity function plot, there is always a main ridge resulting from the autocorrelation operation. The width of this ridge defines the ability of the waveform to resolve a target. The smaller the width of the ridge, the higher will be the resolution of the radar waveform. Ambiguity diagrams sometimes have grating lobes resulting from the repetitive pattern of the waveform. These grating lobes need to be diminished or removed completely to avoid the possibility of a close-by false target or their interference with the return signal from a true close-by target. Other than the grating lobes, the immediate sidelobes also become a trouble in the measurement of target range parameters. Therefore, sidelobes are needed to be reduced as much as possible.

Fig. 4.12 and 4.13 show AF plots for OFDM and the proposed SC-DMA for Frank-16 each with 32 subcarriers with pulse width and the chip width of 6.250×10^{-5} s and 1.95×10^{-6} s respectively. In the case of SC-FDMA, the bandwidth spreading factor is 2 i.e. the sequence of 16 coded symbols is repeated 2 times in time domain multiplied by a scaling factor of $1/2$. The plots in Fig. 4.12 and 4.13 show diagonal ridges which are due to the selection of Frank code as the base signal in both OFDM and SC-FDMA. The width of these ridges along the delay axis represents range resolution. It is clear from Fig. 4.12 & 4.13 that the width of the major ridge in the proposed SC-FDMA signal is lesser than that of the OFDM plot. It is therefore inferred that the range resolution of Sc-FDMA radar is higher than OFDM radar for the same number of multiplexed subcarriers.

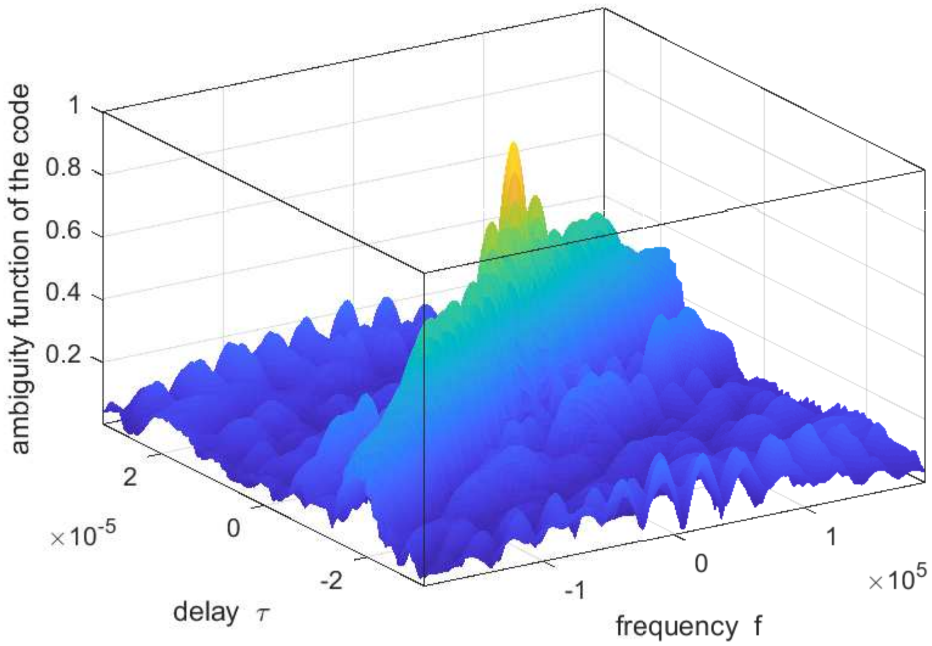

(a)

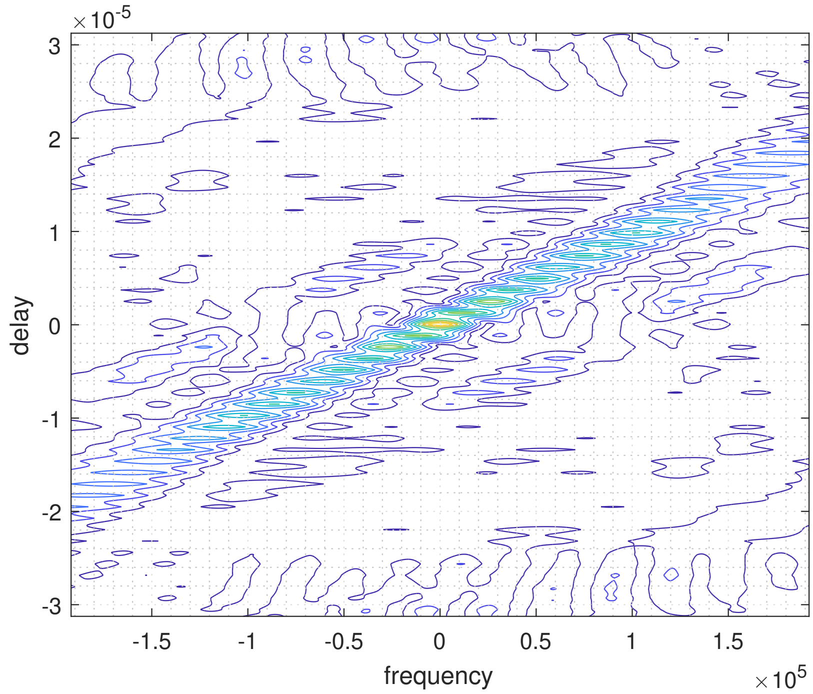

(b)

FIGURE 4.12: Ambiguity function plots for 4-phased 16-element Frank sequence with 32 OFDM subcarriers (a) 3-D ambiguity plot (b) Contour plot

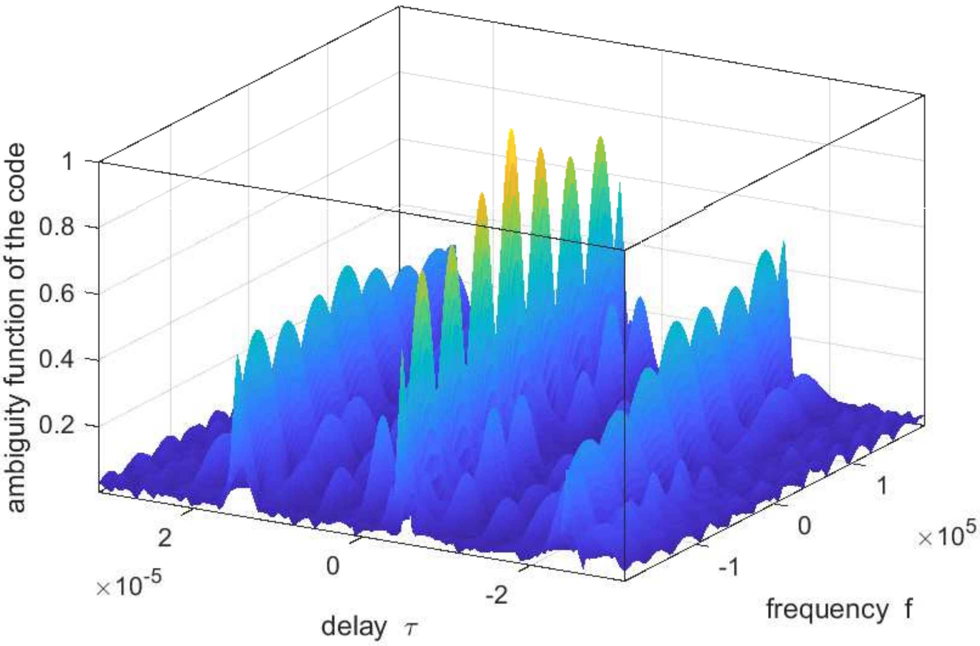

(a)

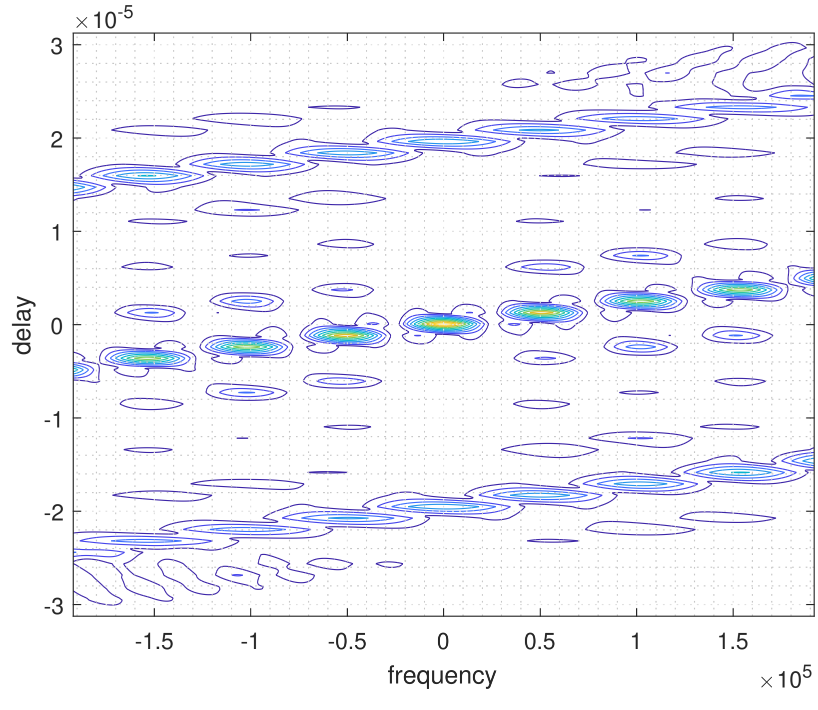

(b)

FIGURE 4.13: Ambiguity function plots for 4-phased 16-element Frank sequence with 32 subcarriers of the proposed SC-FDMA waveform (a) 3-D ambiguity plot (b) Contour plot

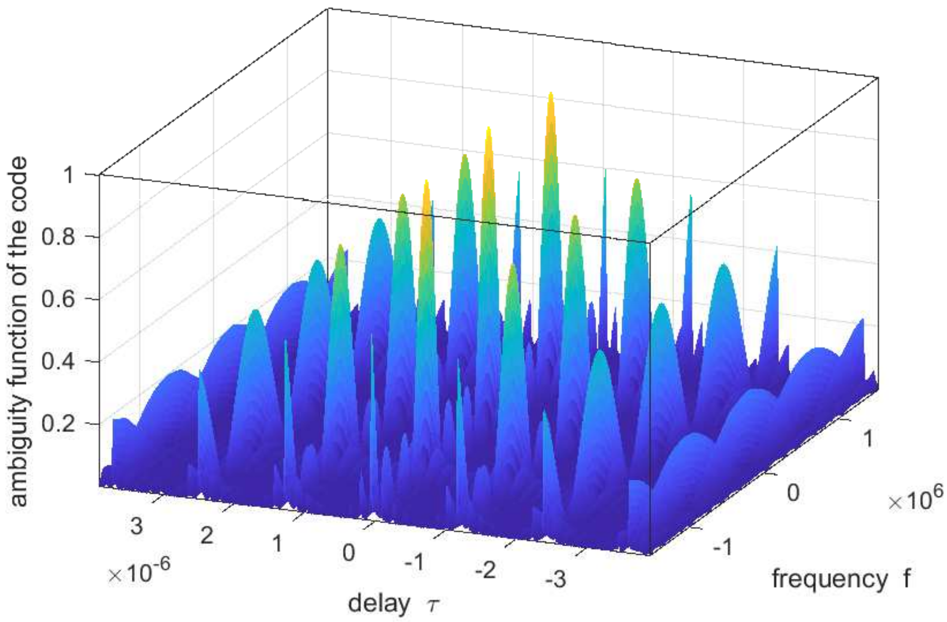

(a)

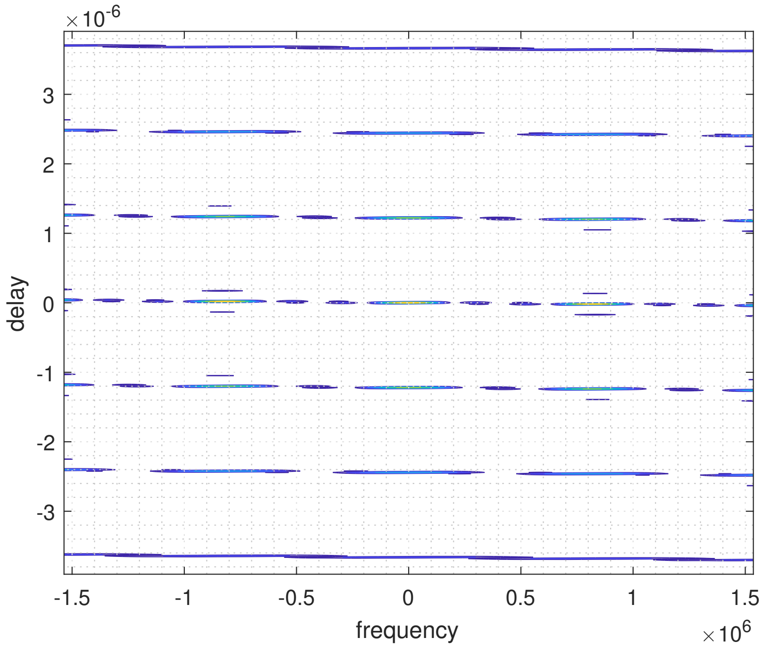

(b)

FIGURE 4.14: Ambiguity function plots for 8-phased 64-element Frank sequence with 256 subcarriers of proposed SC-FDMA waveform (a) 3-D ambiguity plot (b) Zero-Doppler cut ambiguity plot

Fig. 4.14 shows AF plots for the proposed SC-FDMA for the Frank-64 sequence multiplexed with 256 subcarriers. The pulse width and the chip width are $7.8 \times$

10^{-6} s and 3.05×10^{-8} s respectively. The bandwidth spreading factor is 4, i.e. the 64 code symbols are repeated 4 times in the time domain. The plots in Fig. 4.14 show that the range resolution of the proposed SC-FDMA waveform increases as the number of subcarriers (mapped to the base signal) increases.

4.6 Autocorrelation Properties

In addition to orthogonality, good auto-correlation properties of a waveform are required for many radar applications. Good auto-correlation means that a transmitted waveform is uncorrelated to the time-shifted versions of itself. If a transmitted waveform exhibits good auto-correlation properties then the matched filter at the receiver can easily extract the backscattered signal for a given range bin and attenuates backscattered signals of other range bins. The auto-correlation function r of a complex valued radar waveform $y(t)$ is given in (4.21).

Fig. 4.15 shows the autocorrelation function of the unimodular signal generated by using CAN (Cyclic Algorithm-New) proposed by Jian Li *et al.*, in their work in [172] for a MIMO radar with 40 subsequences. It is compared with the proposed SC-FDMA signal with 40 elements generated by the P3 code of 20 elements as initial sequence (40 subcarriers are used for mapping the 20 frequency domain elements of P3 code sequence). It is clear from the figure that the proposed signal exhibits better auto-correlation properties as compared to the signal in [172] except at recurring grating lobe points.

In Fig. 4.16, the autocorrelation properties of a 100-element long waveform, PWCIA (Periodic Correlation Weighted Cyclic Iteration Algorithm) generated by a sequence of 8 phases proposed by Ze Li *et al. in* [174] are compared with our proposed 128-element long, 8-phase SC-FDMA waveform initiated by 64-element Frank code; each with a chip width of $1\mu s$. The plots show that the autocorrelation of our waveform is better than that of the PWCIA waveform except at the recurring grating lobe points.

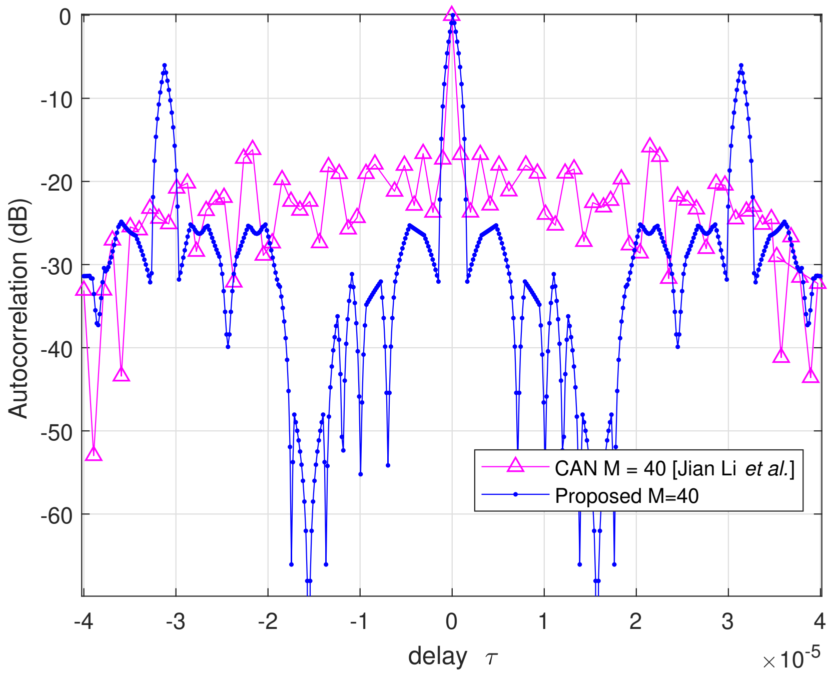

FIGURE 4.15: Auto-correlation of CAN sequence [172] with number of elements M=40 compared with the proposed SC-FDMA waveform, initially using P3 code with number of initial sequence N=20 and number of subcarriers M=40.

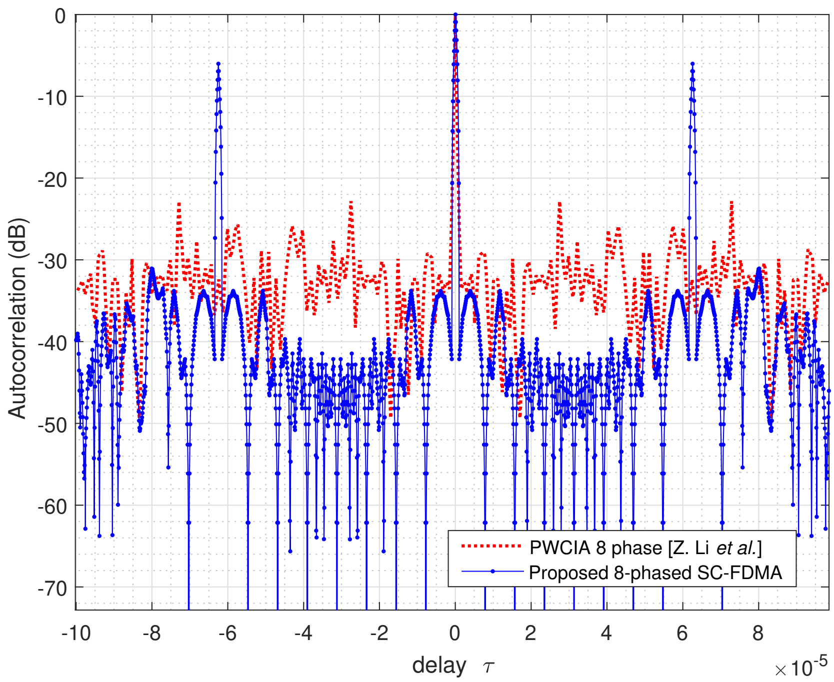

FIGURE 4.16: Autocorrelation of 8-phased PWCIA waveform [174] and the proposed 8-phased SC-FDMA waveform.

4.6.1 Occurrence of Recurrent (Grating) Lobes in SC-FDMA Radar and their Removal

It is observed from Fig. 4.15, & 4.16, that the occurrence of recurring lobes is a serious issue in the autocorrelation of SC-FDMA waveform and thus needs a handful solution. Their position can be predicted intuitively by examining the AF of the proposed SC-FDMA waveform. These occur at the points where secondary diagonal ridges cross the zero Doppler axis in an AF diagram. The presence of secondary ridges is due to the periodicity in the waveform.

We remove these recurrent lobes by adopting the method proposed in [182]. The approach proposed by the authors is based on overlaying an orthogonal coding sequence over a pulse train in which a signal is repeated periodically after a fixed Pulse Repetition Interval (PRI). For a train of K identical pulses of duration KT, the basic pulse of duration T is divided into N slices with a width $T_s = T/N$. In our case, we are dealing with a long pulse of duration KT in which a basic sequence of duration T repeats K times subsequently. We consider T_s as the duration of a single element of the original initial sequence. Each slice is further encoded by the elements of an orthogonal phase-coded scheme represented by $K \times N$ matrix A. In this matrix K rows represent the coding sequence used for K sub-pulses in the main pulse. The new overlaid signal is then given by

$$y(t) = \sum_{k=0}^{K-1} \sum_{n=0}^{N-1} a_{k,n} \frac{1}{K} x_n g[t - (n + kN)T_s] \tag{4.32}$$

where $a_{k,n}$ represents an element of the matrix A and is used to code the nth slice in the kth sequence in the main pulse is given by.

$$a_{k,n} = \exp(j\phi_{k,n}) \tag{4.33}$$

where $\phi_{k,n}$ is the nth phase state of the kth phase-coded sequence.

The matrix A is given as

$$A = \begin{bmatrix} a_{0,0} & a_{0,1} & \cdots & a_{0,n} & \cdots & a_{0,N-1} \\ a_{1,0} & a_{1,1} & \cdots & a_{1,n} & \cdots & a_{1,N-1} \\ & & \ddots & & & \vdots \\ a_{k,0} & \cdots & \cdots & a_{k,n} & \cdots & a_{k,N-1} \\ \vdots & & & \vdots & \ddots & \vdots \\ a_{K-1,0} & \cdots & \cdots & a_{K-1,n} & \cdots & a_{K-1,N-1} \end{bmatrix} \tag{4.34}$$

The grating lobe removal method is solely for radar systems. It was originally utilized by N. Levanon et al. [182] for the repeated pulses in a radar pulse train in order to prevent grating lobes in autocorrelation and ambiguity function graphs. We adopted this method of grating lobe removal that is raised from the repetitive pattern within a single pulse in the proposed ISC-FDMA radar waveform.

Fig. 4.17 shows the same CAN autocorrelation signal plotted in Fig. 4.15 compared with the modified proposed waveform after removal of its grating lobes. Similarly in Fig. 4.18, the PWCIA waveform is compared with the modified proposed waveform after resolving the grating lobes issue. The recurrent grating lobes are removed from the autocorrelation of the signal in a very elegant way so that autocorrelation properties of the originally proposed waveform are improved.

Fig. 4.19, shows the autocorrelation of OFDM waveform, the proposed SC-FDMA waveform, and the proposed SC-FDMA waveform after removing grating lobes; Each waveform contains 64 element in initial Frank phase-coded sequence which are multiplexed with 128 subcarriers (N=64, M=128) and the final pulse is 128 elements long. It is clear from the figure that the autocorrelation properties of our proposed waveform are better than that of the OFDM signal.

In Fig. 4.20, the autocorrelation of our proposed waveform of length 256, generated by 4-phase, 16-element, Frank code is compared with the piecewise nonlinear frequency-modulated waveform proposed in [169]. It is clear from the plots that the peak to sidelobe ratio of our proposed waveform is pretty high as compared to the reference waveforms.

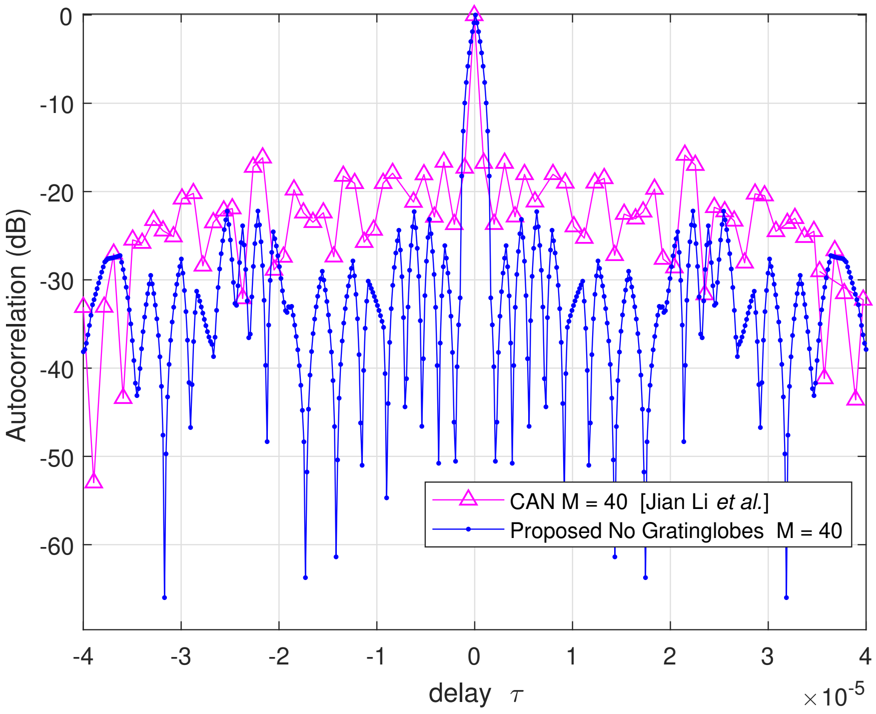

FIGURE 4.17: Auto-correlation of CAN sequence [172] with number of elements M=40 compared with the proposed SC-FDMA waveform after removing grating lobes initially using P3 code with number of initial sequence N=20 and number of subcarriers M=40.

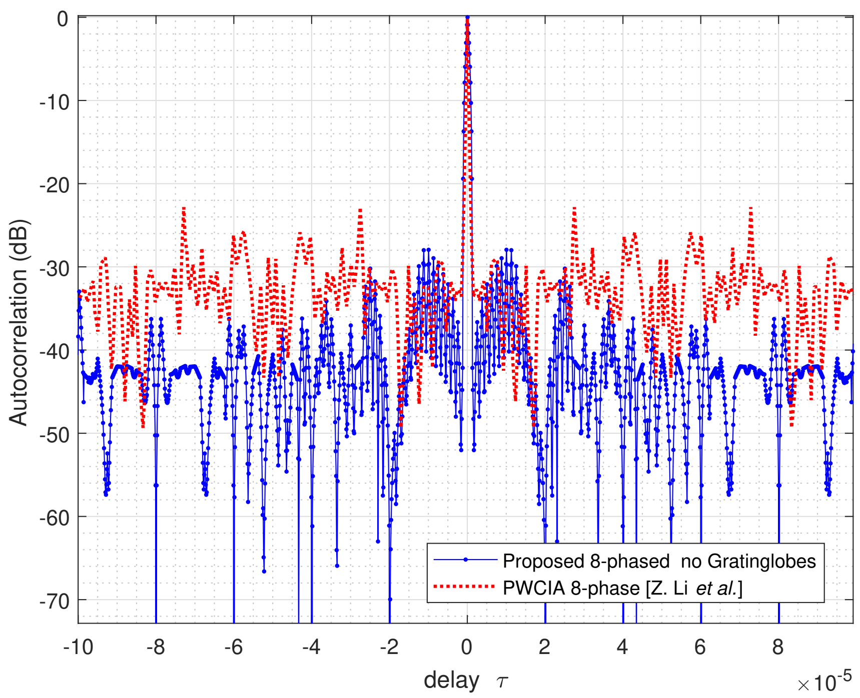

FIGURE 4.18: Autocorrelation of PWCIA waveform with 8-phases and 100 subsequences [174] verses the proposed 8-phased SC-FDMA waveform when grating lobes are resolved.

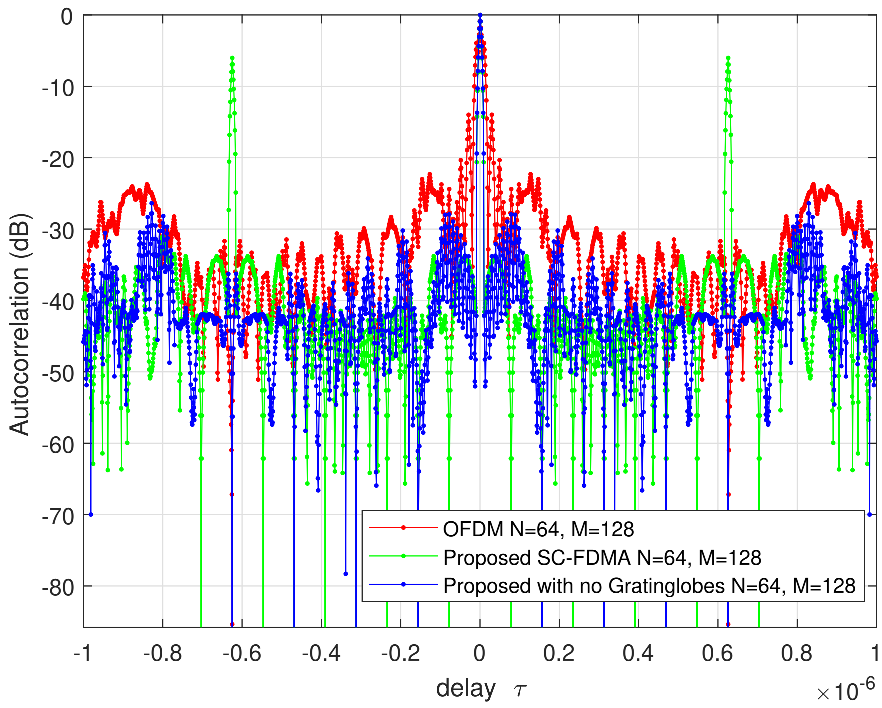

Figure 4.19: Autocorrelation of OFDM waveform and the proposed SC-FDMA waveform before and after the removal of grating lobes; each waveform contains N=64, and M=128.

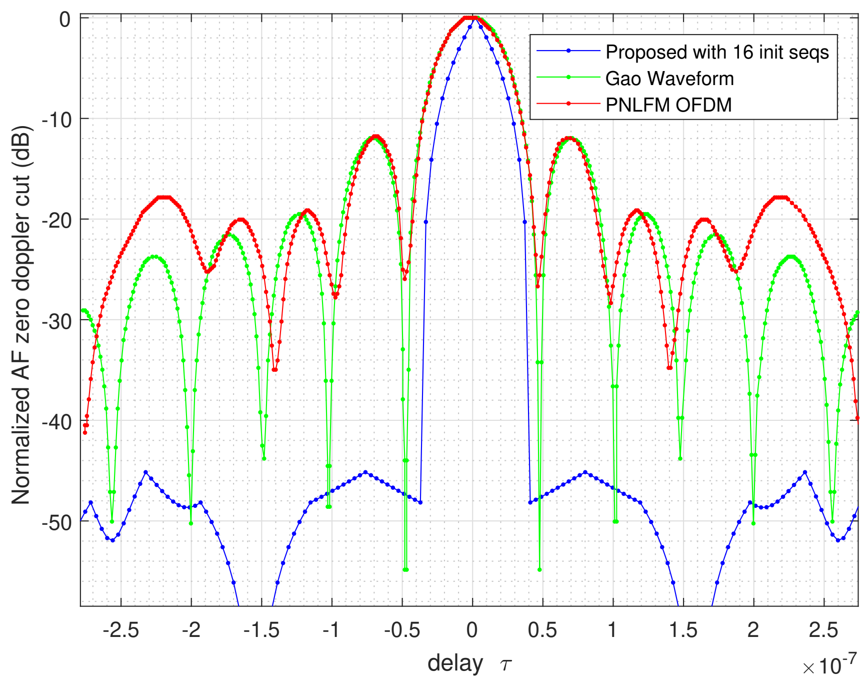

Figure 4.20: Autocorrelation of PNLFM [169] and Gao's waveforms verses autocorrelation of the proposed 4-phase SC-FDMA with 256 subcarriers and 16 initial sequences, zoomed on delay axis with pulsewidth $=8\mu s$.

4.6.2 Peak-to-Sidelobe Ratio

In an auto-correlated signal, peak-to-sidelobe ratio is an important parameter when analyzing a waveform. This relation is given by

$$\mathrm{PSR} = 10\log_{10}\frac{|r_o|^2}{|r_{\mathrm{SL}}|^2} \tag{4.35}$$

where r_o is the peak value and r_{SL} is sidelobe value of autocorrelation function of the waveform $x(t)$ and is given as,

$$r_{\mathrm{SL}} = \max\{r_m\}_{m=1}^{M-1} \qquad m \neq 0 \tag{4.36}$$

where

$$r_m = \left| \frac{1}{K^2}\frac{1}{T}\int_0^T x(t+\frac{mT_s}{2})\, x^*(t-\frac{mT_s}{2})\exp(j2\pi f_d t)dt \right| \tag{4.37}$$

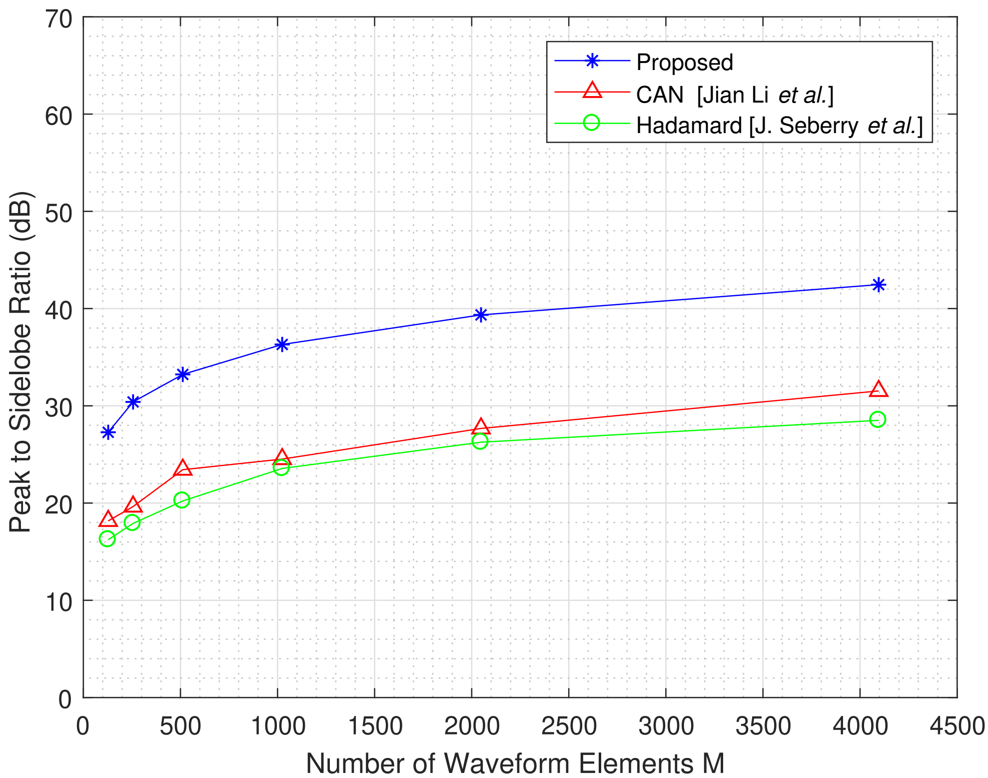

FIGURE 4.21: Sidelobe peaks against the number of waveform elements for the waveforms generated by CAN algorithm [172], waveform generated by Hadamard sequence [183] and the proposed SC-FDMA.

In Fig. 4.21, sidelobe peaks of the proposed SC-FDMA waveform are plotted against the number of waveform elements for $M = 128, 256, 512, 1024, 2048, 4096$. The behavior of these peaks is then compared with the trend shown by the sidelobe peaks of CAN [172] and Hadamard sequence [183]. For these plots, the Hadamard sequence is scrambled with the PN (pseudo-noise) sequence to reduce its correlation sidelobes. It is clear from the comparison, that our proposed waveform exhibits very low sidelobe peaks as compared to the other two waveform sequences.

4.7 Peak-To-Average Power Ratio (PAPR) of a Multicarrier Radar

In multicarrier systems, such as OFDM, the signal usually has a fluctuating envelope that limits the power efficiency of the radar transmitter amplifier. The measure of the envelope variations in a signal is given by Peak-to-Average Power Ratio (PAPR) which is a ratio of the instantaneous peak power of the signal to the average signal power. For a multicarrier signal $s(t)$, the mathematical expression for the PAPR is given by

$$\mathrm{PAPR} = \frac{\max(|s(t)|^2)}{\frac{1}{T}\int_0^T |s(t)|^2 \, dt} \tag{4.38}$$

where T is the duration of the signal.

In multicarrier radar systems, such as OFDM radar, the high PAPR produces signal excursions into the nonlinear operation region of the High Power Amplifier (HPA) of the transmitter. This results in nonlinear distortions leading to inter-carrier interference and spectral spreading [146]. It is, therefore, necessary to use linear amplifiers in the transmitters [147] which are difficult to be employed in radars especially in airborne or vehicular applications where power is a constraint. Therefore, the peak-to-average power ratio must be controlled in these systems.

4.8 Interleaved SC-FDMA: A Constant-Envelope Waveform

The proposed interleaved SC-FDMA (ISC-FDMA) waveform aims at reducing the time-domain fluctuations of the signal, as already discussed in chapter 2. While generating the waveform in the SC-FDMA radar, the DFT operation is incorporated prior to the IDFT, similar to the coding method that is performed to reduce the PAPR of the multicarrier waveforms, as already discussed in section 2.1. In the proposed SC-FDMA waveform, the interleaved subcarrier mapping converts the overall signal into a constant envelope time-domain signal.

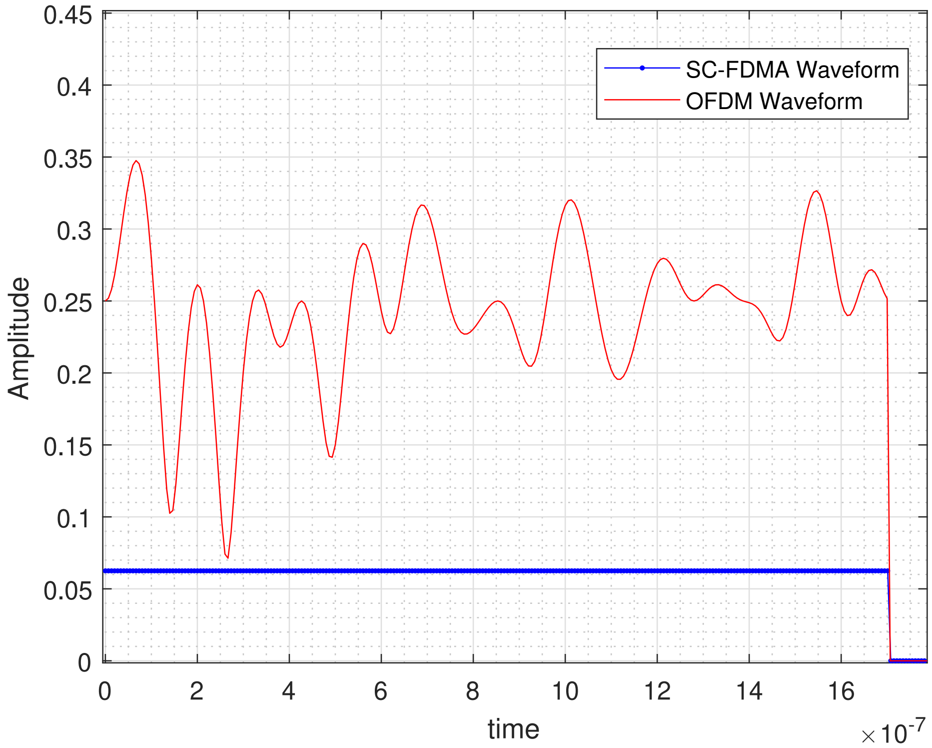

FIGURE 4.22: Waveforms generated by SC-FDMA and OFDM radars with 256 subcarriers by using 4-phased 16-element Frank code as the initial sequence.

The Fig. 4.22 shows the amplitude comparison between the proposed interleaved SC-FDMA time-domain radar signal and the OFDM time-domain radar signal. Both of these signals are generated by using 256 subcarriers with a 16 element Frank code as initial sequence. The OFDM signal in the plot exhibits a chaotic fluctuating envelope with a PAPR of 2.86 dB and follows an approximately random amplitude distribution. The high PAPR limits the efficiency of the HPA of the transmitter by causing nonlinear distortions. In the same figure, the proposed interleaved SC-FDMA signal exhibits a constant envelope resulting in a PAPR value of almost 0 dB. The constant amplitude of the proposed signal eliminates the issue of nonlinear distortion of the transmitter HPA. Therefore, for such radar systems, the transmitter power can be increased to extend the detection range of the radar without compromising the performance efficiency of the transmitter HPA.

4.9 PAPR Analysis of the Proposed SC-FDMA, OFDM and Other Notable Waveforms with Phase-Coded Sequences

In this section, we computed and compared the PAPR values of the proposed interleaved SC-FDMA and OFDM waveforms for different fixed-valued phase-coded initial sequences by using 32 subcarriers as given in Table.4.1. The phase-coded waveforms include Pseudo Random Number (PRN), Frank, Zadoff-Chu, Barker, P1, P3, and Px codes with different code lengths and phase values.

The results given in Table 4.1, show that the PAPR of the proposed Interleaved SC-FDMA is 0 dB for those code sequences in which the number of the subcarriers is an integral multiple of the code length. In addition to this, the PAPR of the proposed waveform has non-zero (though very small) values when the subcarrier number is not the integral multiple of the length of initial sequences. Taking into account the overall results presented in Table.4.1, it is observed that PAPR values of each of the proposed interleaved SC-FDMA signals, generated by using different initial sequences, are much lower than those of the OFDM signals.

Table. 4.2 presents the computed values of the PAPR of the proposed SC-FDMA waveforms in comparison with the unimodular sequences proposed in [172] and

[174] and piecewise nonlinear frequency modulated (PNLFM) signals proposed in [169]. Though the autocorrelation properties of the PNLFM waveform [169], as discussed in chapter 4, are good; however, its PAPR is 3dB which is quite high as compared to the proposed Interleaved SC-FDMA waveform. PAPR of the unimodular sequences of [172] and [174] is 0 dB due to their constant envelope structure which is same as that of our proposed waveform; however, the proposed waveform exhibits better auto-correlation properties as compared to these waveforms, as already discussed in Sec 4.6.

SN	Waveform	Code Length	OFDM PAPR (dB)	Proposed Interleaved SC-FDMA PAPR (dB)
1	PRN	15	4.8072	0.2803
2	Frank	4	2.4753	0
3	Frank	16	2.5859	0
4	Zadoff-Chu	8	2.3226	0
5	Zadoff-Chu	16	2.4473	0
6	Barker	2	3.0103	0
	Barker	3	3.0103	0
7	Barker	11	6.9897	5.0515
8	Barker	13	9.5424	2.4988
9	P1	16	2.5859	0
10	P3	16	2.4473	0
11	Px	4	3.0103	0
12	Px	16	2.3226	0

Table 4.1: PAPR values of the Proposed ISC-FDMA and OFDM radar waveforms with fixed phase-coded sequences.

SN	Waveform	PAPR (dB)
1	OFDM with Frank16, M=32	2.5859
2	PNLFM [169]	3
3	CAN [172]	0
4	PWCIA [174]	0
5	Proposed Interleaved SC-FDMA with Frank-16, M=32	0
6	Proposed Interleaved SC-FDMA with Frank-64, M=128	0

Table 4.2: PAPR comparison between the proposed waveform and those of the notable waveform signals given in [169], [172], and [174]

In case of random modulation sequences, there is statistical approach to find PAPR which is characterized by the *complementary cumulative distribution function* (CCDF). The CCDF function is the likelihood that a given PAPR is greater than a certain PAPR value Z_o, i.e. Prob[PAPR $>$ Z_o]. Z_o is also known as PAPR threshold. Generally, in SC-FDMA systems, two methods are used for the subcarrier mapping i.e. *localized subcarrier mapping* and *interleaved subcarrier mapping,* as already discussed in chapter. On the basis of these mapping schemes, SC-FDMA is subdivided into Interleaved SC-FDMA (ISC-FDMA) and Localized SC-FDMA (LSC-FDMA) waveforms. The proposed ISC-FDMA waveform, while outperforming the OFDM and LSC-FDMA, provides 0 dB PAPR over the range of all probabilities of given random modulation sequences such as BPSK, QPSK, and 8PSK [121]. To avoid the repetition of any previous published work, we did not include the CCDF plots of the random phase coded waveforms in this thesis.

Consequent upon the observations made in Sec. 4.8 and 4.9, it can be inferred that the proposed Interleaved SC-FDMA waveform is the most suitable waveform for multicarrier radar systems in term of achieving minimum possible PAPR. This will enable the power amplifier of the radar transmitter to utilize its maximum capability without compromising its power efficiency and consequently extend the detection range of the radar many folds.

Chapter 5

SC-FDMA Radar: Target Parameter Estimation

In this chapter, an end-to-end SC-FDMA Radar is evaluated for practical consideration. The proposed SC-FDMA radar is investigated for target detection and parameter estimation. The performance of the proposed radar is evaluated and compared with other radars using LFM and OFDM waveforms for range and Doppler estimation. For this purpose, an end-to-end monostatic radar has been simulated in MATLAB®by using the proposed SC-FDMA waveform with different polyphase codes including Frank and P3 codes. Section 5.1 describes the end-to-end radar simulation model. Section 5.2 gives the simulation setup and section 5.3 provides simulation results for four different simulation scenarios.

5.1 Radar Simulation Model

The main objective of radar is target detection and parameter estimation. The major parameters include the range and velocity of the target along with their resolutions. A generalized monostatic radar transmits a pulse of fixed duration with a constant or variable transmission rate known as fixed or staggered pulse repetition frequency (PRF) respectively. The reciprocal to the PRF is the pulse repetition interval (PRI) which is the interval in which a pulse is repeated. After the transmission of pulse, the radar switches to listening mode. The pulse after hitting a remote target is returned back towards the radar as an echo. The echo contains the information of the target. After receiving the echo, the radar performs signal processing and retrieves the information of the range and speed of the target.

5.1.1 Radar Range Equation

The maximum range of a monostatic radar can be determined from radar equation [2] that is given by

$$R_{\max} = \sqrt[4]{\frac{P_t G^2 \lambda^2 \sigma}{(4\pi)^3 P_r}} \tag{5.1}$$

where

P_t = Minimum peak transmit power

G = Transmit and receive antenna gain

λ = Wavelength of the carrier frequency

σ = Radar Cross Section (RCS) of the target

$R_{\max}$ = Radar maximum range

P_r = Minimum received power

5.1.2 Unambiguous Range

A radar may not be able to distinguish between echoes from an earlier transmission and the current one. The resulting range is known as the unambiguous range. The maximum unambiguous range can be acquired from the following relation.

$$R_{\mathrm{ur}} = c\frac{T_{\mathrm{PRI}}}{2} = \frac{c}{2f_{\mathrm{PRF}}} \tag{5.2}$$

where c is the speed of light in free space, T_{PRI} is the Pulse Repetition Interval (PRI) and f_{PRF} is the Pulse Repetition Frequency (PRF).

5.1.3 Radar Link Budget for Transmitter Power

The transmitter power plays an important role in the evaluation of radar performance. In order to determine the minimum required peak power, the signal to noise ratio (SNR) is calculated by using the Albersheim's Equation [184] as,

$$SNR_{\mathrm{mindB}} = -5\log_{10} N_p + \left(6.2 + \frac{4.54}{\sqrt{N_p + 0.44}}\right)\log_{10}\left(A_o + 0.12A_oB_o + 1.7B_o\right) \tag{5.3}$$

where

$$A_o = \ln \frac{0.62}{P_{\mathrm{FA}}}$$

$$B_o = \ln \frac{P_d}{1 - P_d}$$

N_p =Pulse integration number

P_d =Probability of detection

P_{FA} =Probability of false alarm

To determine the minimum SNR, we set the probability of detection $P_d = 0.9$ and probability of false alarm $P_{\mathrm{FA}} = 10^{-6}$ and $N_p = 128$, as the number of pulses for pulse integration. After the calculation of minimum SNR, the radar equation is used to determine the minimum peak transmit power P_t of a monostatic radar for a given maximum range. The radar equation for minimum SNR is then given as

$$\mathrm{SNR}_{\mathrm{mindB}} = \frac{P_r}{P_n} = \frac{P_t G^2 \lambda^2 \sigma}{(4\pi)^3 R_{\mathrm{max}}^4 k_B T_o B F_n L_T} \tag{5.4}$$

where P_n = Noise power

k_B = Boltzmann's constant

B = Bandwidth

T_o = System temperature in Kelvin

F_n = Noise figure of the receiver

L_T = Total losses

Here, the receiver noise has an additive effect and is modeled as a zero mean complex white Gaussian noise vector with variance σ_o^2, given as

$$\sigma_o^2 = k_B T_o B F_n \tag{5.5}$$

5.1.4 Propagation Model

For propagation, the free space pathloss model is used considering that the target is in the far field of the transmitting antenna. The formula for free space pathloss, represented as L_{free}, is derived from the Friis equation [185] and is given by

$$L_{\text{free}} = \frac{(4\pi R)^2}{\lambda^2} \tag{5.6}$$

Pathloss can also be written in terms of frequency f.

$$L_{\text{free}} = \frac{(4\pi R f)^2}{c^2} \tag{5.7}$$

This scenario presumes that there is no obstruction between the target and the radar considering the availability of line of sight (LoS).

5.1.5 Radar Range Doppler Processing

When a target is illuminated by a radar signal, some of the signal energy is reflected towards the radar in the form of an echo of the original signal. The radar after receiving the echo extracts the target parameters including range and velocity from the return signal, as discussed earlier in chapter 3. The maximum range can then be determined from the radar equation given in Eq. 5.1. In the case of the proposed

SC-FDMA radar, the transmitted signal is obtained after performing N-point DFT on a phase-coded sequence, subcarrier mapping, and M-point IDFT, where N is the number of source symbols and M is the number of total number of subcarriers. The proposed radar, after receiving the echo, performs demultiplexing of the signal by applying M-point DFT, demapping the frequency domain symbols, and applying N-point IDFT operations subsequently. As a result, the time domain symbols of the transmitted phase-coded sequence, are expected. Therefore, a matched filter, having the matching coefficient acquired from the copy of the transmitted signal, is applied to the received signal and pulse integration is performed. As described in chapter 3, pulse integration improves the SNR ratio up to a maximum of n times the SNR, where n is the pulse integration number. A processing along the fast time of the data matrix, results in a peak at range axis at a particular range bin representing the presence of a target in it. Moreover, for the computation of the Doppler shift, a DFT or periodogram operation is implemented along the slow-time of the data matrix as described in detail, in Chapter 3. It provides the Doppler frequency resulting in the speed of a moving target.

5.2 Simulation Setup

The simulations are carried out for the automotive radar applications. The modern automotive radars use 77 GHz band. There is an availability of large bandwidth of up to 4 GHz in this band that makes it attractive for applications requiring high range and Doppler resolutions. This band is extremely appealing in short-range radar applications in the automotive industry. Therefore, we also opted a short range radar with a maximum unambiguous range of 4000m. Although the simulations are for automotive radars however this radar architecture can be implemented for air/ ground / maritime based applications. All simulations are performed for multiple target detection scenarios using MATLAB R2017a version 9.2 with Phased Array Toolbox, on a PC with Windows 7 operating system. These scenarios include single and multiple target environments. Also, the SC-FDMA waveform is evaluated for different numbers of subcarriers.

5.2.1 Waveform Selection

For the simulation of an end-to-end radar, SC-FDMA waveform is generated by using Eq. 3.11. The initial phase sequences used to generate the SC-FDMA waveform are Frank code with 16 elements and P3 codes with 16 elements. For performance comparison, OFDM waveforms are generated with the same Frank and P3 codes as initial time domain sequences. Likewise, the LFM waveform is also generated for the sake of comparative analysis. The selected SC-FDMA waveform uses the same number of subcarriers as that of OFDM waveform and same bandwidth as that of LFM waveform.

5.2.2 Transmitter

The transmitter power is adjusted using Albersheim's relation, given in Eq. 5.3, for a given pulse integration number, and defined probabilities of false alarm and detection probabilities.

5.2.3 Transmit and Receive Antenna

For the monostatic radar configuration, the transmitter and receiver share a common antenna. The Phased Array System Toolbox in MATLAB®is used to design sensor array systems in radar. With the help of this toolbox, any antenna with the desired specifications can be modeled. In the simulations, a single isotropic antenna element is modeled whose response is same in all directions. The frequency range covers the desired simulation frequency bands. For achieving high gain the "BackBaffled" property of the antenna object is set to "True".

5.2.4 Target and Radar Platforms

The target is considered as a point target with the non-fluctuating swerling case (swerling case 0; constant RCS). For simulation, the radar platform is considered as ground-based with fixed coordinates. The position of the target platform is given in Cartesian coordinates, placed at point (x, y, z). The values of x, y, and z are given in the Table. 5.1, 5.2, and 5.3 for different positions of the targets in different scenarios; while the radar is positioned at $(0, 0, 0)$.

5.2.5 Range Doppler Processing workflow

In pulse-Doppler processing, the usual workflow involves:

- Target detection in the range dimension (fast-time samples) which allows detecting the relative range bin containing the target.
- Computing DFT of slow-time data samples of a particular range bin that contains the target and identifying the peaks in the Doppler spectrum which are converted into speed values by using Eq. 3.28.

5.3 Simulation Results

Computer simulations for an SC-FDMA radar are performed for single and multiple target environments with different ranges and speeds. OFDM and LFM radars are also simulated for the purpose of performance comparison. These simulations are performed using the following four scenarios. Scenario 1 presents the comparative analysis of the interleaved SC-FDMA waveforms with different number of multicarriers. The results of this scenario are then used to establish a baseline for the selection of characteristic parameters in order to perform a cross technology comparative analysis of the proposed SC-FDMA radar with LFM and OFDM radars in the successive scenarios. In these scenarios, end-to-end radars with the proposed SC-FDMA, OFDM, and LFM waveforms are simulated for single and multiple targets detection.

As the radar simulations are for automotive short range radar, therefore, the selected target speed is the usual speed of the automobiles. The PRI specifies the radar's maximum unambiguous range. The chip width is determined by the bandwidth of the waveform, which is 150 MHz. The range and speed of the moving targets are estimated with the help of matched filter and range-Doppler processing. The results are then compared with the objective to select a waveform as the best candidate for achieving high range and Doppler resolution.

5.3.1 Scenario 1: SC-FDMA Waveform with Different Number of Multicarriers

In this scenario, SC-FDMA waveform has been analyzed for different bandwidth spreading factors and the number of subcarriers. For generating SC-FDMA waveform, 4-phased, 16-element Frank code (Frank-16) has been used as the initial sequence. 16-point FFT is implemented on the time domain symbols of the Frank-16 sequence which is followed by interleaved subcarrier mapping with M = 64, 128, 256, and 512 (number of subcarriers). Then an M-point IFFT is performed for each individual case to generate an SC-FDMA signal. Table 5.1 gives the simulation parameters for the waveform, transmitter, target, and radar processor.

SC-FDMA waveforms with different number of subcarriers, each, initiated with 16-element Frank code are used as radar waveforms for range estimation. The amplitude of the received signal for the four cases of subcarriers is plotted against range in Fig. 5.1. In each case, the pin-pointed peak shows the high resolution feature of these waveforms. However, the strong sidelobes along the peak are noticeably visible in Fig. 5.1 (a), that uses 64 subcarriers; while observe relatively lower sidelobe peaks can be observed in other plots of Fig. 5.1 (b, c, and d). It can also be observed that the gradual reduction of sidelobe peaks in Fig. 5.1 (b, c, and d) gives rise to their spread on the range axis.

This spreading of sidelobes is because of the repetition of original Frank-16 code in the time domain signal of the SC-FDMA waveform, as we have discussed earlier in chapter 4. It is also evident from Fig. 5.1 c and (d) that the sidelobe peaks are almost immersed inside the receiver noise. These results are obtained after

Parameters	Interleaved SC-FDMA
Waveform/ Code	Frank-16
f_c(GHz)	77
Sample Rate (Msps)	150
Subcarriers	64, 128, 256, 512
Chip width (s)	6.67×10^{-9}
PRI (s)	1.467×10^{-5}
Pulse Integration number	128
G (dB)	39
Radar Position (m)	(0,0,0)
Target Position (m)	(1000,0,0)
Target RCS (m^2)	1
Target radial speed (ms^{-1})	35 (closing)

TABLE 5.1: Simulation parameters for Scenario1.

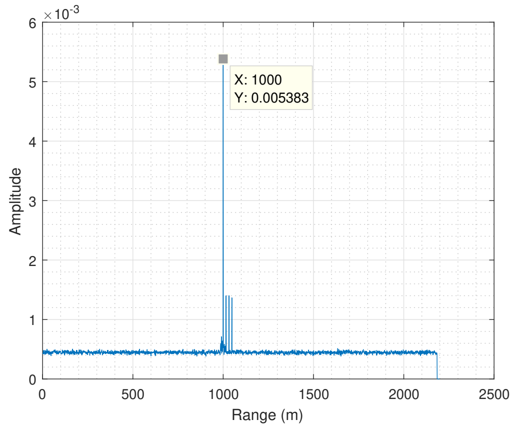

(a)

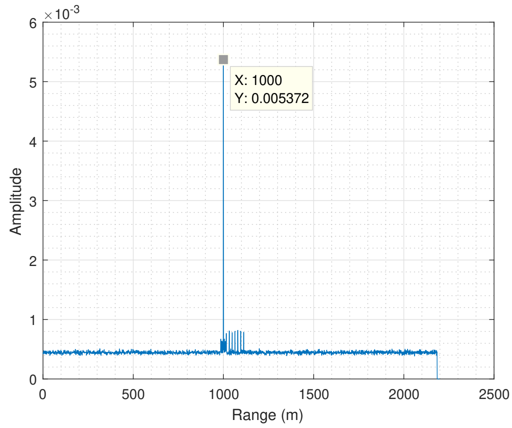

(b)

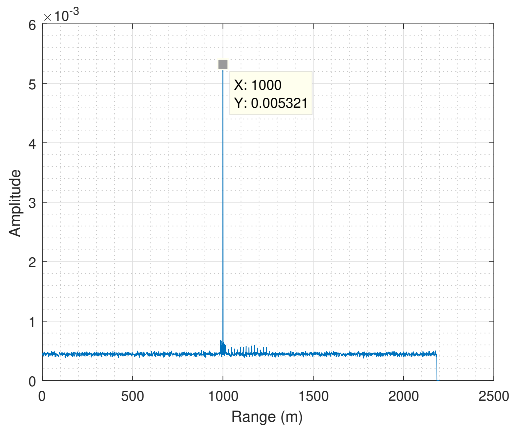

(c)

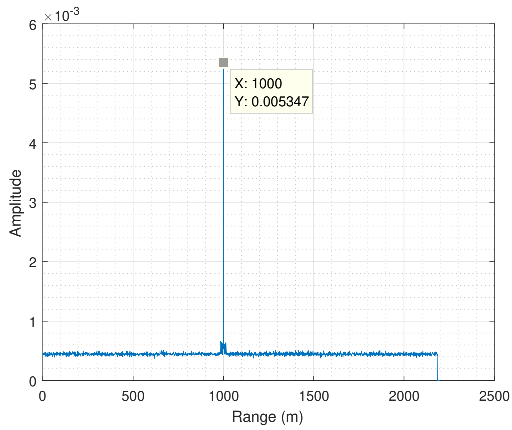

(d)

FIGURE 5.1: Range estimation plots of SC-FDMA waveform (initiated with 16 element Frank code) with M different subcarriers (a) M=64, (b) M = 128, (c) M=256, (d) M = 512

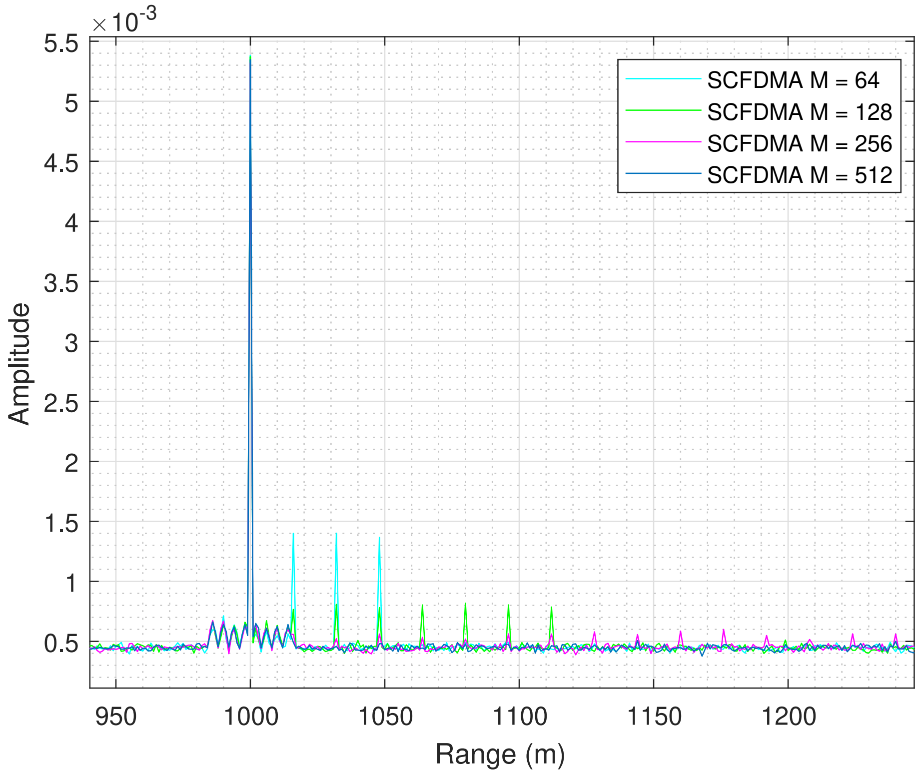

FIGURE 5.2: Zoomed range estimation plots for SCFDMA waveform radar with M subcarriers; M = [64, 128, 256, 512]

the pulse integration of 128 PRIs. It is shown in Fig. 5.1 that the peak level for each case is almost the same and there is no significant loss in the peak power as the spreading factor increases. It is observed that with the increase in the number of subcarriers, the sidelobe peaks are reduced and spreaded over range axis. At $M = 256$ and $M = 512$, when the bandwidth spreading factor is 16 and 32 respectively, we observe that the sidelobe peaks are almost at the level of noise. These sidelobes remain under the detection threshold and therefore have a negligible effect on range and speed estimation. For an elaborative comparison, we combine zoomed plots of all the cases in Fig. 5.2. It is also observed from the results that increasing the number of subcarriers for SC-FDMA waveform prevents the radar processor to detect the sidelobe peaks that could be considered falsely as targets of smaller RCSs.

As discussed earlier, the range estimation plots with 256 and 512 subcarriers showed promising results with negligible sidelobe peaks. We therefore, select M = 256 for cross-technology comparative analysis, because in case of M = 512,

Parameters	LFM	OFDM	ISC-FDMA
Waveform/ Code	LFM	Frank-16	Frank-16
f_c (GHz)	77	77	77
Sample rate (Msps)	150	150	150
Subcarriers	Nil	256	256
Sweep bandwidth (MHz)	75	-	-
Chip width (s)	Nil	6.67×10^{-9}	6.67×10^{-9}
PRI (s)	1.467×10^{-5}	1.467×10^{-5}	1.467×10^{-5}
Pulse integration number	128	128	128
G (dB)	39	39	39
Radar position (m)	(0,0,0)	(0,0,0)	(0,0,0)
Target position (m)	(1000,0,0)	(1000,0,0)	(1000,0,0)
Target RCS (m^2)	1	1	1
Target radial speed (ms^{-1})	35 (closing)	35 (closing)	35 (closing)

Table 5.2: Simulation parameters for Scenario 2

there will be a reduction in the unambiguous range along with the increase in the complexity of the system.

5.3.2 Scenario 2: Range and Speed Estimation of Single Target using SC-FDMA, OFDM and LFM based Radars

In this scenario, end-to-end radar simulations are performed for the proposed SC-FDMA waveform generated on the basis of the selection of initial sequence and the number of subcarriers, made in the previous scenario and their results are then used for a cross technology comparative analysis with LFM and OFDM radars. For this purpose, the results of the proposed multicarrier interleaved SC-FDMA waveform with 256 subcarriers and 16-element Frank code are compared with those of single carrier LFM waveform and multicarrier OFDM waveform with 256 subcarriers and 16-element Frank code.

In this scenario, we consider that a single point target at a distance of 1000 meters away from the static radar is moving with a constant speed of $35ms^{-1}$ towards the radar. The simulation parameters are given in Table. 5.2. The range and speed of the target are estimated by using a matched filter, pulse integrator, and range-Doppler estimator.

Fig. 5.3, 5.4, and 5.5 show the range and velocity plots of the selected waveforms obtained as the result of end-to-end radar simulations. The negative speed in the range-speed plain denotes that the target is moving towards the radar platform and vice versa.

We observe from Fig. 5.3 that the linear frequency modulated (LFM) waveform produces quite high range and Doppler resolutions due to its large bandwidth structure. The range resolution of the target using the OFDM waveform is also good as shown in Fig. 5.4 (b). However, the sidelobe peaks are quite high in the range estimation plot, which may cross the detection threshold raising false alarms for close-by targets, with low signal strength. The same is the case with Doppler estimation, where the signal spreads over the speed axis as shown in Fig. 5.4 (a). The target image shown on the range-speed plane, in Fig. 5.5 (a), illustrates that the proposed SC-FDMA waveform offers higher resolution in both range and velocity as compared to LFM and OFDM. A similar conclusion can also be drawn from the sharp peak of the range plot in Fig. 5.5 (b).

5.3.3 Scenario 3: Range and Speed Estimation of Multiple Targets using SC-FDMA, OFDM and LFM based Radars

In this scenario, end-to-end radars generating SC-FDMA, OFDM, and LFM waveforms are simulated and compared for their performance for multiple target detection and parameter estimation. Each of these waveform use the same simulation parameters as in the case of scenario 2, i.e. OFDM and interleaved SC-FDMA waveform use 256 subcarriers and 16-element Frank code. In this scenario, two point targets i.e. Target 1 and Target 2 having the same RCS, are approaching the radar with radial velocities of 30 ms^{-1} and 20 ms^{-1} at the distances of 2000m

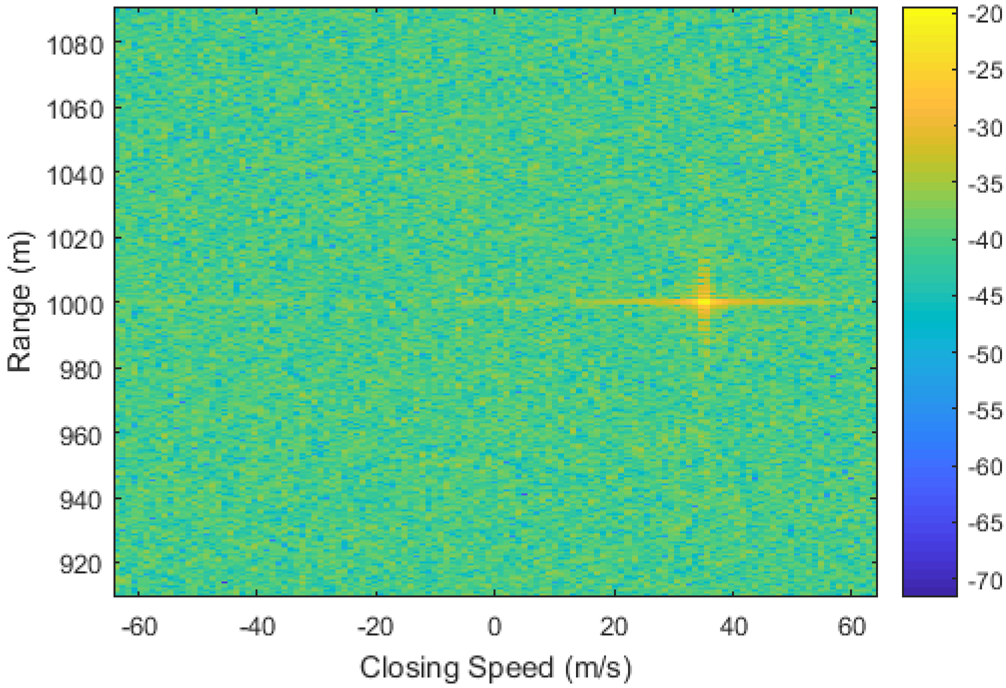

(a)

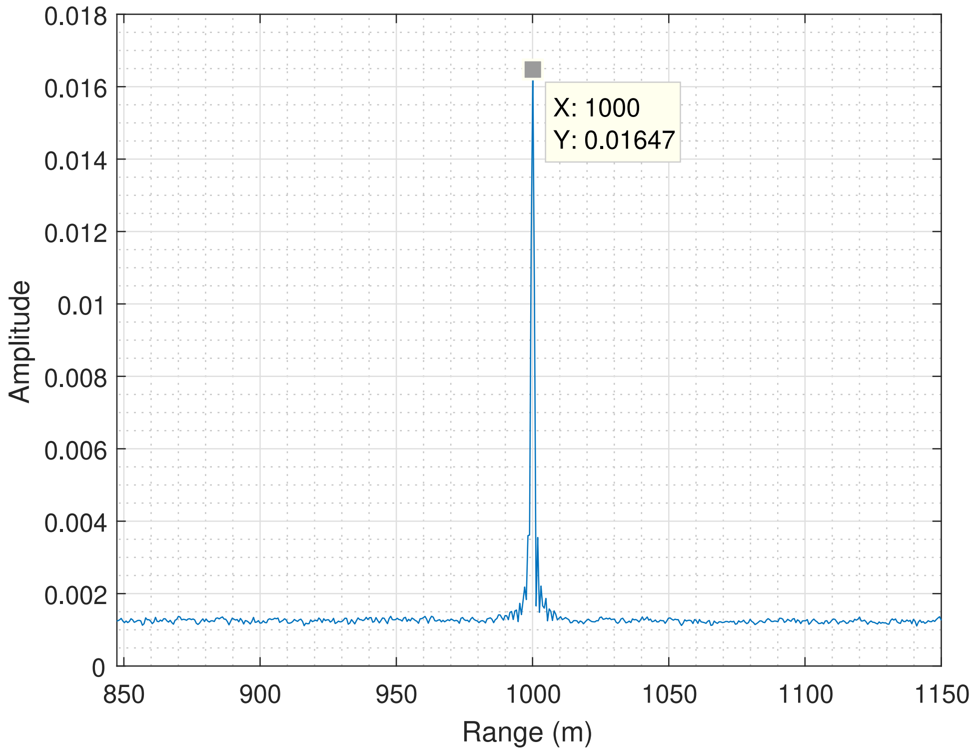

(b)

Figure 5.3: Range and speed estimation of a single moving target using LFM waveform (a) Range-speed plot (b) Range plot.

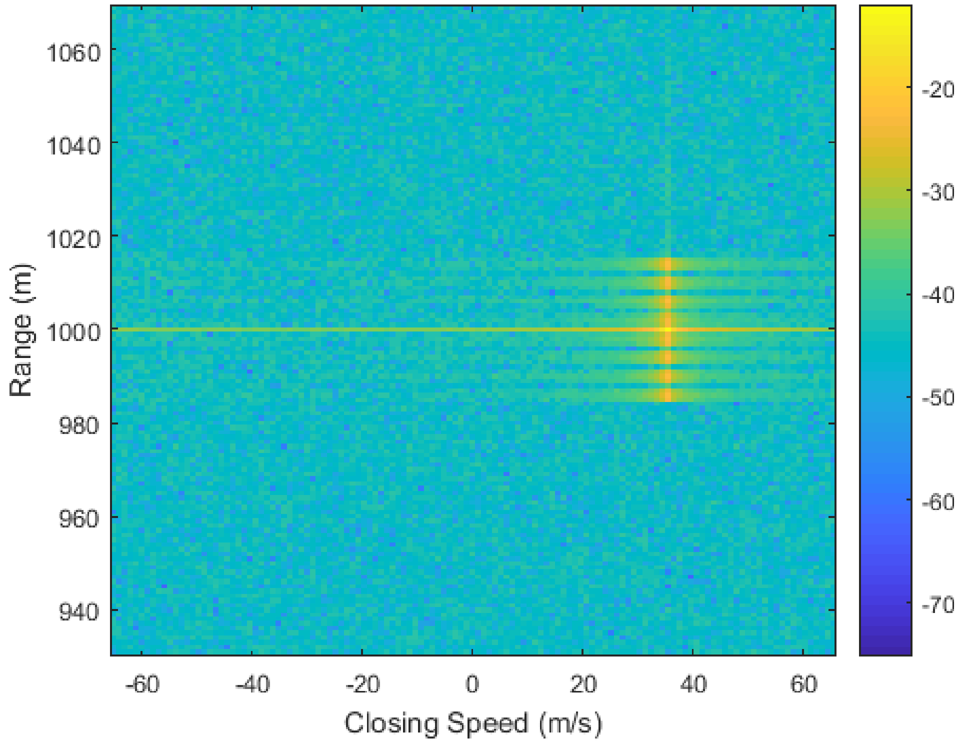

(a)

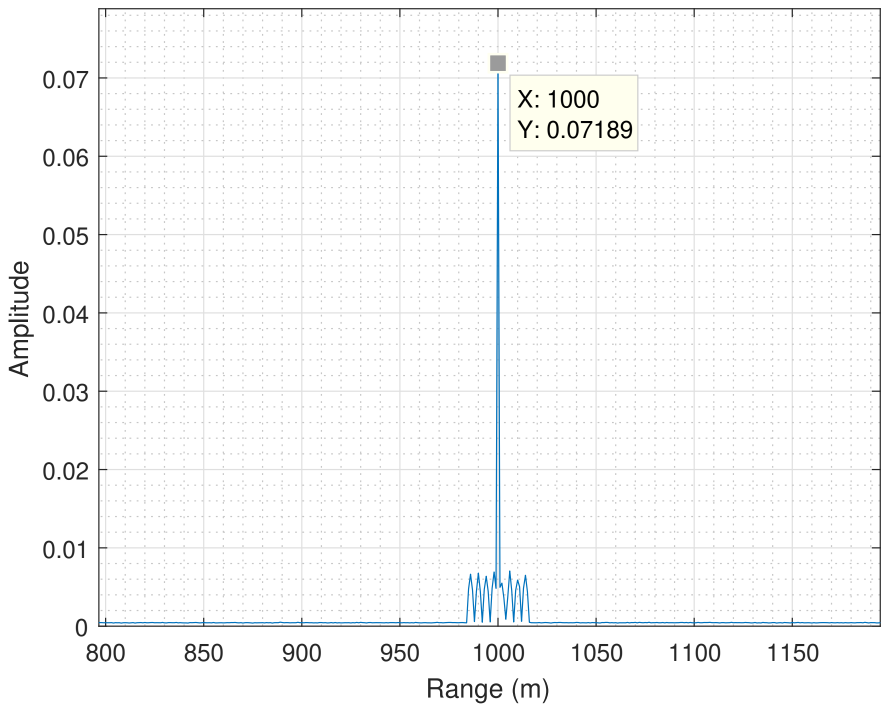

(b)

FIGURE 5.4: Range and speed estimation of a single moving target using OFDM waveform (a) Range-speed plot (b) Range plot.

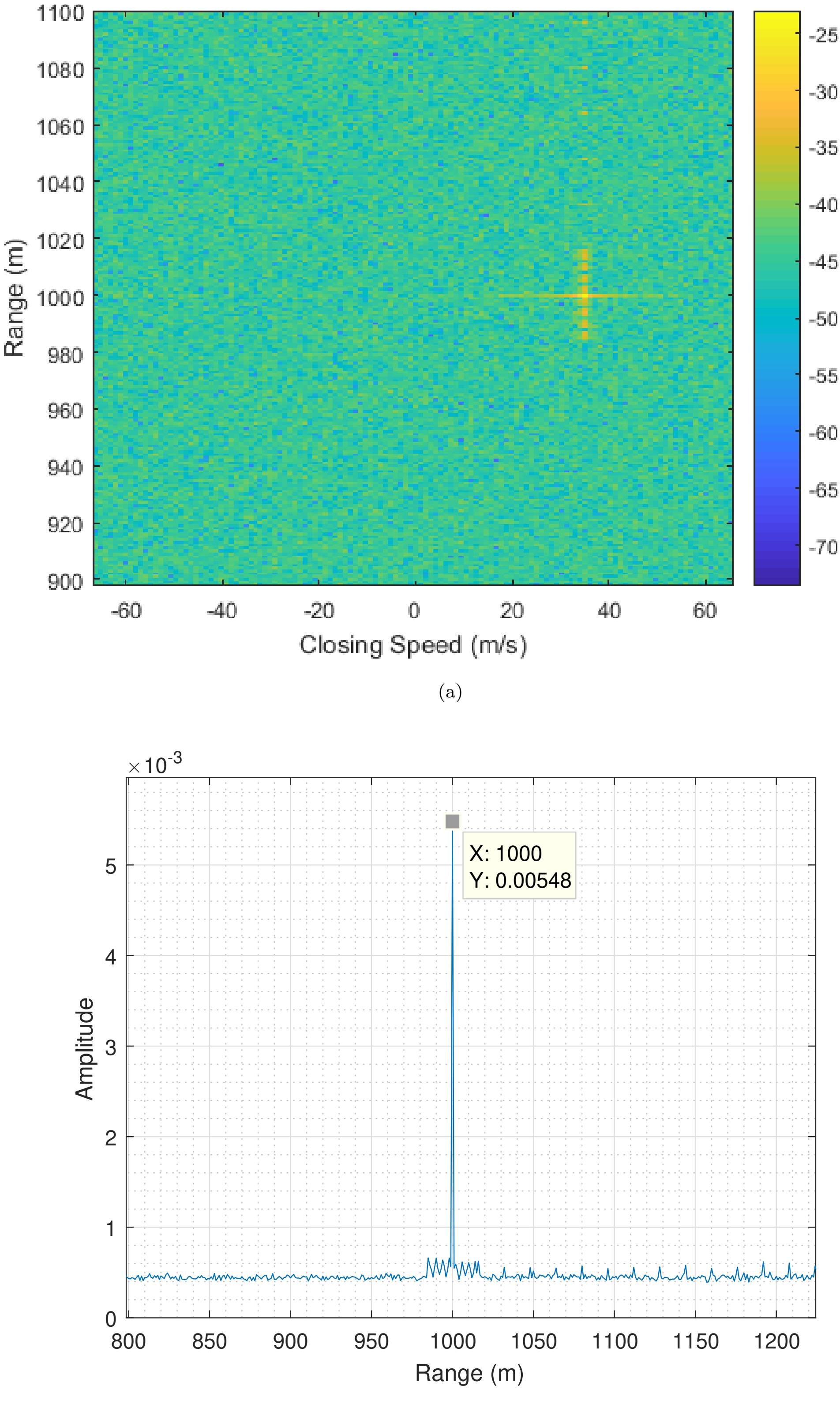

(a)

(b)

FIGURE 5.5: Range and speed estimation of a single moving target using the proposed interleaved SC-FDMA waveform (a) Range-speed plot (f) Range plot.

Parameters	LFM	OFDM	ISC-FDMA
Waveform/ Code	LFM	Frank-16	Frank-16
f_c (GHz)	77	77	77
Sample rate (Msps)	150	150	150
Subcarriers	Nil	256	256
Sweep bandwidth (MHz)	75	-	-
PRI (s)	2.67×10^{-5}	2.67×10^{-5}	2.67×10^{-5}
Chip width (s)	Nil	6.67×10^{-9}	6.67×10^{-9}
Pulse integration number	128	128	128
G (dB)	40	40	40
Radar position (m)	(0,0,0)	(0,0,0)	(0,0,0)
Target 1 position (m)	(2000,0,0)	(2000,0,0)	(2000,0,0)
Target 2 position (m)	(2005,0,0)	(2005,0,0)	(2005,0,0)
Target 1 RCS (m^2)	1	1	1
Target 2 RCS (m^2)	1	1	1
Target-1 speed (ms^{-1})	30	30	30
Target-2 speed (ms^{-1})	20	20	20

Table 5.3: Simulation parameters for Scenario-3

and 2005m from the radar respectively. The simulation parameters are given in Table. 5.3.

In the case of the LFM waveform, as shown in Fig. 5.6 (a) and (b), targets are distinguishable with poor range and Doppler resolutions. In case of OFDM waveform, as shown in Fig. 5.7 (a) and (b), the range and Doppler resolutions of the two targets are even worse. Although the targets are of the same RCS, but the range plot given in Fig. 5.7 (b), shows that the peaks are not even at the same level. This suppression of the peak of the second target occurs due to the sidelobes of first target. Simulation results of the proposed interleaved SC-FDMA waveform are displayed in Fig. 5.8. It is observed from Fig. 5.8 (b) that the range peaks are sharper as compared to those in the cases of LFM and OFDM. On the range-speed plane, depicted in Fig. 5.8 (a), the target images are pin- pointed on their respective estimated range and speed values, illustrating high range and speed resolutions.

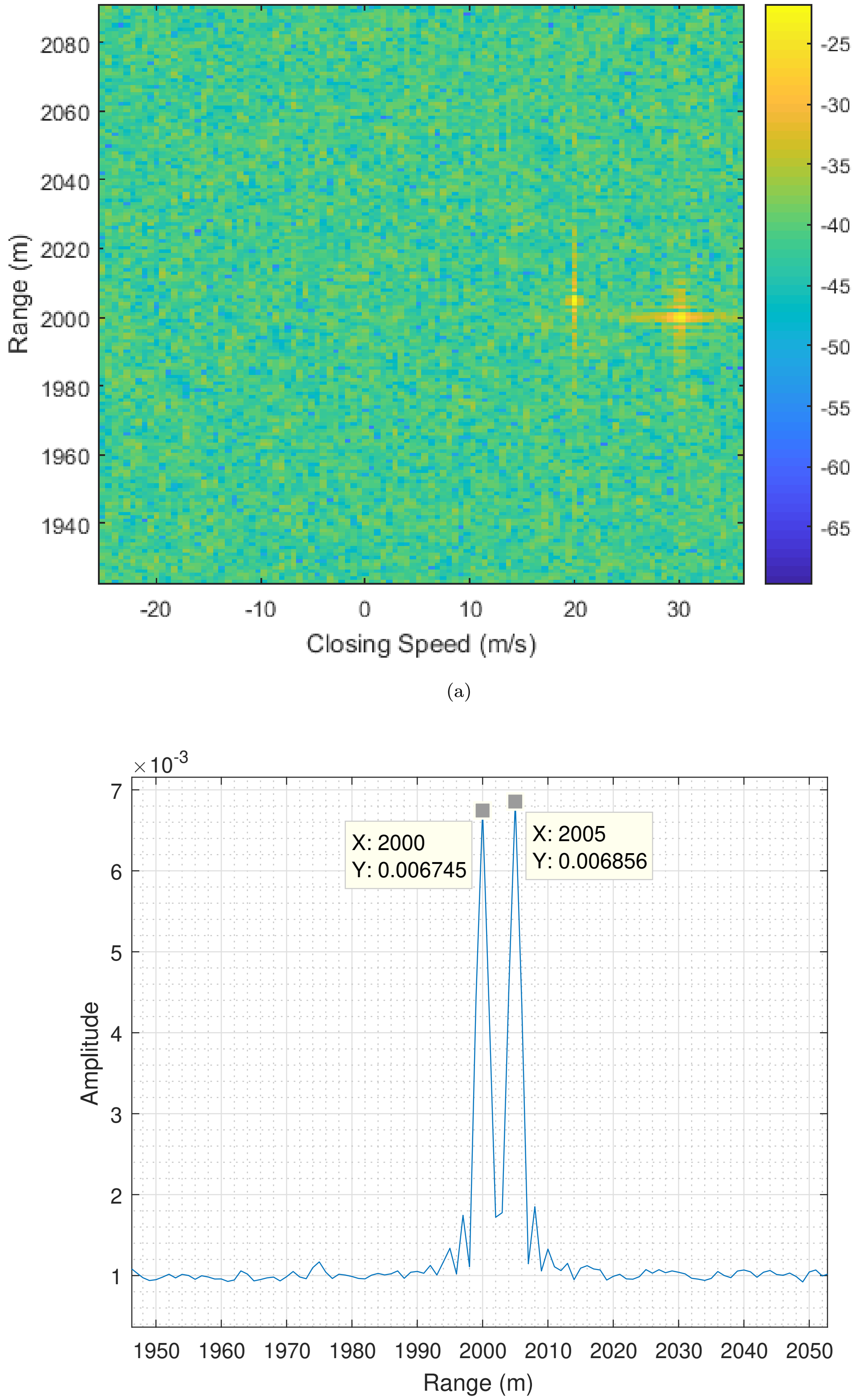

(b)

Figure 5.6: Range and speed estimation of two moving targets using LFM waveform (a) Range-speed plot (b) Range plot.

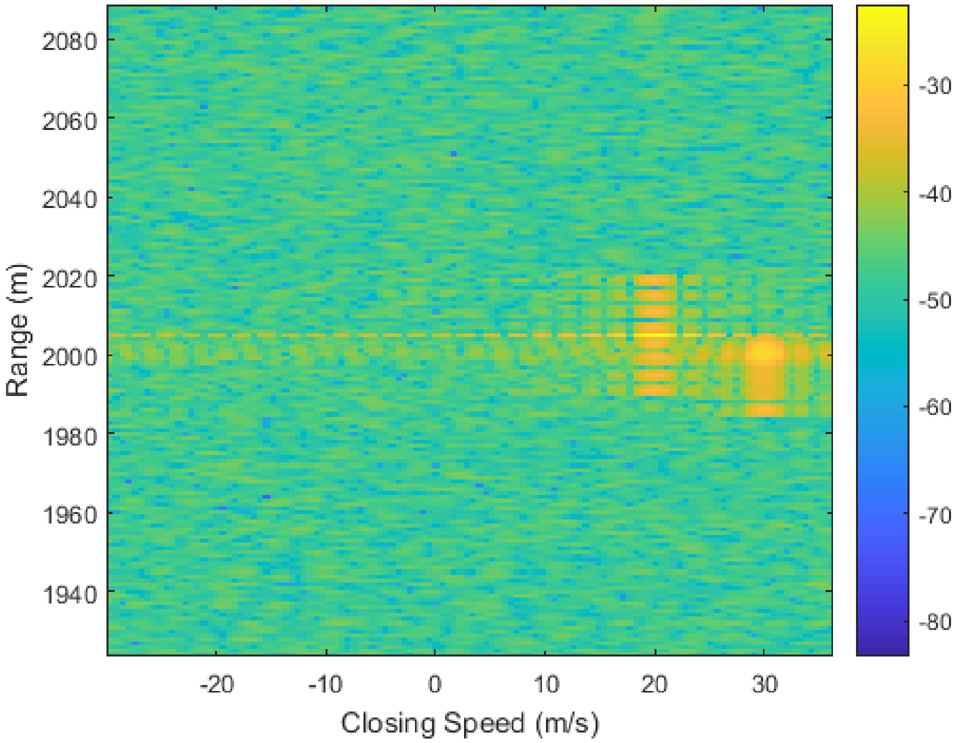

(a)

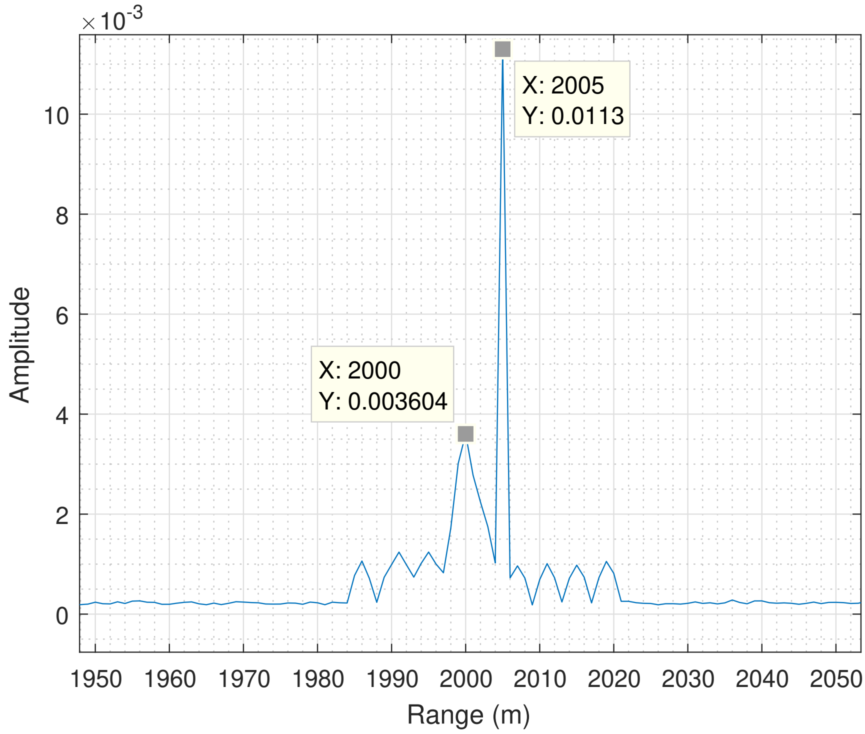

(b)

Figure 5.7: Range and speed estimation of two moving targets using OFDM waveform (a) Range-speed plot (b) Range plot.

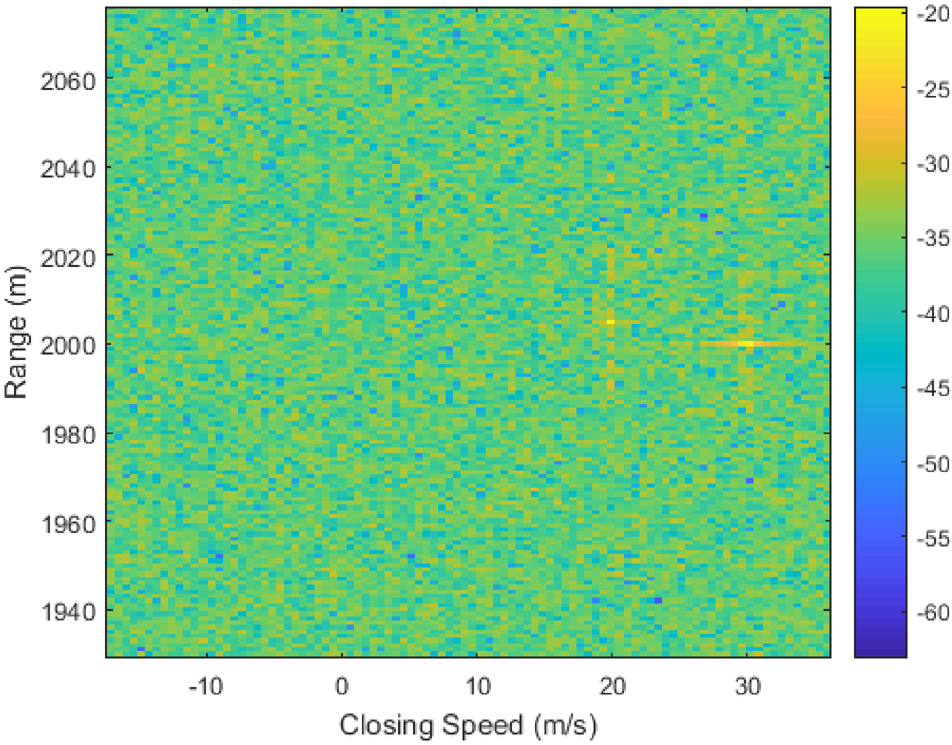

(a)

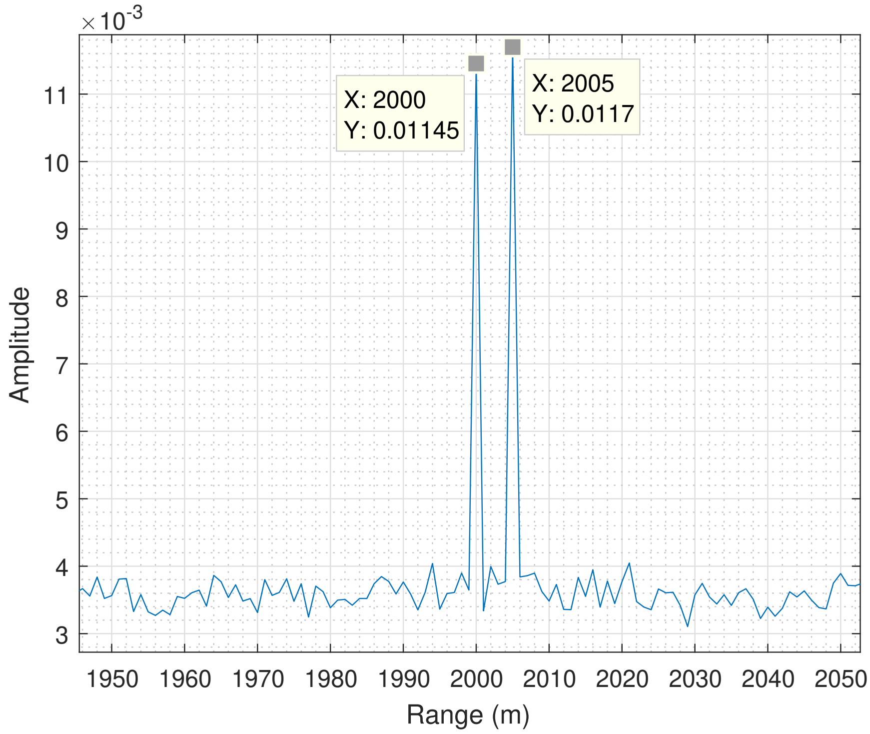

(b)

FIGURE 5.8: Range and speed estimation of two moving targets using the proposed interleaved SC-FDMA waveform (a) Range-speed plot (b) Range plot.

5.3.4 Scenario 4: Range and Speed Estimation of multiple Close-Range Targets Moving with Constant Speed using SC-FDMA, OFDM and LFM based Radars

For further elaboration, we present scenario 4 that depicts the situation when two point targets are moving towards the radar with the constant speed of 30 ms^{-1} and are only 2 meters apart from each other, i.e. at the distances of 2000 m and 2002 m from the radar. Since this scenario is the same as the scenario 3 except for the target speeds and ranges; therefore, the same simulation setup of scenario 3 is used with slight changes of target parameters as given in Table. 5.4.

In the previous scenarios, LFM based radar performed poorly in the detection of the targets distinctively. However, in the current scenario, in which the targets are quite close to each other, LFM radar is not even able to resolve the two targets on range axis as shown in Fig. 5.9 (a) and (b). The range plot shows only a single peak, providing an erroneous range value for both targets, i.e. 2001 m.

In the case of OFDM radar, we can observe in the range-speed plot given in Fig. 5.10 (a), that instead of two targets only a single target is visible at a range of 2002 m. In Fig. 5.10 (b), we see a major peak at 2002 m and a minor peak at 2000 m, which is too small to be detected as an independent target as it is shadowed by the high sidelobes of the major peak. Therefore, we detect only a single target above the detection threshold. This simulation scenario illustrates the limitation of OFDM and LFM based radars.

The proposed interleaved SC-FDMA radar shows impressive results in this case. Despite the fact that the two targets are quite close to each other in range and moving with the same speed, each target is detected independently as shown in

Parameters	Target 1	Target 2
Position (m)	$(2000, 0, 0)$	$(2002, 0, 0)$
Closing speed (ms^{-1})	30	30
RCS (m^2)	1	1

TABLE 5.4: Target parameters for Scenario 4

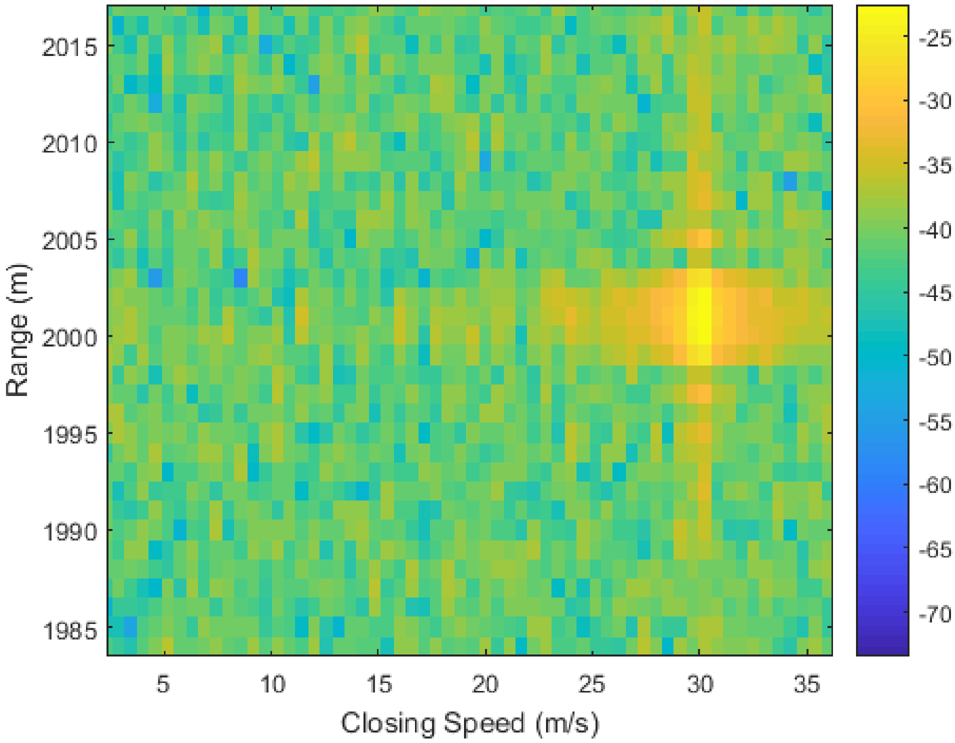

(a)

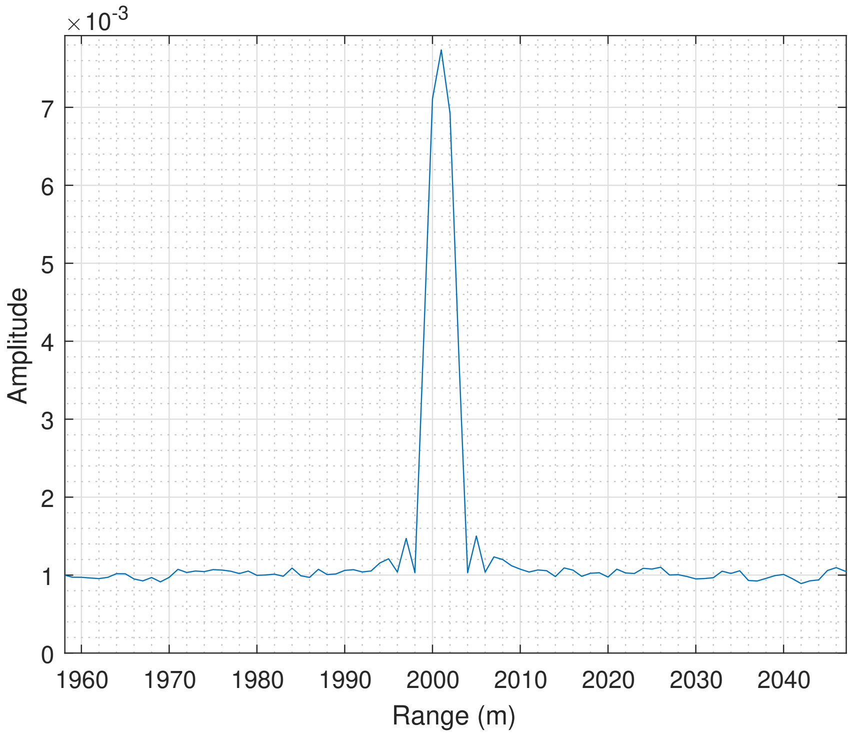

(b)

FIGURE 5.9: Range and velocity estimation of two targets, very close in range and having same radial speed using LFM waveform (a) Range-speed plot (b) Range plot.

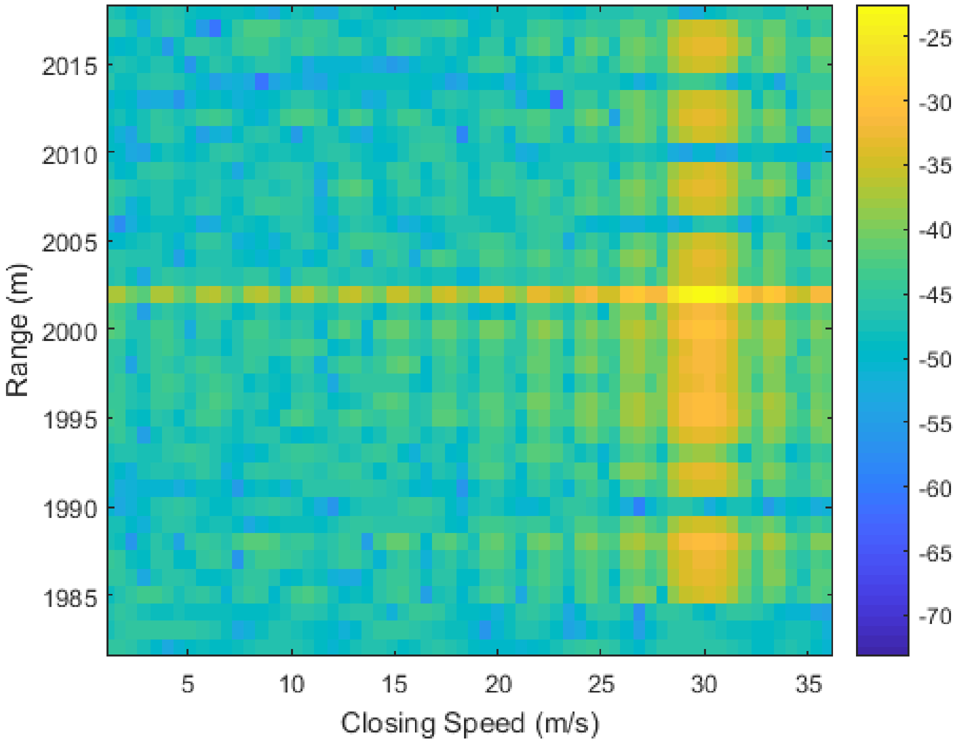

(a)

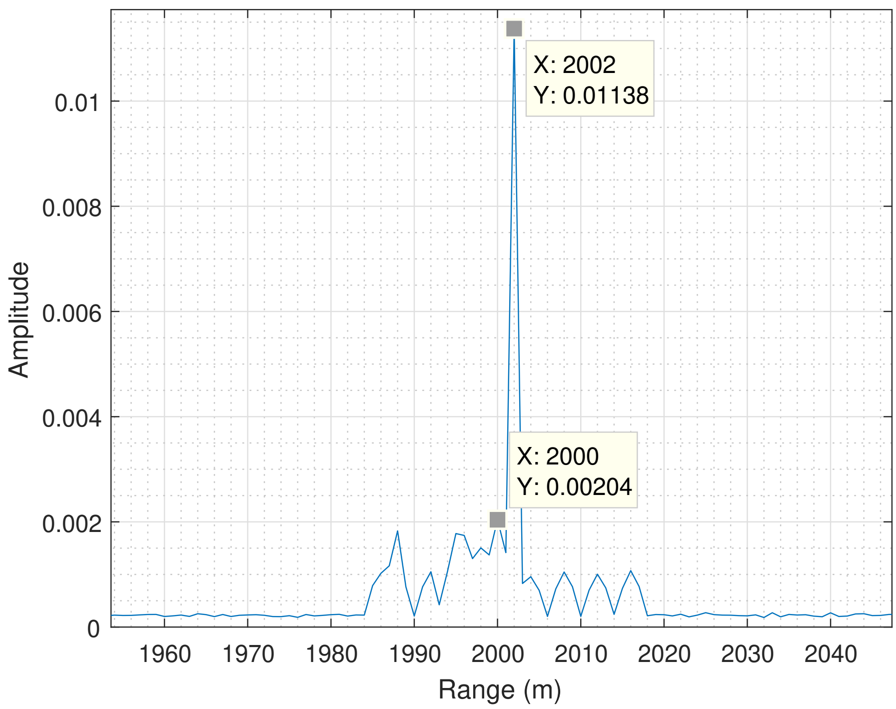

(b)

FIGURE 5.10: Range and velocity estimation of two targets, very close in range and having same radial speed using OFDM waveform (a) Range-speed plot (b) Range plot.

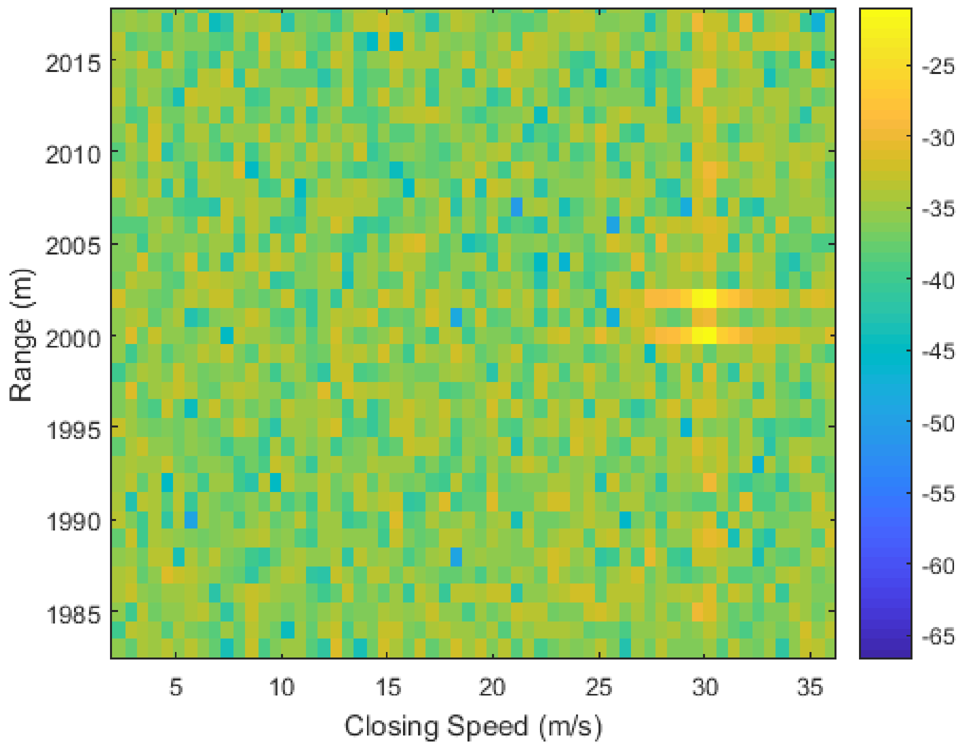

(a)

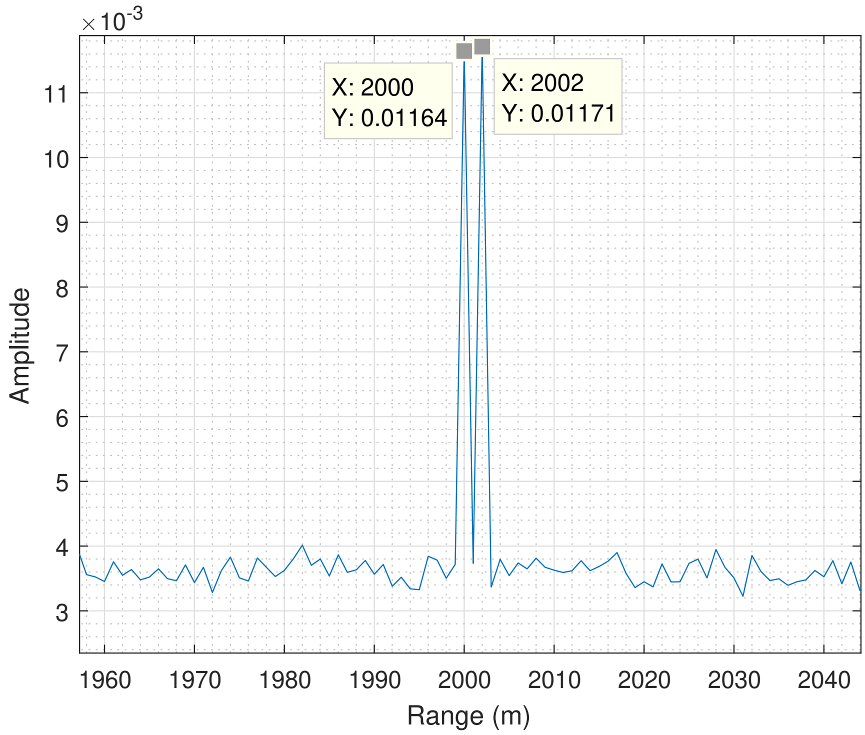

(b)

FIGURE 5.11: Range and velocity estimation of two targets, very close in range and having same radial speed using the proposed interleaved SC-FDMA waveform (a) Range-speed (b) Range plot.

Fig. 5.11 (a). Likewise, the plot in Fig. 5.11 (b), shows two distinct peaks of almost the same strengths, at 2000 m and 2002 m on the range axis.

As we know that range resolution depends upon the bandwidth of the radar waveform. In these simulations the bandwidth of SC-FDMA is taken 150MHz therefore the range resolution is 1 meter. However, the range resolution can be improved by increasing the bandwidth of the SC-FDMA signal. The simulation results show the consistency in the measurement of range resolution for ISC-FDMA Radar.

5.3.5 Scenario 5: Range and Speed Estimation of Two Targets, Close in Range and Speed, one with Large RCS Masking the other Target

This scenario is presented to show the effect of a target with large RCS masking a near-by relatively smaller target. This scenario is similar to the scenario 3 except that these targets are close in range and speeds but their sizes are significantly different from each other. The simulation parameters are identical to those described in scenario 3. The target parameters, however, are altered and are listed in Table.5.5.

Parameters	Target 1	Target 2
Position (m)	$(2000, 0, 0)$	$(2005, 0, 0)$
Closing speed (ms^{-1})	28	30
RCS (m^2)	2	0.1

TABLE 5.5: Target parameters for Scenario 5

As shown in Fig.5.12, the range resolution of LFM waveform is relatively poor and we can observe peaks other than the return signal from target 2. These peaks may lead to the detection of false targets in addition to the real ones. The results for the OFDM waveform are even worse. As shown in Fig.5.13, the range resolution of

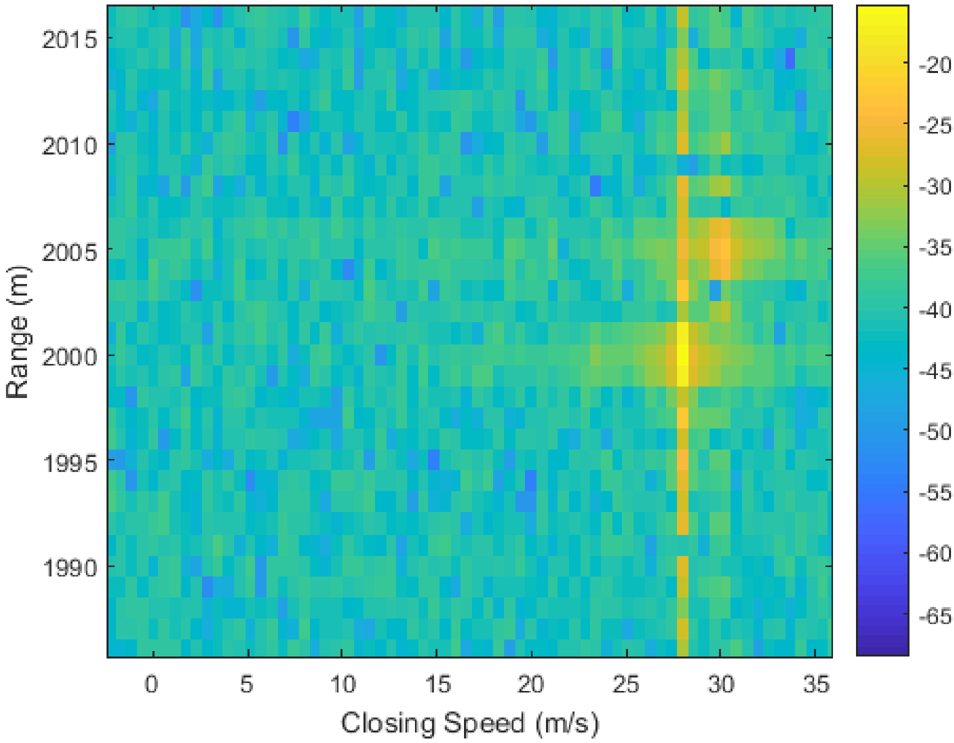

(a)

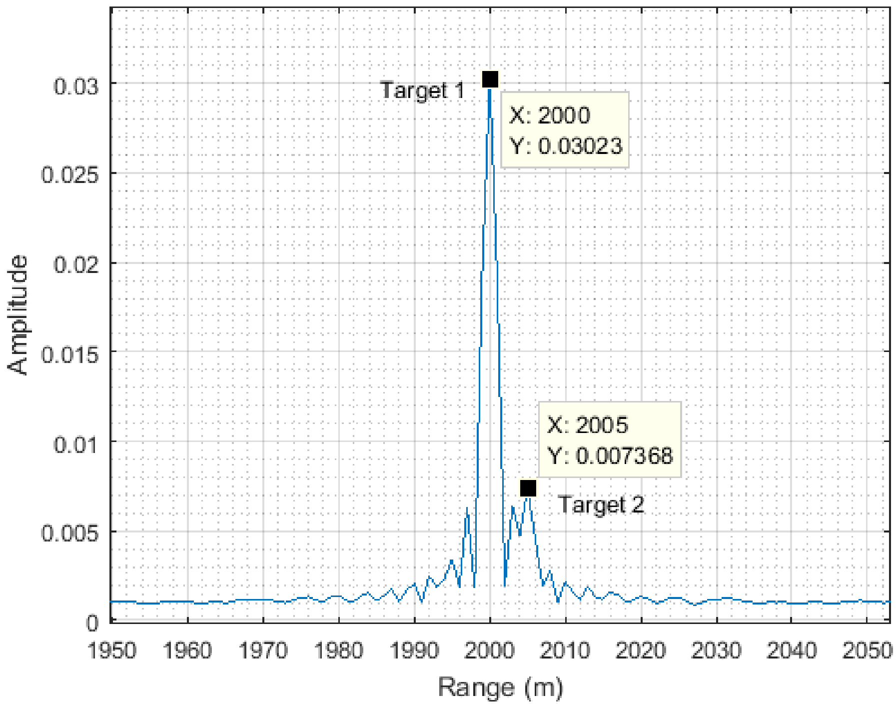

(b)

FIGURE 5.12: Range and velocity estimation using the LFM waveform when two targets, one with a very large RCS masking the other, are very close in range and speed (a) Range-speed plot (b) Range plot.

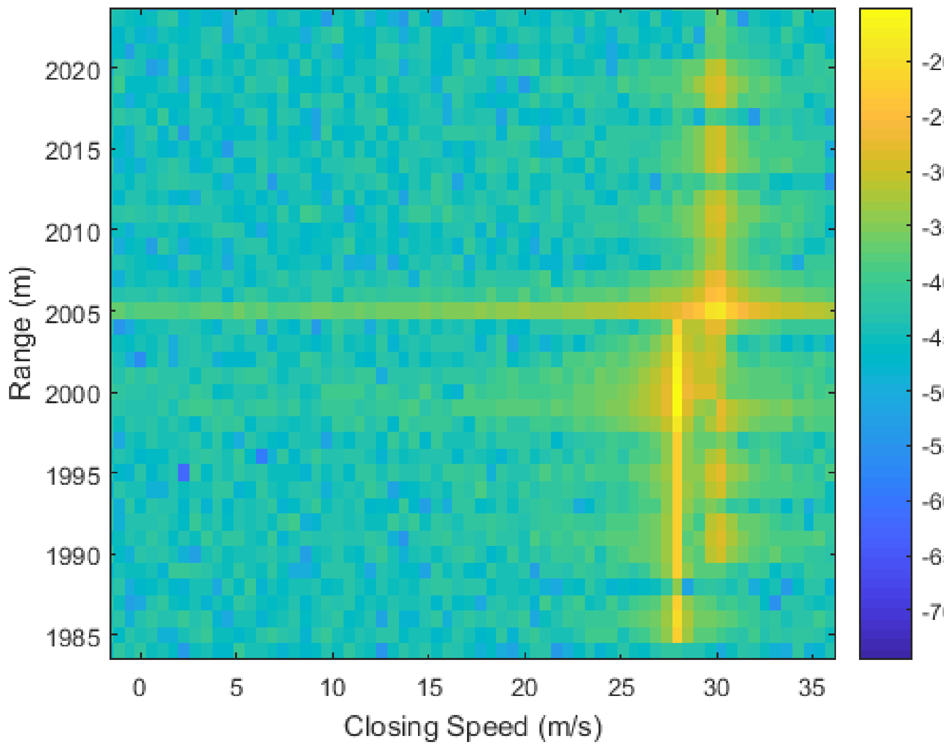

(a)

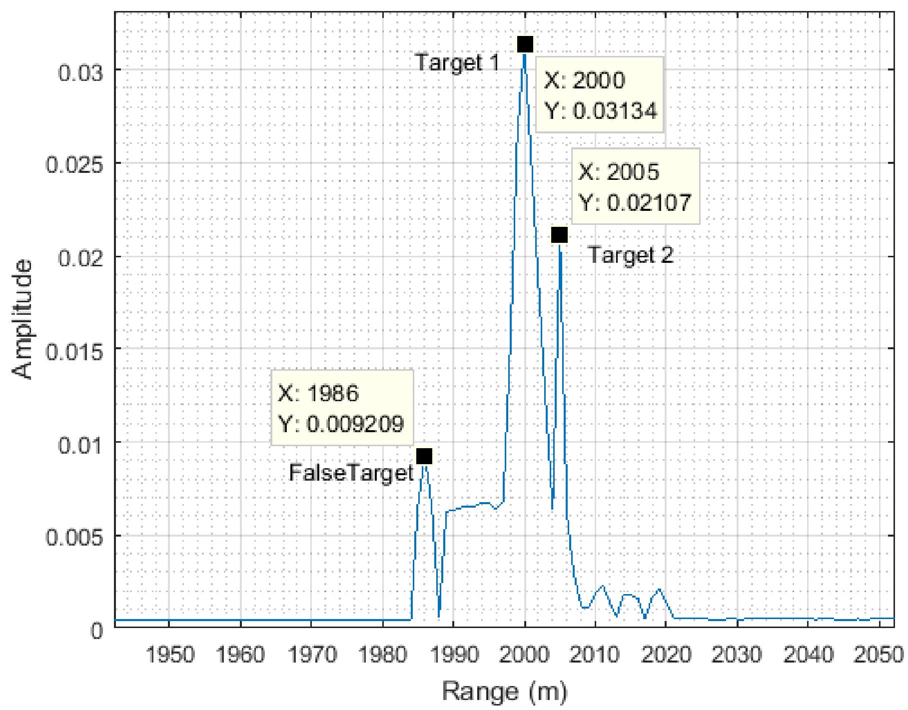

(b)

Figure 5.13: Range and velocity estimation using the OFDM waveform when two targets, one with a very large RCS masking the other, are very close in range and speed (a) Range-speed plot (b) Range plot.

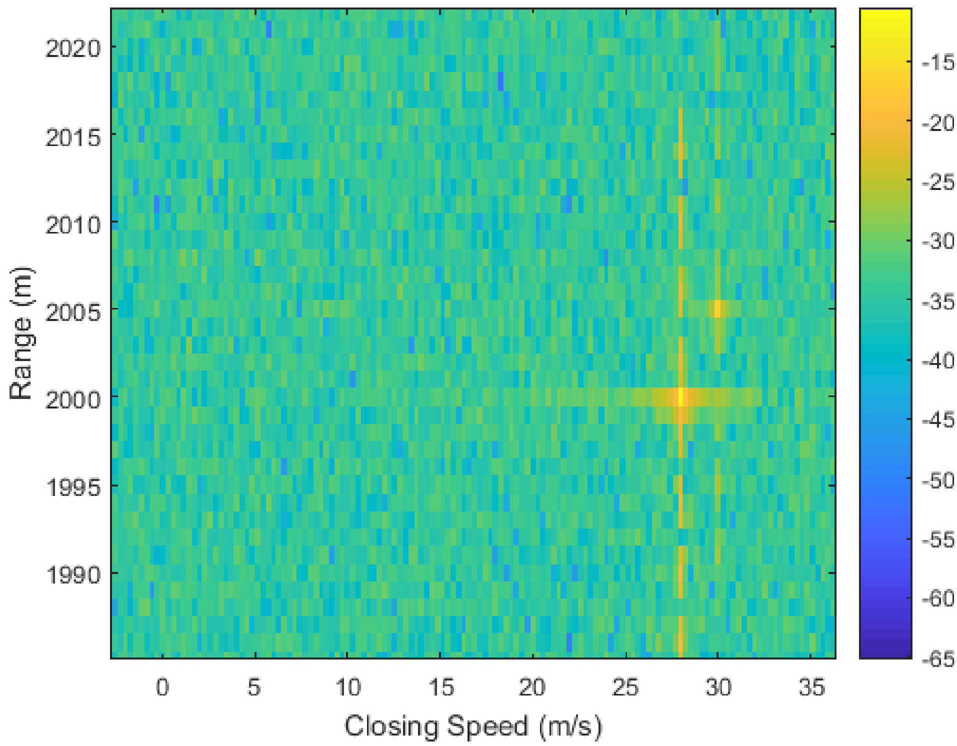

(a)

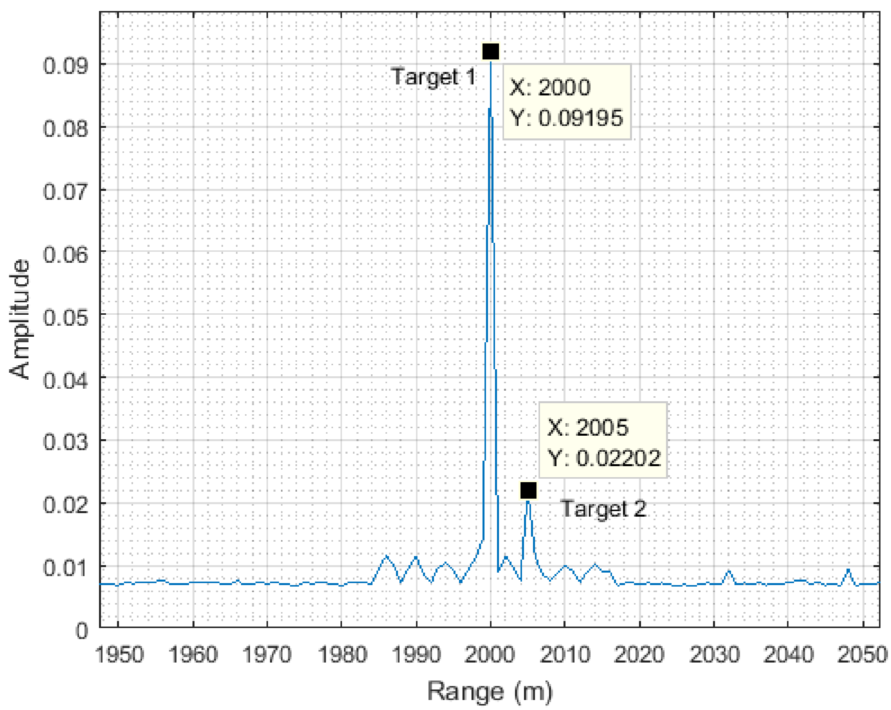

(b)

FIGURE 5.14: Range and velocity estimation using the proposed interleaved SC-FDMA waveform when two targets, one with a very large RCS masking the other, are very close in range and speed (a) Range-speed plot (b) Range plot.

OFDM has deteriorated, where the noise floor has risen along with the appearance of ghost targets.

This scenario, in addition to scenario 4, demonstrates the limitations of radars based on OFDM and LFM. The proposed ISC-FDMA waveform, on the other hand, exhibits promising results in terms of signal detection and range and Doppler resolutions, as shown in Fig. 5.14. Despite the fact that the peak indicating Target 2 is smaller than that of Target 1, it is still discernible. Both of the targets may be detected distinctively by adjusting an appropriate threshold without the involvement of any false target.

It is evident from the simulation results of Scenario 4 and 5 that the proposed Single Carrier-FDMA waveform with interleaved subcarrier mapping not only outperforms OFDM and LFM waveforms in the estimation of target range and Doppler but also in their resolutions. It can also be added on the basis of the conclusions made from all the scenarios that the resolution increases when a phase coded waveform with a higher number of elements is used as the initial sequence and a higher number of subcarriers are selected. The width of the main lobe of the ambiguity function (i.e., the resolution) is directly tied to the code length. The longer codes will produce a narrower main lobe and thus will have better resolution than the shorter ones. Therefore, the proposed SC-FDMA waveform with interleaved subcarrier mapping has the capability to pinpoint a target, even with a very small RCS, at any unambiguous range and velocity.

Chapter 6

Conclusion and Future Work

This chapter presents a brief summary of the dissertation in the first section and then discusses the conclusion and future work in the second section based upon the findings of the research work presented in this dissertation.

6.1 Summary of the Dissertation

Chapter 1 provides the introduction of the thesis and presents a brief history of radars, and their types and applications. The chapter elaborates the basic radar functions, salient target parameters, the concept of pulse compression, and the types of radar waveforms. These types are single and multicarrier waveforms. Single carrier waveforms include PAM, LFM, phase-coded, and CDMA waveforms; whereas the multicarrier waveform include OFDM. This chapter also provides the performance metrics of radar used in this thesis, and the research objectives. In the last section, the outline of this dissertation is given.

Chapter 2 provides the literature review and research directives in radar waveforms. The literature review points out the gray areas in the previous research work and leads the authors to the research gap analysis which ultimately gives the motivation of using SC-FDMA waveform in radar design. This motivation becomes the foundation stone for the problem formulation. In the end, the research methodology to achieve the set goals is presented and the contributions of this research work are listed in a comprehensive manner.

In chapter 3, the proposed SC-FDMA radar architecture and its signal modeling has been discussed in detail. The signal processing mechanism of the proposed radar is also presented in terms of its target detection and range and Doppler estimation capabilities.

In chapter 4, the proposed interleaved SC-FDMA waveform is analyzed for its autocorrelation properties and ambiguity function (AF). The analytical expression for the AF of the proposed SC-FDMA is derived. The 3-D AF diagrams are obtained through simulations for the proposed waveform. These diagrams are then compared with those of some existing waveforms including OFDM, and LFM. Signal correlation properties for the proposed waveform such as autocorrelation and peak-to-sidelobe ratio are analyzed and compared with those of OFDM and some notable phase-coded waveforms. In the last part of this chapter, the peak-to-average power ratios (PAPR) of the proposed interleaved SC-FDMA waveform using different phase-coded sequences are computed and compared with those of OFDM and other notable radar waveforms. The chapter presents an expression for computing the PAPR of multicarrier radars and elaborates the proposed interleaved SC-FDMA waveform as a constant envelope signal that aims at reducing the PAPR. Moreover, the PAPR values of the proposed SC-FDMA and the OFDM waveforms are presented and compared. These waveforms are initialized with fixed phase-coded sequences including PRN, Barker, Frank, Zadoff-Chu, P1, P3, and Px codes.

In Chapter 5, the proposed interleaved SC-FDMA Radar is end-to-end evaluated for practical consideration. The chapter is divided into three major parts; in the first part, the end-to-end radar simulation model is presented which leads to the simulation setup presented in the second part and simulation results are then provided in the third part for four different target scenarios. The proposed

SC-FDMA radar is investigated for target detection and parameter estimation. The performance of the proposed radar is evaluated and compared with other radars using LFM and OFDM waveforms for range and Doppler estimation.

6.2 Conclusion and Future Work

It is well established that the high range resolution of a radar for a given target can be significantly improved by using short duration pulses and large bandwidth. Unfortunately, short duration pulses decrease the transmit pulse energy that ultimately degrade the pulse signal-to-noise ratio (SNR) leading to poor detection probability. This makes the range resolution and the target detectability coupled in an inverse relationship. The solution to this perplexity of pulse energy and range resolution is the pulse compression. The most common waveforms used to increase the bandwidth of a radar signal by pulse compression include LFM, phase-coding, and CDMA waveforms in the case of single carrier and OFDM waveform in the case of multicarrier radar systems. LFM waveform has good spectral efficiency but lacks the sub-pulse level diversity. Whereas the phase-coded compression offers diversity at sub-pulse level but fails to achieve spectral efficiency as its resulting spread spectrum is not effectively rectangular due to abrupt changes in the phase. Likewise, CDMA does not provide control over spectral properties of the signal and OFDM possesses inherited weaknesses, such as the high peak-to-average power ratio (PAPR), high auto-correlation sidelobe peaks, and its vulnerability to spectral nulls. This motivated the authors to propose SC-FDMA for its use as a radar waveform, that not only exploits all the benefits of single and multicarrier waveforms but also offers null PAPR with good autocorrelation properties.

In this dissertation, Interleaved SC-FDMA has been proposed as a radar waveform. The signal design and a complete architecture as well as the signal processing mechanism of the proposed Interleaved SC-FDMA radar is presented. It has been observed that in the proposed radar waveform the DFT operation prior to the subcarrier mapping is similar to the coding performed usually in multicarrier radar signals for the reduction of PAPR. After the subcarrier mapping, the IDFT operation converts the overall signal into evenly-spaced non-overlapping multicarriers over a large spectrum. The proposed interleaved SC-FDMA waveform aims at reducing the time-domain fluctuations of the signal which is a major issue in multicarrier radar systems. The high PAPR limits the efficiency of the HPA of the transmitter by causing nonlinear distortions. The proposed interleaved SC-FDMA signal exhibits a constant envelope resulting in a PAPR value of almost 0 dB. The constant amplitude of the proposed signal eliminates the issue of nonlinear distortion of the transmitter HPA. From the PAPR analysis results, it can be inferred that the proposed Interleaved SC-FDMA waveform is the most suitable waveform for multicarrier radar systems in term of achieving minimum possible PAPR. This will enable the power amplifier of the radar transmitter to utilize its maximum capability without compromising its power efficiency and consequently extend the detection range of the radar many folds.

The wideband characteristics of the proposed waveform provide the opportunity to achieve high range resolution and facilitate to stabilize the spectral nulls which in turn lower the sensitivity to frequency offset. It also has the ability to provide resilience and covertness against active and passive interference including jamming and deception signals due to its interleaved multicarrier mapping structure. In the proposed radar, the phase-coded sequences are used to generate the SC-FDMA waveform that provides diversity at the sub-pulse level.

In order to confirm the ability of the proposed radar to serve the set objective regarding the range resolution, an analysis of its ambiguity function (AF) has been carried out. It has been observed that the width of the major ridge in the AF plot of the proposed SC-FDMA waveform is lesser than that of the OFDM waveform. It is, therefore, inferred that the range resolution of the proposed SC-FDMA radar is higher than that of the OFDM radar for the same number of subcarriers. In addition to a favorable AF, the proposed radar also exhibits good auto-correlation properties for the diverse radar applications. It is evident from the simulation results, that the proposed waveform has a pretty high peak-to-sidelobe ratio, and its autocorrelation properties are better than that of the OFDM and other notable waveforms.

In order to investigate the efficacy of the proposed radar architecture, end-to-end radar system simulations have been conducted for target detection and parameter estimation. Four scenarios of the target motion dynamics have been taken into account. The comparative analysis of the simulation results for each scenario show that the proposed radar outperforms the LFM and OFDM radars for target detection and its range and velocity estimation with extremely high resolutions. Even in multiple target scenario, the ability of the proposed radar to pinpoint very close targets both in range and velocity, is outstanding.

Hence in nutshell, it has been concluded that the proposed radar waveform outperforms OFDM and other notable single and multiple carrier waveforms by achieving higher range resolution, better autocorrelation properties, lower PAPR, and better discrimination between very close targets in range and velocity.

The research work in this thesis can be extended, as a future work, in the following directions.

1. Rad-Comm Hybrid Applications: The proposed waveform can be used to develop multiple tasking radars as the different source signals may correspond to independent tasks to be performed simultaneously. The proposed work can thus be extended to develop an SC-FDMA radar framework allowing multiple tasks to be carried out simultaneously by taking the advantage of its multiple access structure and translating sources into radar tasks while assigning each task a subset of subcarriers. The proposed extension can not only find its applications in Radar-Communications (Rad-Comm) hybrid systems but also in multiple target tracking radars.

2. Multiple Target Tracking Radars: The proposed ISC-FDMA radar shows great potential in tracking radar applications. In a multiple target environment, the large bandwidth can be divided into relatively narrowband sections, with each section associated to individual target

allowing simultaneous parameter estimation of each target. It is, therefore, recommended to evaluate the ISC-FDMA radar performance in tracking radars as a future work.

3. A Blend with DS-CDMA: In the potential applications of SC-FDMA radar, such as, Rad-Comm, the multiple data sources may use different subcarrier mappings, spreaded by the orthogonal direct sequence spread spectrum technique, prior to SC-FDMA modulation. This makes both interleaved and localized (e.g. the mapping used in LTE) mappings coexist with overlapping subcarriers separated in code domain. The scheme referred to as Single Carrier Code-Frequency Division Multiple Access (SC-CFDMA) can be viewed as a combination of DS-CDMA and SC-FDMA for the counter-interception applications of Rad-Comm systems. In such systems, multiple data sensors may keep themselves separated in both the frequency domain and code domain.

4. Implementation in Phased Array and Beamforming: The research work presented in this thesis has been carried out for single transmit and receive antenna system. This work can be implemented in phased array radars for beamforming to achieve higher gain and improved detection probability.

5. Implementation in MIMO radars: The proposed research work can also be extended to design an SC-FDMA MIMO radar. MIMO Radars not only provide better angular resolution and higher sensitivity for moving target detection [186], but also exhibit better capability to identify the large number of targets distinctively as compared to the conventional SISO radars. OFDM has been investigated extensively, in the literature, for MIMO radar applications. As a rule in OFDM, each antenna element utilizes a bandwidth chunk due to its block wise share in the total number of subcarriers. This reduces the range resolution of the MIMO OFDM radar system by a factor equal to its number of radar spatial data streams. However, as an alternative, in a MIMO SC-FDMA radar with interleaved subcarrier mapping, each

antenna element enjoys the total number of subcarriers simultaneously and hence retains its full resolution as compared to MIMO-OFDM radar.

6. Covertness and Resilience against Clutter/Jammers: The wideband characteristics of the proposed SC-FDMA waveform make it resistant against active and passive interference. Jammers and deception devices are examples of active interference, whereas clutter is an example of passive interference. The performance of the SC-FDMA waveform against jammers and clutter can be analyzed in the future work.

Bibliography

[1] M. I. Skolnik, "Fifty years of radar," *Proceedings of the IEEE*, vol. 73, no. 2, pp. 182–197, 1985.

[2] Skolnik, *Introduction to Radar Systems.* New York: McGraw-Hill, 1980.

[3] I. Immoreev and T.-H. Tao, "UWB radar for patient monitoring," *IEEE Aerospace and Electronic Systems Magazine*, vol. 23, no. 11, pp. 11–18, 2008.

[4] K.-M. Chen, D. Misra, H. Wang, H.-R. Chuang, and E. Postow, "An X-band microwave life-detection system," *IEEE Transactions on Biomedical Engineering*, no. 7, pp. 697–701, 1986.

[5] A. Leshem and A.-J. Van der Veen, "Radio-astronomical imaging in the presence of strong radio interference," *IEEE Transactions on Information Theory*, vol. 46, no. 5, pp. 1730–1747, 2000.

[6] G. Galati, *Advanced radar techniques and systems.* Univ. Press of Mississippi, 1993, no. 4.

[7] W.-D. Wirth, *Radar techniques using array antennas.* London: IET, 2001, vol. 10.

[8] B. R. Mahafza, *Radar Systems Analysis and Design Using MATLAB Second Edition.* Chapman and Hall/CRC, 2005.

[9] F. E. Nathanson, J. P. Reilly, and M. N. Cohen, "Radar design principles-Signal Processing and the Environment," *NASA STI/Recon Technical Report A*, vol. 91, 1991.

[10] D.-Y. Kim, M.-K. Chong, S.-K. Kim, S.-M. Chon, H.-G. Na, S.-H. Baik, C.-S. Ahn, and S.-J. Kim, "T/R Module Development for X-Band Active Phased-Array Radar," *The journal of Korean institute of electromagnetic engineering and science*, vol. 20, no. 12, pp. 1243–1251, 2009.

[11] H. Hommel and H.-P. Feldle, "Current status of airborne active phased array (AESA) radar systems and future trends," in *Proc. IEEE MTT-S International Microwave Symposium Digest*, 2005, pp. 4–pp.

[12] A. K. Agrawal, B. A. Kopp, M. H. Luesse, and K. W. O Haver, "Active phased array antenna development for modern shipboard radar systems," *Johns Hopkins APL technical digest*, vol. 22, no. 4, pp. 600–613, 2001.

[13] B. Friedlander, "On the relationship between MIMO and SIMO radars," *IEEE Transactions on Signal Processing*, vol. 57, no. 1, pp. 394–398, 2009.

[14] M. Lesturgie, "Improvement of high-frequency surface waves radar performances by use of multiple-input multiple-output configurations," *IET radar, sonar & navigation*, vol. 3, no. 1, pp. 49–61, 2009.

[15] W.-Q. Wang, M. Sellathurai, F. K. W. Chan, W. Xu, and S. Zhu, "MIMO antennas in radar applications," *International Journal of Antennas and Propagation*, vol. 2015, 2015.

[16] N. Levanon, "Multifrequency complementary phase-coded radar signal," in *Proc. IEE Proceedings-Radar, Sonar and Navigation*, vol. 147, no. 6. IET, 2000, pp. 276–284.

[17] E. Knott, *Radar Cross Section Measurements.* SciTech Pub., 2006.

[18] P. Swerling, "Probability of detection for fluctuating targets," *IRE Transactions on Information theory*, vol. 6, no. 2, pp. 269–308, 1960.

[19] J. D. Echard, "Estimation of radar detection and false alarm probability," *IEEE Transactions on Aerospace and Electronic Systems*, vol. 27, no. 2, pp. 255–260, 1991.

[20] B. Magaz, A. Belouchrani *et al.*, "Automatic threshold selection in OS-CFAR radar detection using information theoretic criteria," *Progress In Electromagnetics Research*, vol. 30, pp. 157–175, 2011.

[21] M. A. Richards, *Fundamentals of radar signal processing.* Tata McGraw-Hill Education, 2005, ch. 4, pp. 169–198.

[22] C. E. Cook, "Pulse compression-key to more efficient radar transmission," *Proceedings of the IRE*, vol. 48, no. 3, pp. 310–316, 1960.

[23] E. C. Farnett and G. H. Stevens, *Pulse compression radar.* McGraw-Hill New York, 1990, vol. 2.

[24] C. Allen, "Radar Pulse Compression," *June*, vol. 17, pp. 1–19, 2004.

[25] P. Woodward, *Probability and Information Theory: With Applications to Radar*, ser. Electronics and Waves. Elsevier Science & Technology, 1953.

[26] J. Ville, "Theory and applications of the notion of the analytic signal," *Cables et Transmission*, vol. 2, no. 1, pp. 61–74, 1948.

[27] P. M. Woodward, "Radar ambiguity analysis," Royal Radar Establishment Malvern, United Kingdom, Tech. Rep., 1967.

[28] R. Blahut, W. Miller, and C. Wilcox, *Radar and Sonar*, ser. IMA volumes in mathematics and its applications. Springer-Verlag, 1991.

[29] J.-C. Guey and M. R. Bell, "Diversity waveform sets for delay-Doppler imaging," *IEEE Transactions on Information Theory*, vol. 44, no. 4, pp. 1504–1522, 1998.

[30] A. Rihaczek, *Principles of High-resolution Radar*, ser. Artech House radar library. Artech House, New York, 1969.

[31] N. Levanon, *Radar Principles.* New York: Wiley, May 1988.

[32] I. Gladkova, "Families of waveforms with good auto and cross ambiguity properties," in *Proc. IEEE Radar Conference (RadarConf01)*, 2001, pp. 138–140.

[33] L. G. Weiss, "Wavelets and wideband correlation processing," *IEEE signal processing magazine*, vol. 11, no. 1, pp. 13–32, 1994.

[34] L. Sibul and L. Ziomek, "Generalized wideband cross-ambiguity function," in *Proc. IEEE International Conference on Acoustics, Speech, and Signal Processing (ICASSP'81)*, vol. 6, 1981, pp. 1239–1242.

[35] T. Jiang and Y. Wu, "An overview: Peak-to-average power ratio reduction techniques for OFDM signals," *IEEE Transactions on broadcasting*, vol. 54, no. 2, pp. 257–268, May 2008.

[36] R. H. Dicke, "Object detection system," U.S. Patent 2 624 876, Jan 6, 1953.

[37] J. R. Klauder, A. Price, S. Darlington, and W. J. Albersheim, "The theory and design of chirp radars," *Bell System Technical Journal*, vol. 39, no. 4, pp. 745–808, 1960.

[38] R. H. Barker, *Communication Theory*, W. Jackson ed. Academic Press, 1953, ch. Group synchronizing of binary digital system, pp. 273–287.

[39] R. L. Frank, "Phase-coded communication system," U.S. Patent 3 099 795A, July, 1963.

[40] R. Frank, "Polyphase codes with good nonperiodic correlation properties," *IEEE Transactions on Information Theory*, vol. 9, no. 1, pp. 43–45, 1963.

[41] B. Lewis and F. Kretschmer, "A new class of polyphase pulse compression codes and techniques," *IEEE Transactions on Aerospace and Electronic Systems*, vol. AES-17, no. 3, pp. 364–372, 1981.

[42] B. L. Lewis and F. F. Kretschmer, "Linear frequency modulation derived polyphase pulse compression codes," *IEEE Transactions on Aerospace and Electronic Systems*, vol. AES-18, no. 5, pp. 637–641, 1982.

[43] H. Wang, J. Wang, and H. Li, "Target detection using CDMA based passive bistatic radar," *Journal of Systems Engineering and Electronics*, vol. 23, no. 6, pp. 858–865, Dec. 2012.

[44] A. Munshi and S. Unnikrishnan, "Vehicle to Vehicle Communication Using DS-CDMA Radar," *Procedia Computer Science*, vol. 49, pp. 235–243, 2015.

[45] R. Bera, J. Bera, S. Sil, D. Mondal, S. Dhar, and D. Kandar, "CDMA Technology for Intelligent Transportation Systems," *arXiv preprint arXiv:0705.2084*, 2007.

[46] N. Levanon and E. Mozeson, *Radar Signals.* John Wiley & Sons, 2004, ch. 11, pp. 327–372.

[47] R. Calderbank, S. D. Howard, and B. Moran, "Waveform diversity in radar signal processing," *IEEE Signal Processing Magazine*, vol. 26, no. 1, pp. 32–41, 2009.

[48] R. F. Tigrek, "A processing technique for OFDM-modulated wideband radar signals," Ph.D. dissertation, 2010.

[49] G. Lellouch, P. Tran, R. Pribic, and P. Van Genderen, "OFDM waveforms for frequency agility and opportunities for Doppler processing in radar," in *Proc. IEEE Radar Conference (RadarConf08)*, 2008, pp. 1–6.

[50] R. Tigrek, W. De Heij, and P. Van Genderen, "Solving Doppler ambiguity by Doppler sensitive pulse compression using multi-carrier waveform," in *Proc. European Radar Conference, (EuRAD2008), IEEE*, 2008, pp. 72–75.

[51] M. Li, W.-Q. Wang, and Z. Zheng, "Communication-embedded OFDM chirp waveform for delay-Doppler radar," *IET Radar, Sonar & Navigation*, 2017.

[52] W.-Q. Wang, Z. Zheng, and S. Zhang, "OFDM Chirp waveform diversity for co-designed radar-communication system," in *Proc. 18th International Radar Symposium (IRS).* IEEE, 2017, pp. 1–9.

[53] A. Babaei, W. H. Tranter, and T. Bose, "A nullspace-based precoder with subspace expansion for radar/communications coexistence," in *Proc. IEEE Global Communications Conference (GLOBECOM)*, 2013, pp. 3487–3492.

[54] A. R. Chiriyath, B. Paul, G. M. Jacyna, and D. W. Bliss, "Inner bounds on performance of radar and communications co-existence," *IEEE Transactions on Signal Processing*, vol. 64, no. 2, pp. 464–474, 2016.

[55] J. G. Metcalf, C. Sahin, S. D. Blunt, and M. Rangaswamy, "Analysis of symbol-design strategies for intrapulse radar-embedded communications," *IEEE Transactions on Aerospace and Electronic Systems*, vol. 51, no. 4, pp. 2914–2931, 2015.

[56] A. Turlapaty and Y. Jin, "A joint design of transmit waveforms for radar and communications systems in coexistence," in *Proc. IEEE Radar Conference (RadarConf14)*, 2014, pp. 0315–0319.

[57] B. Paul, A. R. Chiriyath, and D. W. Bliss, "Joint communications and radar performance bounds under continuous waveform optimization: The waveform awakens," in *Proc. IEEE Radar Conference (RadarConf16)*, 2016, pp. 1–6.

[58] A. de Oliveira, R. Sampaio-Neto, and J. M. Fortes, "Robust radar-embedded sidelobe level modulation using constrained optimization design," in *Proc. IEEE Radar Conference (RadarConf08)*, 2016, pp. 1–5.

[59] J. Guerci and R. Guerci, "RAST: Radar as a subscriber technology for wireless spectrum cohabitation," in *Proc. IEEE Radar Conference (RadarConf14)*, 2014, pp. 1130–1134.

[60] M. Scharrenbroich and M. Zatman, "Joint radar-communications resource management," in *Proc. IEEE Radar Conference (RadarConf16)*, 2016, pp. 1–6.

[61] J. R. Krier, M. C. Norko, J. T. Reed, R. J. Baxley, A. D. Lanterman, X. Ma, and J. R. Barry, "Performance bounds for an OFDM-based joint radar and communications system," in *Military Communications Conference, MILCOM 2015-2015 IEEE*. IEEE, 2015, pp. 511–516.

[62] Y. Xie, R. Tao, and T. Wang, "Method of waveform design for radar and communication integrated system based on CSS," in *First International Conference on Instrumentation, Measurement, Computer, Communication and Control.* IEEE, 2011, pp. 737–739.

[63] B. Knoedler, R. Zemmari, and U. Nickel, "GSM passive radar: Range resolution improvement using data-dependent non parametric approach," in *Proc. IEEE Radar Conference (RadarConf14)*, 2014, pp. 1035–1039.

[64] A. R. Chiriyath, B. Paul, and D. W. Bliss, "Joint radar-communications information bounds with clutter: The phase noise menace," in *Proc. IEEE Radar Conference (RadarConf16).* IEEE, 2016, pp. 1–6.

[65] D. Garmatyuk, J. Schuerger, K. Kauffman, and S. Spalding, "Wideband OFDM system for radar and communications," in *Proc. IEEE Radar Conference (RadarConf09)*, 2009, pp. 1–6.

[66] L. Han and K. Wu, "24-GHz integrated radio and radar system capable of time-agile wireless communication and sensing," *IEEE Transactions on Microwave Theory and Techniques*, vol. 60, no. 3, pp. 619–631, 2012.

[67] J. Moghaddasi and K. Wu, "Improved joint radar-radio (RadCom) transceiver for future intelligent transportation platforms and highly mobile high-speed communication systems," in *Proc. IEEE International Wireless Symposium (IWS)*, 2013, pp. 1–4.

[68] C. Sturm and T. Zwick, "Joint radar sensing and communications based on OFDM signals for intelligent transportation networks," *LS Telecom Summit, Lichtenau, Germany*, pp. 1–4, 2010.

[69] P. Ubolkosold, "Frequency estimation for single-carrier and OFDM signals in communication and radar systems," Ph.D. dissertation, 2009.

[70] A. R. Chiriyath, B. Paul, and D. W. Bliss, "Joint Radar-Communications Performance Inner Bounds: Data versus Estimation Information Rates," *arXiv preprint arXiv:1409.4159*, 2014.

[71] D. Ciuonzo, A. De Maio, G. Foglia, and M. Piezzo, "Pareto-theory for enabling covert intrapulse radar-embedded communications," in *Proc. IEEE Radar Conference (RadarConf15)*, 2015, pp. 0292–0297.

[72] D. Gaglione, C. Clemente, A. R. Persico, C. V. Ilioudis, I. K. Proudler, and J. J. Soraghan, "Fractional Fourier Transform Based Co-Radar Waveform: Experimental Validation," in *Proc. Sensor Signal Processing for Defence (SSPD), IEEE*, 2016, pp. 1–5.

[73] L. Hu, Z. Du, and G. Xue, "Radar-communication integration based on OFDM signal," in *Proc. IEEE International Conference on Signal Processing, Communications and Computing (ICSPCC)*, 2014, pp. 442–445.

[74] D. Erricolo, H. Griffiths, L. Teng, M. Wicks, and L. L. Monte, "On the spectrum sharing between radar and communication systems," in *Proc. International Conference on Electromagnetics in Advanced Applications (ICEAA)*, 2014, pp. 890–893.

[75] Y. L. Sit, C. Sturm, and T. Zwick, "One-stage selective interference cancellation for the OFDM joint radar-communication system," in *Proc. The 7th German Microwave Conference (GeMiC), IEEE*, 2012, pp. 1–4.

[76] Y. L. Sit, L. Reichardt, C. Sturm, and T. Zwick, "Extension of the OFDM joint radar-communication system for a multipath, multiuser scenario," in *Proc. IEEE Radar Conference (RadarConf11)*, 2011, pp. 718–723.

[77] Y. L. Sit and T. Zwick, "MIMO OFDM radar with communication and interference cancellation features," in *Proc. IEEE Radar Conference (RadarConf14)*. IEEE, 2014, pp. 0265–0268.

[78] M. Braun, C. Sturm, and F. K. Jondral, "On the Frame Design for Joint OFDM Radar and Communications," in *Proc. 15th International OFDM Workshop, Hamburg*, 2010.

[79] J. Moghaddasi and K. Wu, "Multifunctional transceiver for future radar sensing and radio communicating data-fusion platform," *IEEE Access*, vol. 4, pp. 818–838, 2016.

[80] X. Shen, R. Yang, X. Li, and M. Huang, "The Research on DS-OFDM in Integrated Radar and Communication," in *Wireless Communications, Networking and Applications*. Springer, 2016, pp. 729–740.

[81] R. Tigrek, W. De Heij, and P. Van Genderen, "Multi-carrier radar waveform schemes for range and Doppler processing," in *Proc. IEEE Radar Conference*, 2009, pp. 1–5.

[82] C. Sturm, M. Braun, T. Zwick, and W. Wiesbeck, "A multiple target Doppler estimation algorithm for OFDM based intelligent radar systems," in *Proc. European Radar Conference (EuRAD), IEEE*, 2010, pp. 73–76.

[83] Y. L. Sit, C. Sturm, L. Reichardt, W. Wiesbeck, and T. Zwick, "Verification of an OFDM-based range and Doppler estimation algorithm with ray-trace OFDM," in *Proc. IEEE-APS Topical Conference on Antennas and Propagation in Wireless Communications (APWC)*, 2011, pp. 808–811.

[84] M. Braun, C. Sturm, and F. K. Jondral, "Maximum likelihood speed and distance estimation for OFDM radar," in *Proc. IEEE Radar Conference (RadarConf10)*, 2010, pp. 256–261.

[85] G. Lellouch, "Waveform design and processing techniques in OFDM radar," Ph.D. dissertation, University of Cape Town, 2015.

[86] S. Hadizadehmoghaddam, F. Yusufali, and R. S. Adve, "Interference-aware power allocation in OFDMA radar," in *Proc. IEEE Radar Conference (RadarConf18)*, 2018, pp. 0821–0826.

[87] S. Hadizadehmoghaddam and R. S. Adve, "Simultaneous execution of multiple radar tasks using OFDMA," in *Proc. Radar Conference (RadarConf17)*, 2017, pp. 0622–0626.

[88] S. Sen, "PAPR-constrained pareto-optimal waveform design for OFDM-STAP radar," *IEEE Transactions on Geoscience and Remote Sensing*, vol. 52, no. 6, pp. 3658–3669, 2014.

[89] S. Sen and C. W. Glover, "Frequency adaptability and waveform design for OFDM radar space-time adaptive processing," in *Proc. IEEE Radar Conference (RadarConf16)*, 2012, pp. 0230–0235.

[90] S. Sen, "Adaptive OFDM radar for target detection and tracking," Ph.D. dissertation, 2010.

[91] S. Sen and A. Nehorai, "Adaptive OFDM radar for target detection in multipath scenarios," *IEEE Transactions on Signal Processing*, vol. 59, no. 1, pp. 78–90, 2011.

[92] S. Sen, M. Hurtado, and A. Nehorai, "Adaptive OFDM radar for detecting a moving target in urban scenarios," in *Proc. International Waveform Diversity and Design Conference*, Feb. 2009, pp. 268–272.

[93] Y.-H. Cao, X.-G. Xia, and S.-H. Wang, "IRCI free colocated MIMO radar based on sufficient cyclic prefix OFDM waveforms," *IEEE Transactions on Aerospace and Electronic Systems*, vol. 51, no. 3, pp. 2107–2120, 2015.

[94] T. Zhang, X.-G. Xia, and L. Kong, "CP-based MIMO OFDM radar IRCI free range reconstruction using real orthogonal designs," *Science China Information Sciences*, vol. 60, no. 2, p. 022301, 2017.

[95] G. Hakobyan and B. Yang, "A novel OFDM-MIMO radar with non-equidistant subcarrier interleaving and compressed sensing," in *Proc. IEEE 17th International Radar Symposium (IRS)*, 2016, pp. 1–5.

[96] Y. L. Sit and T. Zwick, "Automotive MIMO OFDM radar: Subcarrier allocation techniques for multiple-user access and DOA estimation," in *Proc. 11th European Radar Conference (EuRAD), IEEE*, 2014, pp. 153–156.

[97] S. Sen and A. Nehorai, "OFDM MIMO radar with mutual-information waveform design for low-grazing angle tracking," *IEEE Transactions on Signal Processing*, vol. 58, no. 6, pp. 3152–3162, 2010.

[98] C. Sturm, Y. L. Sit, M. Braun, and T. Zwick, "Spectrally interleaved multi-carrier signals for radar network applications and multi-input multi-output radar," *IET Radar, Sonar & Navigation*, vol. 7, no. 3, pp. 261–269, 2013.

[99] X. Wu, A. Kishk, and A. Glisson, "MIMO-OFDM radar for direction estimation," *IET Radar, Sonar & Navigation*, vol. 4, no. 1, pp. 28–36, 2010.

[100] Y. L. Sit, C. Sturm, J. Baier, and T. Zwick, "Direction of arrival estimation using the MUSIC algorithm for a MIMO OFDM radar," in *Proc. IEEE Radar Conference*, 2012, pp. 0226–0229.

[101] X.-R. Li, Z. Zhang, W.-X. Mao, X.-M. Wang, J. Lu, and W.-S. Wang, "A study of frequency diversity MIMO radar beamforming," in *Proc. IEEE 10th International Conference on Signal Processing (ICSP)*, 2010, pp. 352–356.

[102] Y. L. Sit, M. Agatonovic, and T. Zwick, "Neural network based direction of arrival estimation for a MIMO OFDM radar," in *Proc. 9th European Radar Conference (EuRAD), IEEE*, 2012, pp. 298–301.

[103] P. De Silva and C. K. Seow, "Performance of MIMO radar using two-way MUSIC," 2013.

[104] C. W. Kim, B. Luo, Y.-C. Liang, and M. Y. W. Chia, "MIMO-OFDM radar array configuration for resolving DOA ambiguity," in *Proc. IEEE International Conference on Communication Systems (ICCS)*, 2012, pp. 85–89.

[105] J. Wang, X. Liang, and L. Chen, "MIMO SAR system using digital implemented OFDM waveforms," in *Proc. IEEE International Geoscience and Remote Sensing Symposium (IGARSS)*, 2012, pp. 7428–7431.

[106] W.-Q. Wang, "MIMO SAR OFDM chirp waveform diversity design with random matrix modulation," *IEEE Transactions on Geoscience and Remote Sensing*, vol. 53, no. 3, pp. 1615–1625, 2015.

[107] J. Wang, X. Liang, C. Ding, L. Chen, L. Zhou, and Y. Dong, "An improved OFDM chirp waveform used for MIMO SAR system," *Science China Information Sciences*, vol. 57, no. 6, pp. 1–9, 2014.

[108] Y.-H. Cao and X.-G. Xia, "IRCI-Free MIMO-OFDM SAR Using Circularly Shifted Zadoff–Chu Sequences," *IEEE Geoscience and Remote Sensing Letters*, vol. 12, no. 5, pp. 1126–1130, 2015.

[109] X.-G. Xia, T. Zhang, and L. Kong, "MIMO OFDM radar IRCI free range reconstruction with sufficient cyclic prefix," *IEEE Transactions on Aerospace and Electronic Systems*, vol. 51, no. 3, pp. 2276–2293, 2015.

[110] J. Kim, M. Younis, A. Moreira, and W. Wiesbeck, "A novel OFDM waveform for fully polarimetric SAR data acquisition," in *Proc. 8th European Conference on Synthetic Aperture Radar (EUSAR), VDE*, 2010, pp. 1–4.

[111] J. Wang, L.-Y. Chen, X.-D. Liang, C.-b. Ding, and K. Li, "Implementation of the OFDM chirp waveform on MIMO SAR systems," *IEEE Transactions on Geoscience and Remote Sensing*, vol. 53, no. 9, pp. 5218–5228, 2015.

[112] W.-Q. Wang, "MIMO SAR chirp modulation diversity waveform design," *IEEE Geoscience and Remote Sensing Letters*, vol. 11, no. 9, pp. 1644–1648, 2014.

[113] J.-H. Kim, M. Younis, A. Moreira, and W. Wiesbeck, "Spaceborne MIMO synthetic aperture radar for multimodal operation," *IEEE Transactions on Geoscience and Remote Sensing*, vol. 53, no. 5, pp. 2453–2466, 2015.

[114] D. Garmatyuk and K. Kauffman, "Radar and data communication fusion with UWB-OFDM software-defined system," in *IEEE International Conference on Ultra-Wideband*, 2009, pp. 454–458.

[115] T. Zhang and X.-G. Xia, "OFDM synthetic aperture radar imaging with sufficient cyclic prefix," *IEEE Transactions on Geoscience and Remote Sensing*, vol. 53, no. 1, pp. 394–404, 2015.

[116] V. Riché, S. Méric, J.-Y. Baudais, and É. Pottier, "Investigations on OFDM signal for range ambiguity suppression in SAR configuration," *IEEE Transactions on Geoscience and Remote Sensing*, vol. 52, no. 7, pp. 4194–4197, 2014.

[117] J.-H. Kim, M. Younis, A. Moreira, and W. Wiesbeck, "A novel OFDM chirp waveform scheme for use of multiple transmitters in SAR," *IEEE Geoscience and Remote Sensing Letters*, vol. 10, no. 3, pp. 568–572, 2013.

[118] T. Zhang, X.-G. Xia, and L. Kong, "IRCI free range reconstruction for SAR imaging with arbitrary length OFDM pulse," *IEEE Transactions on Signal Processing*, vol. 62, no. 18, pp. 4748–4759, 2014.

[119] D. Garmatyuk, "Cross-range SAR reconstruction with multicarrier OFDM signals," *IEEE Geoscience and Remote Sensing Letters*, vol. 9, no. 5, pp. 808–812, 2012.

[120] H. G. Myung, J. Lim, and D. J. Goodman, "Single carrier FDMA for uplink wireless transmission," *IEEE Vehicular Technology Magazine*, vol. 1, no. 3, pp. 30–38, 2006.

[121] H. G. M. D. J. Goodman, *Single Carrier FDMA- A New Air Interface for Long Term Evolution.* John Wiley & Sons, Ltd, Oct 2008.

[122] M. Jankiraman, B. Wessels, and P. Van Genderen, "System Design and verification of the PANDORA multifrequency Radar," in *Proc. International conference on Radar Systems*, May 1999.

[123] G. Franken, H. Nikookar, and P. Van Genderen, "Doppler tolerance of OFDM-coded radar signals," in *Proc. 3rd European Radar Conference, (EuRAD), IEEE*, 2006, pp. 108–111.

[124] M. Braun, C. Sturm, A. Niethammer, and F. K. Jondral, "Parameterization of joint OFDM-based radar and communication systems for vehicular applications," in *Proc. IEEE 20th International Symposium on Personal, Indoor and Mobile Radio Communications*, 2009, pp. 3020–3024.

[125] S. Sen and A. Nehorai, "Target detection in clutter using adaptive OFDM radar," *IEEE signal processing letters*, vol. 16, no. 7, pp. 592–595, Apr. 2009.

[126] C. Sturm, E. Pancera, T. Zwick, and W. Wiesbeck, "A novel approach to OFDM radar processing," in *Proc. IEEE Radar Conference*, 2009, pp. 1–4.

[127] C. Sturm, T. Zwick, and W. Wiesbeck, "An OFDM system concept for joint radar and communications operations," in *Proc. IEEE 69th Vehicular Technology Conference (VTC Spring)*, 2009, pp. 1–5.

[128] M. Bică and V. Koivunen, "Generalized multicarrier radar: Models and Performance," *IEEE Transactions on Signal Processing*, vol. 64, no. 17, pp. 4389–4402, 2016.

[129] G. Lellouch, A. K. Mishra, and M. Inggs, "Design of OFDM radar pulses using genetic algorithm based techniques," *IEEE Transactions on Aerospace and Electronic Systems*, vol. 52, no. 4, pp. 1953–1966, 2016.

[130] N. Prasad, V. Shameem, U. Desai, and S. Merchant, "Improvement in target detection performance of pulse coded Doppler radar based on multicarrier modulation with fast Fourier transform (FFT)," *IEE Proceedings-Radar, Sonar and Navigation*, vol. 151, no. 1, pp. 11–17, 2004.

[131] N. Levanon, "Train of diverse multifrequency radar pulses," in *Proc. IEEE Radar Conference (RadarConf01)*, 2001, pp. 93–98.

[132] M. Fuhr, M. Braun, C. Sturmz, L. Reichardtz, and F. K. Jondral, "An SDR-based experimental setup for OFDM-based radar," in *Proc. 7th Karlsruhe Workshop on Software Radio Karlsruhe, Citeseer*, 2012.

[133] Y. L. Sit, B. Nuss, S. Basak, M. Orzol, and T. Zwick, “Demonstration of interference cancellation in a multiple-user access OFDM MIMO radar-communication network using USRPs,” in *Proc. IEEE MTT-S International Conference on Microwaves for Intelligent Mobility (ICMIM)*, 2016, pp. 1–4.

[134] S. A. Holder, “Linear frequency modulated signals VS orthogonal frequency division multiplexing signals for synthetic aperture radar systems,” NAVAL Postgraduate School Monterey CA, Tech. Rep., 2014.

[135] J. Fink and F. K. Jondral, “Comparison of OFDM radar and Chirp sequence radar,” in *Proc. 16th International Radar Symposium (IRS), IEEE*, 2015, pp. 315–320.

[136] K. Chen, Y. Liu, and W. Zhang, “Study on integrated radar-communication signal of OFDM-LFM based on FRFT,” in *Proc. IET International Radar Conference*, 2015, pp. 1–6.

[137] X. Ouyang and J. Zhao, “Orthogonal chirp division multiplexing,” *IEEE Transactions on Communications*, vol. 64, no. 9, pp. 3946–3957, 2016.

[138] K. Huo, B. Deng, Y. Liu, W. Jiang, and J. Mao, “High resolution range profile analysis based on multicarrier phase-coded waveforms of OFDM radar,” *Journal of Systems Engineering and Electronics*, vol. 22, no. 3, pp. 421–427, 2011.

[139] M. Ruggiano, E. Stolp, and P. Van Genderen, “Multi-target performance of LMMSE filtering in radar,” *IEEE Transactions on Aerospace and Electronic Systems*, vol. 48, no. 1, pp. 170–179, 2012.

[140] J. Zuo, R. Yang, S. Luo, and Y. Zhou, “Range sidelobe suppression for OFDM-integrated radar and communication signal,” *The Journal of Engineering*, vol. 2019, no. 21, pp. 7624–7627, 2019.

[141] W.-Q. Wang, “An orthogonal frequency division multiplexing radar waveform with a large time-bandwidth product,” *Defence Science Journal*, vol. 62, no. 6, pp. 427–430, 2012.

[142] S.-J. Cheng, W.-Q. Wang, and H.-Z. Shao, "Spread spectrum-coded OFDM chirp waveform diversity design," *IEEE Sensors Journal*, vol. 15, no. 10, pp. 5694–5700, 2015.

[143] M. Sebt, A. Sheikhi, and M. Nayebi, "Orthogonal frequency-division multiplexing radar signal design with optimized ambiguity function and low peak-to-average power ratio," *IET radar, sonar & navigation*, vol. 3, no. 2, pp. 122–132, 2009.

[144] R. Tigrek, W. de Heij, and P. van Genderen, "Relation between the peak to average power ratio and Doppler sidelobes of the multi-carrier radar signal," in *Proc. International Radar Conference-Surveillance for a Safer World.* IEEE, 2009, pp. 1–6.

[145] R. F. Tigrek, W. J. A. De Heij, and P. Van Genderen, "OFDM signals as the Radar Waveform to solve Doppler Ambiguity," *IEEE Transactions on Aerospace and Electronic Systems*, vol. 48, no. 1, pp. 130–143, Jan. 2012.

[146] Y. Rahmatallah and S. Mohan, "Peak-to-average power ratio reduction in OFDM systems: A survey and taxonomy," *IEEE communications surveys & tutorials*, vol. 15, no. 4, pp. 1567–1592, Mar. 2013.

[147] A. De Maio, Y. Huang, M. Piezzo, S. Zhang, and A. Farina, "Radar code design with a Peak to average power Ratio constraint: A randomized approximate approach," in *Proc. 19th European Signal Processing Conference, IEEE*, 2011, pp. 436–440.

[148] X. Li and L. J. Cimini, "Effects of clipping and filtering on the performance of OFDM," in *Proc. IEEE 47th Vehicular Technology Conference*, vol. 3, May 1997, pp. 1634–1638.

[149] G. Azarnia and A. A. Sharifi, "Clipping-based PAPR reduction of optical OFDM signals using compressive sensing: Bayesian signal reconstruction approach," *Optical Fiber Technology*, vol. 64, p. 102527, 2021.

[150] X. Liu, X. Zhang, L. Zhang, P. Xiao, J. Wei, H. Zhang, and V. C. Leung, "PAPR reduction using iterative clipping/filtering and ADMM approaches for OFDM-based mixed-numerology systems," *IEEE Transactions on Wireless Communications*, vol. 19, no. 4, pp. 2586–2600, 2020.

[151] X. Wang, T. T. Tjhung, and C. Ng, "Reduction of Peak-to-average power ratio of OFDM system using a companding technique," *IEEE transactions on broadcasting*, vol. 45, no. 3, pp. 303–307, Sep. 1999.

[152] P. O. Börjesson, H. G. Feichtinger, N. Grip, M. Isaksson, N. Kaiblinger, P. Ödling, and L.-E. Persson, "A low-complexity PAR-reduction method for DMT-VDSL," in *Proc. International Symposium on Digital Signal Processing for Communication Systems*, 1999, pp. 164–169.

[153] S. Cha, M. Park, S. Lee, K.-J. Bang, and D. Hong, "A new PAPR reduction technique for OFDM systems using advanced peak windowing method," *IEEE Transactions on Consumer Electronics*, vol. 54, no. 2, pp. 405–410, Jul. 2008.

[154] R. Musabe, M. B. Lionel, V. M. Ushindi, M. Atupenda, J. Ntaganda, and G. Bajpai, "PAPR reduction in LTE network using both peak windowing and clipping techniques," *Journal of Electrical Systems and Information Technology*, vol. 6, no. 1, pp. 1–11, 2019.

[155] H. Ochiai and H. Imai, "Performance analysis of deliberately clipped OFDM signals," *IEEE Transactions on communications*, vol. 50, no. 1, pp. 89–101, Jan. 2002.

[156] T. Wattanasuwakull and W. Benjapolakul, "PAPR reduction for OFDM transmission by using a method of tone reservation and tone injection," in *Proc. 5th International Conference on Information Communications Signal Processing*, Dec. 2005, pp. 273–277.

[157] R. W. Bauml, R. F. Fischer, and J. B. Huber, "Reducing the peak-to-average power ratio of multicarrier modulation by selected mapping," *Electronics letters*, vol. 32, no. 22, pp. 2056–2057, 1996.

[158] S. H. Muller and J. B. Huber, "OFDM with reduced Peak-to-average power ratio by optimum combination of partial transmit sequences," *Electronics letters*, vol. 33, no. 5, pp. 368–369, 1997.

[159] A. D. Jayalath and C. Tellambura, "Reducing the peak-to-average power ratio of orthogonal frequency division multiplexing signal through bit or symbol interleaving," *Electronics Letters*, vol. 36, no. 13, pp. 1161–1163, 2000.

[160] Z. Wang, F. Tigrek, O. Krasnov, F. Van Der Zwan, P. Van Genderen, and A. Yarovoy, "Interleaved OFDM radar signals for simultaneous polarimetric measurements," *IEEE Transactions on Aerospace and Electronic Systems*, vol. 48, no. 3, pp. 2085–2099, 2012.

[161] P. Tu, X. Huang, and E. Dutkiewicz, "Peak-to-average power ratio performance of interleaved spread spectrum OFDM signals," in *Proc. International Symposium on Communications and Information Technologies.* IEEE, 2007, pp. 82–86.

[162] B. S. Krongold and D. L. Jones, "PAR reduction in OFDM via active constellation extension," *IEEE Transactions on broadcasting*, vol. 49, no. 3, pp. 258–268, 2003.

[163] A. Aggarwal and T. H. Meng, "Minimizing the peak-to-average power ratio of OFDM signals using convex optimization," *IEEE Transactions on Signal Processing*, vol. 54, no. 8, pp. 3099–3110, 2006.

[164] M. Hosseinzadeh Aghdam and A. A. Sharifi, "PAPR reduction in OFDM systems: An efficient PTS approach based on particle swarm optimization," *ICT Express*, vol. 5, no. 3, pp. 178–181, 2019.

[165] R. Sayyari, J. Pourrostam, and H. Ahmadi, "Efficient PAPR reduction scheme for OFDM-NOMA systems based on DSI & precoding methods," *Physical Communication*, vol. 47, p. 101372, 2021.

[166] H.-J. Ahn, Y. Shin, and S. Im, “A block coding scheme for peak-to-average power ratio reduction in an orthogonal frequency division multiplexing system,” in *Proc. IEEE 51st Vehicular Technology Conference Proceedings (Cat. No. 00CH37026)*, vol. 1, 2000, pp. 56–60.

[167] J. A. Davis and J. Jedwab, “Peak-to-mean power control in OFDM, Golay complementary sequences, and Reed-Muller codes,” *IEEE Transactions on information theory*, vol. 45, no. 7, pp. 2397–2417, 1999.

[168] A. A. Abouda, “PAPR reduction of OFDM signal using turbo coding and selective mapping,” in *Proc. 6th Nordic Signal Processing Symposium*, 2004, pp. 248–251.

[169] Y. Zhao, X. Lu, J. Yang, W. Su, and H. Gu, “OFDM wavefroms designed with piecewise nonlinear frequency modulation pulse for MIMO radar,” *International journal of remote sensing*, vol. 39, no. 23, pp. 8746–8765, 2018.

[170] E. Mozeson and N. Levanon, “Multicarrier radar signals with low peak-to-mean envelope power ratio,” *IEE Proceedings-Radar, Sonar and Navigation*, vol. 150, no. 2, pp. 71–77, 2003.

[171] Y. Balal, M. Pinchas, and Y. Pinhasi, “Constant Envelope Modulation Techniques for Limited Power Millimeter Wave Links,” *Electronics*, vol. 8, no. 12, p. 1521, 2019.

[172] H. He, P. Stoica, and J. Li, “Designing unimodular sequence sets with good correlations, including an application to MIMO radar,” *IEEE Transactions on Signal Processing*, vol. 57, no. 11, pp. 4391–4405, 2009.

[173] P. Stoica, H. He, and J. Li, “New algorithms for designing unimodular sequences with good correlation properties,” *IEEE Transactions on Signal Processing*, vol. 57, no. 4, pp. 1415–1425, 2009.

[174] Z. Li, P. Li, X. Hao, and X. Yan, “Optimal unimodular sequences design method for active sensing systems,” *Mathematical Problems in Engineering*, vol. 2018, pp. 1–13, May 2018.

[175] Z. Souad and B. Ridha, "SOCP approach for reducing PAPR system SC-FDMA in uplink via tone reservation," *International Journal of Computer Networks & Communications*, vol. 3, no. 6, p. 157, 2011.

[176] W. Wiesbeck, L. Sit, M. Younis, T. Rommel, G. Krieger, and A. Moreira, "Radar 2020: The future of radar systems," in *Proc. IEEE International Geoscience and Remote Sensing Symposium (IGARSS)*, 2015, pp. 188–191.

[177] L. Kong, W. Xu, H. Zhang, and C. Zhao, "R-OFDM Transmission Scheme for Visible Light Communication Using RGBA-LED," in *Proc. IEEE 84th Vehicular Technology Conference (VTC-Fall)*, 2016, pp. 1–6.

[178] J. Zhu, X. Wang, X. Huang, S. Suvorova, and B. Moran, "Golay Complementary Waveforms in Reed–müller Sequences for Radar Detection of Nonzero Doppler Targets," *Sensors*, vol. 18, no. 1, p. 192, 2018.

[179] P. Stoica, H. He, and J. Li, "On designing sequences with impulse-like periodic correlation," *IEEE Signal Processing Letters*, vol. 16, no. 8, pp. 703–706, Aug. 2009.

[180] Y. Huang, S. Hu, S. Ma, Q. Luo, D. Huang, Y. Gao, and R. Shi, "Constant envelope OFDM RadCom fusion system," *EURASIP Journal on Wireless Communications and Networking*, vol. 2018, no. 1, pp. 1–15, 2018.

[181] D. Schleher, *MTI and Pulsed Doppler Radar with MATLAB*, ser. Artech House Remote Sensing Library. Boston: Artech House, 2010.

[182] E. Mozeson and N. Levanon, "Removing autocorrelation sidelobes by overlaying orthogonal coding on any train of identical pulses," *IEEE Transactions on Aerospace and Electronic Systems*, vol. 39, no. 2, pp. 583–603, 2003.

[183] J. Seberry and M. Yamada, *Contemporary Design Theory - A Collection of Surveys*. John Wiley and Sons, 1992, ch. Hadamard matrices, Sequences, and Block Designs, Contemporary Design Theory, pp. 431–560.

[184] W. J. Alberhseim, "A closed-form approximation to Robertson's detection characteristics," *Proceedings of the IEEE*, vol. 69, no. 7, pp. 839–839, 1981.

[185] H. T. Friis, "A note on a simple transmission formula," *Proceedings of the IRE*, vol. 34, no. 5, pp. 254–256, 1946.

[186] J. Li and P. Stoica, *MIMO Radar Signal Processing.* Hoboken, New Jersey: Wiley - IEEE, 2009.